

OFFICIAL FILE COPY

AFWAL-TR-81-4092

ADA117904

PHYSICAL-CHEMICAL PROPERTIES OF ARTICULATED RODLIKE POLYMERS



G. C. Berry
Y. Einaga
R. Furukawa
C. C. Lee

Carnegie-Mellon University
4400 Fifth Avenue
Pittsburgh, PA 15213

October 1981

Final Report for Period March 1980 - February 1981

Approved for Public Release, Distribution Unlimited

OFFICIAL FILE COPY

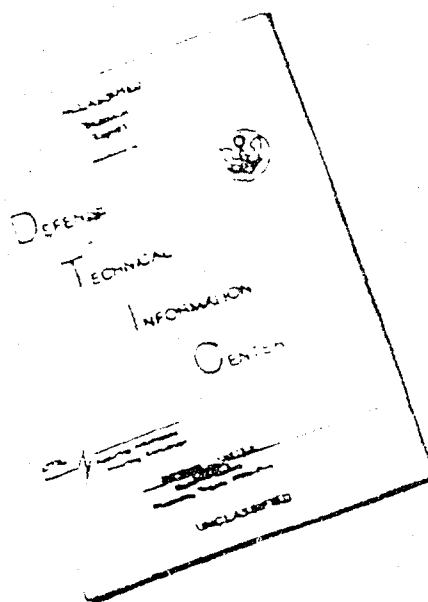
MATERIALS LABORATORY
AIR FORCE WRIGHT AERONAUTICAL LABORATORIES
AIR FORCE SYSTEMS COMMAND
WRIGHT-PATTERSON AIR FORCE BASE, OHIO 45433

BEST AVAILABLE COPY

20040226/97

~~SECRET~~

DISCLAIMER NOTICE



THIS DOCUMENT IS BEST
QUALITY AVAILABLE. THE COPY
FURNISHED TO DTIC CONTAINED
A SIGNIFICANT NUMBER OF
PAGES WHICH DO NOT
REPRODUCE LEGIBLY.

REPRODUCED FROM
BEST AVAILABLE COPY

NOTICE

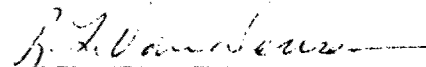
When Government drawings, specifications, or other data are used for any purpose other than in connection with a definitely related Government procurement operation, the United States Government thereby incurs no responsibility nor any obligation whatsoever; and the fact that the Government may have formulated, furnished, or in any way supplied the said drawings, specifications, or other data, is not to be regarded by implication or otherwise as in any manner licensing the holder or any other person or corporation, or conveying any rights or permission to manufacture, use, or sell any patented invention that may in any way be related thereto.

This report has been reviewed by the Office of Public Affairs (ASD/PA) and is releasable to the National Technical Information Service (NTIS). At NTIS, it will be available to the general public, including foreign nations.

This technical report has been reviewed and is approved for publication.



Project Scientist



R. L. VAN DEUSEN
Chief, Polymer Branch

FOR THE COMMANDER



F. D. CHERRY, Chief
Nonmetallic Materials Division

"If your address has changed, if you wish to be removed from our mailing list, or if the addressee is no longer employed by your organization please notify AFWAL/MLBP, W-PAFB, Ohio 45433 to help us maintain a current mailing list.

Copies of this report should not be returned unless return is required by security considerations, contractual obligations, or notice on a specific document.

UNCLASSIFIED

SECURITY CLASSIFICATION OF THIS PAGE (When Data Entered)

REPORT DOCUMENTATION PAGE		READ INSTRUCTIONS BEFORE COMPLETING FORM
1. REPORT NUMBER AFWAL TR-81-4092	2. GOVT ACCESSION NO.	3. RECIPIENT'S CATALOG NUMBER
4. TITLE (and Subtitle) PHYSICAL-CHEMICAL PROPERTIES OF ARTICULATED RODLIKE POLYMERS		5. TYPE OF REPORT & PERIOD COVERED Annual Report March 1980 - February 1981
		6. PERFORMING ORG. REPORT NUMBER
7. AUTHOR(s) G.C. Berry, Principal Investigator, C.C. Lee Y. Einaga R. Furukawa		8. CONTRACT OR GRANT NUMBER(s) F33615-79-C-5034
9. PERFORMING ORGANIZATION NAME AND ADDRESS Carnegie-Mellon University 4400 Fifth Avenue Pittsburgh, PA 15213		10. PROGRAM ELEMENT, PROJECT, TASK AREA & WORK UNIT NUMBERS 2419-04-20
11. CONTROLLING OFFICE NAME AND ADDRESS AFWAL/MLBP Air Force Wright Aeronautical Laboratories Wright-Patterson AFB, Ohio 45433		12. REPORT DATE October 1981
		13. NUMBER OF PAGES 180
14. MONITORING AGENCY NAME & ADDRESS (if different from Controlling Office)		15. SECURITY CLASS. (of this report) UNCLASSIFIED
		15a. DECLASSIFICATION/DOWNGRADING SCHEDULE N/A
16. DISTRIBUTION STATEMENT (of this Report) Approved for Public Release, Distribution Unlimited		
17. DISTRIBUTION STATEMENT (of the abstract entered in Block 20, if different from Report)		
18. SUPPLEMENTARY NOTES		
19. KEY WORDS (Continue on reverse side if necessary and identify by block number)		
20. ABSTRACT (Continue on reverse side if necessary and identify by block number) Investigation on solutions of rodlike poly(p.phenylene benzobisthiozole), PBT, and articulated modification of PBT and poly (p.phenylene benzobisoxazole), PBO, are reported in three parts: dilute solution characterization of PBT and articulated PBO and PBT copolymers; rheological and rheo-optical studies on concentrated solutions of PBT; and solution processing of PBT into oriented ribbons using an improved version of the Wong-apparatus. In the first section,		

UNCLASSIFIED

SECURITY CLASSIFICATION OF THIS PAGE(When Data Entered)

the effects of interchain association are studied. It is found that each of four articulated PBO copolymers studied is aggregated, even in dilute solution, and that the aggregation of a PBT sample studied depends on its solution/precipitation history. In the second section, the transient behavior leading to steady state flow, and the relaxation subsequent to cessation of flow are studied, with recommendations for solution processing. In the third section, solution processing methods to fabricate well oriented ribbons of PBT are studied, leading to a ribbon with a modulus of 600 g/denier for the specimen with highest modulus.

UNCLASSIFIED

SECURITY CLASSIFICATION OF THIS PAGE(When Data Entered)

FOREWORD

This report on the "Physical-Chemical Properties of Articulated Rodlike Polymers" was prepared in the Department of Chemistry, Carnegie-Mellon University, 4400 Fifth Avenue, Pittsburgh, Pennsylvania 15213, under Contract F33615-79-C-5034 (Project No. 24190420). It was administered under the direction of the Materials Laboratory, Air Force Wright Aeronautical Laboratories, Wright-Patterson Air Force Base, Ohio, by Dr. T. E. Helminiak.

The report covers work conducted from 1 March 1980 to 29 February 1981. It was submitted in June 1981. Authors are G. C. Berry, Principal Investigator, C. C. Lee, R. Furukawa, and S. Venkatraman.

TABLE OF CONTENTS

I.	Studies on Dilute Solutions of PBT and Articulated PBT and PBO Polymers	1
1.	Introduction	1
2.	Physical-Chemical Characterization	2
3.	Experimental	10
3.1	Materials	10
3.2	Freezing Point Depression	13
3.3	Partial Specific Volume	13
3.4	Light Scattering Apparatus	14
3.5	Light Scattering Methods	20
3.6	Fluorescence and Absorption Spectroscopy	22
4.	Results	33
4.1	Freezing Point Depression	33
4.2	Partial Specific Volume	35
4.3	Fluorescence and Absorption Spectroscopy of PBT Polymers	35
4.4	Light Scattering on PBT Polymers	38
4.4.1	Total Intensity Light Scattering	38
4.4.2	Photon Correlation Light Scattering	40
4.5	Investigation of Articulated Copolymers	42
4.5.1	Phase Equilibria	42
4.5.2	Size Exclusion Chromatography	43
4.5.3	Light Scattering Behavior	43
5.	Discussion	80
5.1	Cryoscopy and Densitometry	80
5.2	Light Scattering Behavior for PBT Polymers	82
5.3	Light Scattering Behavior for Articulated PBO Copolymers	90
5.4	Fluorescence and Absorption Spectroscopy on PBT Polymers	92
6.	Conclusions	96
II.	Rheological and Rheo-optical Studies on Solutions of PBT	98
1.	Introduction	98
2.	Relations for Rheological and Rheo-optical Analysis	99
3.	Experimental Methods	106
4.	Viscoelastic Measurements on PBT in Polyphosphoric Acid Solution	113
5.	Rheological and Rheo-optical Measurements on PBT in Methane Sulfonic Acid Solution	116
5.1	Steady-State Behavior	116
5.1.1	Viscosity and Recoverable Compliance	116
5.1.2	Flow Birefringence	118
5.2	Creep and Stress-Growth Behavior	124
5.3	Stress and Flow Birefringence Relaxation	126
III.	Solution Processing of Rodlike Polymers into Ribbons	143
1.	Introduction	143
2.	Fabrication of Ribbons by Solution Processing	144
2.1	Apparatus	144
2.2	Solutions	145
2.2.1	PBT in PPA	145
2.2.2	BBL in MSA	147
3.	Tensile Creep and Recovery	149
3.1	Apparatus	149
3.1.1	Results	149

Table of Contents (concluded)

3.1.2	Young's Modulus	150
3.1.3	Tensile Creep Compliance	153
3.1.4	Other Experiments	153
4.	X-ray Diffraction	156
4.1	Experimental Conditions	156
4.2	Results	156
5.	Conclusions	158
	References	167

LIST OF ILLUSTRATIONS

Figure		Page
1	Schematic diagram of light scattering apparatus showing the principal components discussed in the text.	27
2	The distribution $P(n, \gamma)$ determined for a polystyrene solution for several values of $\Delta\tau$. Numbers on each curve give $\log \Delta\tau/\tau_h$. The solid curves were constructed with Eqn. 35 using the experimental $n^{(2)}$ to compute $m^{-1} = n^{(2)} - 1$.	28
3	The coherence factor $f(A)$ determined for several values of the pinhole diameter D . The curve is a theoretical estimate fitted to the data by use of an arbitrary proportionality between D^2 and the coherence area A .	29
4	Example of $\log (g^{(2)}(\tau) - 1)$ versus τ for several combinations of pinhole diameter, number of $G^{(2)}(\tau)$ results averaged, and the presence or absence of a focusing lens in the incident beam. The value of $f(A)$ is entered on the diagram.	30
5	Light scattering cells used for a) total intensity scattering and b) photon correlation scattering.	31
6	Illustration of modulation effect on $g^{(2)}(\tau)$ caused by excessive heating on absorption of the incident beam; the dashed curve represents $g^{(2)}(\tau)$ for the same material obtained under conditions to suppress the heating effect.	32
7	The partial specific volume $(1 - \Delta\rho_c)\rho_s^{-1}$ versus solute concentration for PBT 72-8 in MSA, \circ , and CSA, \square ; PBT 72-7 in MSA, Δ ; and PBT model in MSA, \bullet and CSA, \blacksquare . Here MSA and CSA are methane and chlorosulfonic acids, respectively.	63
8	a) Extinction coefficient for PBT 72-7 and 72-8 in solution in methane sulfonic acid: — 72-7 and 72-8; ---; and — — — 72-7. b) $(\langle n \rangle_{FL} / \langle n \rangle_{STD})_B$ for PBT 72-7 or 72-8 for four excitation wavelengths; ---, 288; — — —, 476; — — —, 488; —, 514; — — —, 613 nm.	64
9	a) Extinction coefficient for PBO in solution in methane sulfonic acid: spectrum below 450 nm is for all PBO samples, whereas the numerals identify the PBO 160 samples for longer wavelength. b) $(\langle n \rangle_{FL} / \langle n \rangle_{STD})_B$ for PBO samples for four excitation wavelengths; ---, 288; — — —, 488; — — —, 514; and 633 nm, — — —.	65

List of Illustrations (continued)

Figure		Page
10	Example of a plot of $\log (\langle n \rangle_{FL} / \langle n \rangle_{STD})_P / (\langle n \rangle_{FL} / \langle n \rangle_{STD})_P^0$ versus path length for PBO 160-1 ($c = 1.04$ g/ml) for three wavelengths: 514, 0; 547, -0; and 686 nm, 0. Below 1 mm path length the illuminated volume of solution decreases.	66
11	Examples of plot of $\log [(\langle n \rangle_{FL} / \langle n \rangle_{STD})_P]_{\ell = \ell'} = 0$ versus c used to evaluate the quenching parameter K_q . Data are for PBO 160 series number given on the figure.	67
12	Examples of $\log R_{VV}/c$ versus h^2 for solutions of PBT 72-7, ● ($c = 0.614$ mg/ml) and 72-8, 0 ($c = 0.631$ mg/ml) in methane sulfonic acid: a) precentrifuged stock solution, diluted and filtered into light scattering cell; b) as in a), but also centrifuged in the cell after the filtration.	68
13	Examples of (c/R_{VV}) and (c/R_{HV}) versus h^2 for PBT 72-7, ● ($c = 0.364$ mg/ml) and 72-8, 0 ($c = 0.332$ mg/ml) for solutions treated by all four methods of clarification discussed in the text.	69
14	Plots of $[Kc/R_{VV}(0)]^{1/2}$ and $[Kc/R_{HV}(0)]^{1/2}$ versus c for PBT 72-7, ● and 72-8, 0 for solutions in methane sulfonic acid.	70
15	Bilogarithmic plots of $n^{(2)}(\gamma) - 1$ versus $h^2 \Delta \tau$ for PBT 72-7, ● ($c = 0.36$ mg/ml) and 72-8, 0 ($c = 0.33$ g/ml), for 45 and 90 degree scattering angle (pips up and down, respectively). The curves represent Eqn. 8 and 11.	71
16	Plots of $\ln (g^{(2)}(\tau) - 1)$ versus $h^2 \tau$ for PBT 72-7, ● ($c = 0.36$ mg/ml) and 72-8, 0 ($c = 0.33$ mg/ml), for 45 and 90 degree scattering angle (pips up and down, respectively).	72
17	Plots of $[\langle \tau_h \rangle \sin^2 \psi / 2]^{-1}$ versus c for solutions of PBT 72-8 in methane sulfonic acid.	73
18	Examples of $\ln R_{VV}$ versus h^2 for solutions of articulated PBO copolymers ($c \sim 0.5 - 0.6$ mg/ml). In each case the sample treatment is designated as filtered, ●, or filtered and centrifuged, 0: a) 292-80 in MSA, 633 nm; b) 292-96 in MSA, 514 nm; c) 352-4 in CSA, 633 nm; and d) 352-4 in MSA, 514 nm.	74
19	Examples of I_+ fluorescence spectra for solutions of articulated PBO copolymers ($c \sim 0.4 - 0.6$ mg/ml). Excitation wavelengths are 388, — —; 514, ----, or 633 nm, ——. In each case the R_{HV} scattering may be seen superposed on I_+ at the excitation wavelength, and intensities are normalized by the peak value of R_{HV} : a) 292-80 in MSA; b) 292-96 in MSA; c) 352-4 in CSA; and d) 352-4 in MSA.	75

List of Illustrations (continued)

Figure		Page
20	Example of Kc/R_{VV} versus h^2 for 292-80 in MSA; 633 nm. Symbols as in Fig. 18.	76
21	Example of Kc/R_{VV} versus h^2 for 292-96 in MSA; 514 nm. Symbols as in Fig. 18.	76
22	Example of Kc/R_{VV} versus h^2 for 352-39 in MSA; 633 nm. Symbols as in Fig. 18.	76
23	Example of Kc/R_{VV} versus h^2 for 352-4 in CSA; 633 nm. Symbols as in Fig. 18.	76
24	Example of Kc/R_{VV} versus h^2 for 352-4 in MSA; 514 nm. Symbols as in Fig. 18.	76
25	Plots of $(Kc/R(0))^{1/2}$ versus concentration for 292-80 in MSA; 633 nm: a) R_{VV} data and b) R_{HV} data. Symbols as in Fig. 18.	77
26	Plots of $(Kc/R(0))^{1/2}$ versus concentration for 352-39 in MSA; 633 nm: a) R_{VV} data and b) R_{HV} data. Symbols as in Fig. 18.	77
27	Plots of $(Kc/R_{VV}(0))^{1/2}$ versus concentration for 292-96 in MSA; 514 nm. Symbols as in Fig. 18.	78
28	Plots of $(Kc/R_{VV}(0))^{1/2}$ versus concentration for 352-4 in CSA; 633 nm. Symbols as in Fig. 18.	78
29	Plots of $(Kc/R_{VV}(0))^{1/2}$ versus concentration for 352-4 in MSA; 514 nm. Symbols as in Fig. 18.	78
30	Plots of $n^{(2)}(\Delta\tau/\tau_h)$ versus $\Delta\tau \times \sin^2 \psi/2$ for a solution of 292-80 in MSA ($c = 0.10$ mg/ml). Filled and unfilled symbols as in Fig. 18. Angles indicated as no pip, 45° ; pip down, 60° ; pip up, 75° ; pip right, 90° ; and pip left, 105° .	79
31	η' , J' and J'' versus frequency ω for a solution of PBT in PPA (10% polymer by weight). The data are for temperature of 28°C (no pips); 89°C (pips left); 102°C (pips up); and 145°C (pips right).	114
32	Creep — and recoverable — compliance for a solution of PBT in PPA (10% polymer by weight), temperature 91.5°C .	115
33	Phase diagram for PBT 53 in methane sulfonic acid, 0, and MSA plus 3% chlorosulfonic acid, 8.	130
34	Plot of η_∞/η_0 and R_∞/R_0 for an isotropic (2.55 wt %) solution of PBT.	131

List of Illustrations (continued)

Figures		Page
35	Plot of η_{κ}/η_0 and R_{κ}/R_0 for a solution that undergoes a transition in the range $10^{\circ} < T < 60^{\circ}\text{C}$ (3.23 wt %).	132
36	Plot of η_{κ}/η_0 and R_{κ}/R_0 for a nematic solution (4.27%).	133
37	The birefringence versus a reduced square shear rate (see text) for solution of PBT in MSA at the indicated temperature (2.55 wt %).	134
38	Rheological time constant τ_N (Eqn. 93) versus the characteristic time (Eqn. 94) for solution of PBT in methane sulfonic acid.	135
39	Creep compliance plotted against t/τ_c for various stress levels for an isotropic solution (2.55% at 300°C).	136
40	Creep compliance curves plotted against t/τ_c for various stress levels, for the 3.23% solution at 198°C (nematic). Also shown is the transient recovery curve for a particular stress level.	137
41	Stress growth curves plotted against t/τ_c for the 4.27% solution of PBT-53 in MSA at 10.5°C (nematic).	138
42	Inverse of the critical strains γ_m and γ^* as a function of concentration for solutions of PBT-53 in MSA.	139
43	Plot of the parameter κt_c from stress-growth measurements against κ for the three different concentrations.	140
44	The time t_m to reach a maximum stress in stress growth as as function of shear rate for solutions of PBT-53 in MSA.	141
45	A typical birefringence relaxation curve, showing the resolution into two exponentials.	142
46	Ribbon fabrication apparatus	159
47	Schematic drawing of tensile creep apparatus.	160
48	Creep and recovery for several ribbons prepared with 9.2 weight percent PBT solution: a) 9-540 C, b) 9-540 U, c) 9-733 U, d) 9-1000 U. Series U are prior to removal of PPA solvent, and series C are after removal of PPA.	161
49	Creep and recovery for several ribbons prepared with 10 weight percent PBT; all prior to removal of PPA solvent: a) 10-280 U, b) 10-150 U, c) 10-200 U, d) 10-100 U.	162
50	Creep and recovery for several ribbons prepared with 10 weight percent PBT; all after removal of PPA solvent: a) 10-100 C, b) 10-130 C, c) 10-200 C, d) 10-200 C.	163

List of Illustrations (concluded)

Figures		Page
51	Creep and recovery for PBT ribbons given post formation creep treatment prior to removal of PPA solvent. Data are for ribbons after removal of PPA: a) 10-130*, b) 9-540*.	164
52	X-ray diffraction from ribbon PBT 3-100 U. Specimen 6 cm from film.	165
53	X-ray diffraction from ribbon PBT 10-100 U; a) before creep; b) after creep and recovery. Specimen 6 cm from film with ribbon axis vertical and x-ray became perpendicular to the plane of the ribbon. Major equatorial reflections are at 3.45 and 5.17 Å.	165
54	X-ray diffraction from ribbon PBT 10-200 U after creep and recovery. Conditions are as specified in Fig. 53 caption.	166
55	X-ray diffraction from ribbon PBT 9-540* after creep and recovery. Conditions are as specified in Fig. 53 caption.	166

LIST OF TABLES

Table		Page
1	Rodlike polymers used in this study.	25
2	Articulated PBT and PBO copolymers investigated.	26
3	Degree of protonation from the freezing point depression in 100 percent sulfuric acid.	47
4	Partial specific volume of PBT, PBO and model compounds.	48
5	Absorption and fluorescence parameters for PBT .	49
6	Absorption and fluorescence parameters for PBO.	50
7	Total intensity light scattering parameters for PBT.	51
8	Photon correlation light scattering data for two PBT polymers at two positions in light scattering cell.	52
9	Photon correlation light scattering data for two PBT polymers.	53
10	Phase equilibria data for solutions in methane sulfonic acid.	54
11	Total intensity light scattering parameters for articulated PBO polymers.	55
12	Photon correlation light scattering data for two articulated PBO polymers at two positions in light scattering cell.	56
13a	Photon correlation light scattering data for articulated PBO polymer 292-80.	57
13b	Photon correlation light scattering data for articulated PBO polymer 292-96.	58
13c	Photon correlation light scattering data for articulated PBO polymer 352-4.	59
14a	Photon correlation light scattering data for articulated PBO polymer 292-80.	60
14b	Photon correlation light scattering data for articulated PBO polymer 292-96.	61
14c	Photon correlation light scattering data for articulated PBO polymer 352-4.	62
15	Apparent contour lengths for two PBT polymers.	95

List of Tables (concluded)

Table		Page
16	Rheological data for PBT-53 in methane sulfonic acid.	119
17	Relaxation time constants observed for a PBT-53 solution.	129
18	Uncoagulated ribbons.	146
19	Ribbons coagulated in water.	146
20	Conditions for ribbon formation.	148
21	Properties of PBT ribbons.	152
22	Creep and recovery data.	154

1. INTRODUCTION

Molecular properties and the effects of intermolecular association have been investigated for rodlike PBT polymers and articulated PBT and PBO polymers. Methods based on the use of the polarized components of the total intensity light scattering described in previous work ¹⁻⁴ have been utilized along with additional methods involving photon (auto-)correlation light scattering. Some results on intermolecular quenching of fluorescence emission, measurements of the partial specific volume, and the freezing point depression will also be given. The latter reflects directly the protonation of the heterocyclic polymers in the strong sulfonic acids used as solvents.

This section of the report is separated into several sections including i) a compilation of equations used to analyze the total integrated and photon correlation light scattering data; ii) a description of the experimental methods, with emphasis on the computer-based light scattering apparatus used; iii) results of the physical-chemical studies on PBT and the articulated PBT and PBO polymers; and iv) discussion of the results. The principal conclusions are that PBT is a rodlike chain, susceptible to formation of metastable aggregates that depend on the dissolution-precipitation history of the polymer, and that the articulated PBT and PBO polymers studied do not have rodlike conformations in dilute solution, and also are susceptible to the formation of rodlike aggregates.

2. PHYSICAL-CHEMICAL CHARACTERIZATION

Characterization of a rodlike polymer and its model compound by studies of the partial specific volume \bar{v} and freezing point depression will permit assessment of the extent of the protonation of the solute that leads to formation of the macroion and elucidate some of the effects of this protonation on intermolecular interactions. Evaluation of the extent of protonation from the freezing-point depression $\Delta\theta$ requires interpretation of $\Delta\theta$ by the relation ⁵

$$\Delta\theta/K_f = \sum_i m_i + \sum_{ij} m_i m_j B_{ij} + \dots \quad (1)$$

where K_f is a constant, the m_i are the molalities of all species formed on addition of the solute, and the B_{ij} are interaction coefficients.

Since the m_i include the conjugate ions formed on protonation of polymer P by acid RSO_3H :



the extent of protonation ν can be deduced. The coefficients B_{ij} are dominated by electrostatic interactions among the small ions ^{6,7}. These may also influence \bar{v} . For example, values of the excess volume ΔV^E are sometimes negative and large for systems with electrostatic interactions. Here, ΔV^E is defined by the relation

$$V = V_1 + V_2 + \Delta V^E$$

for additivity of volumes V_1 and V_2 of solvent and solute to give the volume V of the solution. If ΔV^E is zero, \bar{v} is equal to the specific volume v of the solute.

In previous studies,¹⁻³ the vertical and horizontal components R_{Vv} and R_{Hv} of the Rayleigh ratio, respectively, of the light scattered with vertically polarized incident light have been determined and analyzed with the expressions

$$\left(\frac{Kc}{R_{Vv}}\right)^{1/2} = \left[\left(\frac{Kc}{R_{Vv}}\right)^0\right]^{1/2} \left\{1 + \frac{A_2^M}{(1 + \frac{4}{5}\delta^2)} c + \dots\right\} \quad (2a)$$

$$\left(\frac{R_{Vv}}{KcM}\right)^0 = (1 + \frac{4}{5}\delta^2) - \frac{1}{3} [1 - \frac{4}{5}f_1\delta + \frac{4}{7}(f_2\delta)^2]u + \dots \quad (2b)$$

$$\frac{Kc}{R_{Hv}} \simeq \left(\frac{Kc}{R_{Hv}}\right)^0 + o(c) \quad (3a)$$

$$\left(\frac{R_{Hv}}{KcM}\right)^0 = \frac{3}{5}\delta^2 - \frac{9}{35}(f_3\delta)^2 u + \dots \quad (3b)$$

where c is the polymer concentration, A_2 is the light scattering second virial efficient, K is an optical constant, u is $(R_G h)^2$, with R_G the root-mean-square radius of gyration, $h = (4\pi n/\lambda_0) \sin \theta/2$, and the functions f_i and the molecular anisotropy δ depend on the ratio ρ/L of the

persistence length ρ and the contour length L . The latter is M/M_L , where M_L is the mass per unit length along the chain contour. Here, as elsewhere, the superscript 0 denotes a quantity extrapolated to infinite dilution. The mean-square radius of gyration may be obtained from

$$R_G^2 = [7/3 f_3^2 (c/R_{Hv}(0))^0] (\partial(c/R_{Hv})/\partial h^2)^0 \quad (4)$$

without knowledge of δ (if $\delta \neq 0$ and $f_3 \sim 1$), and from

$$R_G^2 = [3/(c/R_{Vv}(0))^0] J(\delta) (\partial(c/R_{Vv})/\partial h^2)^0 \quad (5a)$$

$$J(\delta) = [1 + \frac{4}{5} \delta^2] / [1 - \frac{4}{5} f_1 \delta + \frac{4}{7} (f_2 \delta)^2] \quad (5b)$$

For rodlike molecules ($L/\rho = 0$), L is the length of the rod, and all f_i are unity.²

Previous work has revealed that self-association of rodlike chains in dilute solution has far more effect on R_{Vv} than on R_{Hv} .¹⁻³ For example, frequently R_{Hv} is little affected by centrifugation treatments that result in substantial change of R_{Vv} and $\partial Kc/R_{Vv}/\partial h^2$. One consequence of this is that the apparent value of δ determined from the ratio $(c/R_{Vv}(0))^0/(c/R_{Hv}(0))^0$ can be seriously affected by association, see below.

Photon-correlation light scattering offers a means to further characterize the chain, and any intermolecular association through the coherence time τ_h for the relaxation of fluctuations of the polarizability of scattering volume elements. The intensity (auto-) correlation

$g^{(2)}(\tau)$ and the factorial moments $n^{(r)}$ are accessible statistical properties of the scattered light that provide measures of τ_h .⁸

Here,

$$g^{(2)}(\tau) = \langle n_0 n_\tau \rangle / \langle n \rangle^2 \quad (6)$$

for $\tau > 0$, and

$$n^{(r)} = \langle n(n-1) \cdots (n-r+1) \rangle / \langle n \rangle^r \quad (7)$$

where n is the number of photons scattered in a time interval $\Delta\tau$, $\langle n \rangle$ is the average value of n , and subscripts 0 and τ indicate the values of n for intervals separated by time τ . For dilute solutions, the experimental quantities $g^{(2)}(\tau)$ and $n^{(r)}$ can be related to τ_h . For a monodisperse solute:⁸

$$n^{(2)}(\gamma) - 1 = f(A)h(2\gamma) \quad (8)$$

$$g^{(2)}(\tau, \gamma) - 1 = f(A)q(2\gamma) |g^{(1)}(\tau/\tau_h)|^2 \quad (9)$$

Here $\gamma = \Delta\tau/\tau_h$, $f(A)$ is a coherence factor fixed by the detector optics, and

$$q(2\gamma) = \left(\frac{\sinh \gamma}{\gamma} \right)^2 \quad (10)$$

$$h(\gamma) = \frac{2}{\gamma} - \frac{2}{\gamma^2} (1 - e^{-\gamma}) \quad (11)$$

For the usual case of an optically isotropic polymer studied in dilute solutions under conditions with $R_G h < 1$, the amplitude correlation function $|g^{(1)}(\tau)|$ is given by

$$|g^{(1)}(\tau/\tau_h)| = \exp(-\tau/\tau_h) \quad (12)$$

where the mutual diffusion coefficient $D_m = (\tau_h h^2)^{-1}$ is expected to be independent of h ; Eqn. (12) has been used to obtain Eqns. 10 and 11.

Following the usual practice, τ_h is obtained from Eqn. (9) by calculation of the first cumulant K_1 , for which (with Eqn. 12):

$$K_1 h^{-2} = -\frac{h^{-2}}{2} \lim_{\tau \rightarrow 0} \frac{\partial \ln(g^{(2)}(\tau)-1)}{\partial \tau} = (\tau_h h^2)^{-1} \quad (13)$$

is expected to be independent of h unless $R_G h$ is greater than about 1.⁹ Evaluation of τ_h from Eqn. (8) can be accomplished by use of a bilogarithmic plot of $\log[n^{(2)}(\gamma)-1]$ versus $\log \Delta\tau h^2$ to determine the value $\Delta\tau^*$ of the sample interval for which the crossover of Eqn. (11) from its limiting value $f(A)$ for small $\Delta\tau$ to its asymptotic form $f(A)/\Delta\tau$ for large $\Delta\tau$ to give $\tau_h = \Delta\tau^*$.

For heterodisperse solute these relations are more complex. For example, at low concentrations,

$$n^{(2)}(\langle\gamma\rangle)-1 = f(A) \sum_i \sum_j r_i r_j h [(\gamma_i + \gamma_j)] \quad (14)$$

with $\gamma_i = \Delta\tau/(\tau_h)_i$, and the r_i representing the fraction of light scattered by solute with coherence time $(\tau_h)_i$. The sums run over all components, with $\sum r_i = 1$. Similarly,

$$g^{(2)}(\tau) - 1 = f(A) \sum_i \sum_j r_i r_j q(\gamma_i + \gamma_j) |g^{(1)}(\tau)|_i |g^{(1)}(\tau)|_j \quad (15)$$

with $|g^{(1)}(\tau)|_i = \exp[-\tau/(\tau_h)_i]$. Analysis of these relations will result in average values of the τ_h . For example, use of the first cumulant leads to the result

$$\langle \tau_h \rangle_{g^{(2)}} = 2 \left\{ \sum_i \sum_j r_i r_j \left[\frac{1}{\tau_{h,i}} + \frac{1}{\tau_{h,j}} \right] \right\}^{-1} \quad (16)$$

whereas use of $\Delta\tau^*$ gives

$$\langle \tau_h \rangle_n(2) = 2 \sum_i \sum_j r_i r_j \frac{\tau_{h,i} \tau_{h,j}}{\tau_{h,i} + \tau_{h,j}} \quad (17)$$

(In Eqn. (16) it is assumed that $q(\gamma/2) = q(\gamma) = 1$, which is the usual condition used to study $g^{(2)}(\tau)$).

An associated species may have τ_h much larger than that for the dissociated components. In the extreme, with only two such components having a wide disparity between values of τ_h , Eqn. (14) and (15) reduce to the results for the scattering from a solute mixed with light from a local oscillator, which gives

$$n^{(2)}(\gamma)-1 = f(A)\{2r(1-r)h(\gamma)+r^2h(2\gamma)\} \quad (18)$$

$$g^{(2)}(\tau, \gamma)-1 = f(A)\{2r(1-r)q(\gamma/2)|g^{(1)}(\tau)| + r^2 q(\gamma) |g^{(1)}(\tau)|^2\} \quad (19)$$

where $1-r$ is the fraction of light from the local oscillator. (Equations 18 and 19 may be obtained from Eqn. 14 and 15 for the special case of two components, with $\gamma = 0$ for one component). The presence of a local oscillator may not be readily apparent for data on $n^{(2)}(\gamma)$ and $g^{(2)}(\tau, \gamma)$ determined at fixed h , unless $f(A)$ is known for the instrument. For example, the composite function for $n^{(2)}(\gamma)-1$ has nearly the same form on a bilogarithmic plot as $h(\gamma)$, so that the principal effect of the local oscillator is to increase $\Delta\tau^*$, such that τ_h is given by

$$\tau_h = \frac{2-r}{4-3r} \Delta\tau^* \quad (20)$$

and to decrease the limiting value of $n^{(2)}(\gamma)-1$ at small γ from $f(A)$ to $r(2-r)f(A)$. Similarly, the first cumulant is decreased, with τ_h given by

$$\tau_h = 1/(2-r)K_1 \quad (21)$$

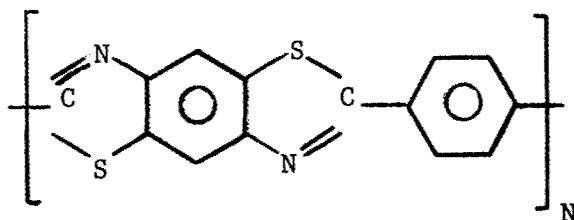
and $g^{(2)}(0)-1$ is decreased by the factor $r(2-r)$. If r is small, the estimates of τ_h based on $\Delta\tau^*$ and K_1 would be the same, so that only

the apparent decrease of $f(A)$ would indicate the presence of the local oscillator for the data at fixed h . Because the scattering from large particles is most intense at small angles, r would be expected to increase with h , so that evaluation of K_1 and $\Delta\tau^*$ as a function of h is another means to detect the local oscillator, if it is known that hR_G is small enough so that $h^2 K_1$ and $h^2 \Delta\tau^*$ should be independent of h .

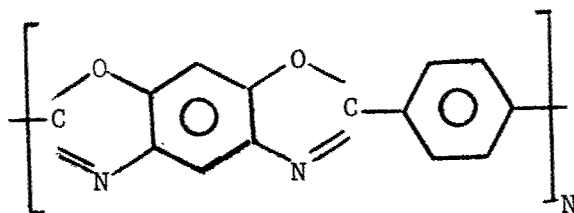
3. EXPERIMENTAL

3.1 Materials

Rodlike polymers used in this study include poly(1,4-phenylene-2,6-benzobisthiazole), PBT:

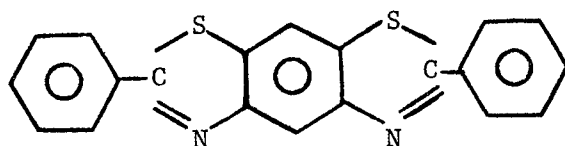


poly(1,4-phenylene-2,6-benzobisoxazole), PBO:

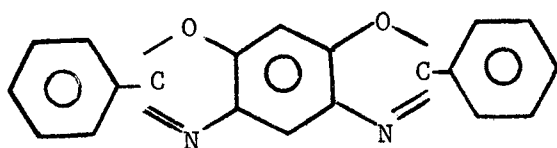


and poly(1,4-phenylene terephthalamide), PPTA. Polymer identifications and values of $[\eta]$ for solutions in methane sulfonic acid are listed in Table 1. Sources include SRI International (J.F. Wolfe), PBT 31, 43, 72-7 and 72-8; the Air Force Materials Laboratory, Polymer Branch (F.E. Arnold), PBO 2 and 6; our laboratory (D. B. Cotts), PBO 160/1, 3, 4, 5 and 8; and Centre de'Recherches sur les Macromolecules, Strasbourg (C. Strazielle), PPTA 2. The PBO 160 series were prepared in a study of the kinetics of the polymerization reaction.¹⁰ Methods used to prepare the other PBO and PBT polymers are described elsewhere.¹¹⁻¹² Characterization of the PPTA polymer used will be described elsewhere.¹³

The model compounds with structures



PBT Model



PBO Model

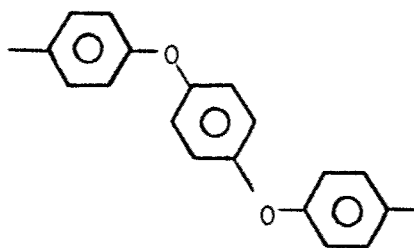
were received from Air Force Materials Laboratory (F.E. Arnold).

Crystallographic studies show these to be nearly planar in the crystal with lengths 1.710 and 1.655 nm for the PBT and PBO models, respectively.¹⁴

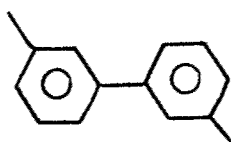
The two samples of PBT 72 differ only in the post-polymerization processing. Aliquots from a polymerization carried out in polyphosphoric acid, PPA, were given different treatments in recovering the dry polymer. With PBT 72-8 the polymer was precipitated in water directly from PPA, extensively washed and then dried under vacuum. With PBT 72-7, the PPA solution was diluted with methane sulfonic acid, precipitated in water, extensively washed and then dried under vacuum.

Articulated PBT and PBO copolymers were received from Air Force Materials Laboratory (R. Evers). These were prepared by copolymerization of the usual PBO or PBT monomers with one of four dicarboxylic acids that resulted in structures with a fraction n of the phenylene moieties of PBO or PBT by one of the aromatics following moieties as shown in Table 2.

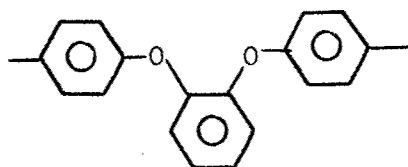
I



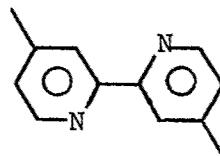
II



III



IV



Solvents were distilled under reduced nitrogen pressure, and stored under nitrogen prior to use.

3.2 Freezing Point Depression

Melting temperatures T_m were determined by methods described in detail elsewhere.⁷ Fresh 100 percent sulfuric acid was prepared by the method given previously. The relatively high viscosity of the polymer solutions required care to avoid breakage of the helical glass stirrer used in the cryostat. Melting temperatures determined from heating curves were recorded to 0.001°C using a platinum resistance thermometer with 0.0001°C accuracy.

3.3 Partial Specific Volume

Densities were determined with a Sodev Densimeter (Model 02D) equipped with a stainless steel hollow vibrating fork. The vibration period P of the fork filled with the test fluid was determined to within $\pm 50 \mu\text{s}$. The difference ΔP between the periods measured for two fluids is proportional to the difference $\Delta \rho$ of their densities:¹⁵

$$\Delta \rho = 2K\bar{P} \Delta P \quad (22)$$

where K is a calibration constant ($4.89 \times 10^{-7} \text{ g/ml}(\mu\text{s})^2$) and \bar{P} is the average period. The partial specific volume \bar{v} is calculated from the variation of $\Delta \rho/c$ with concentration, with one of the fluids being the solvent with density ρ_s :

$$\frac{\Delta \rho}{c} = \frac{\rho - \rho_s}{c} = \left(\frac{\partial \rho}{\partial c} \right)^0 + \frac{1}{2} \left(\frac{\partial^2 \rho}{\partial c^2} \right)^0 c + \dots \quad (23)$$

Since

$$\frac{\Delta \rho}{c} \sim \left(\frac{\partial \rho}{\partial c} \right)_{n_1} = \frac{1 - \rho \bar{v}}{1 - c \bar{v}} \quad (24)$$

(where n_1 is the number of solvent molecules)

the data give \bar{v}^0 by extrapolation to infinite dilution:

$$\bar{v} = \left(1 - \frac{\Delta \rho}{c} \right) \rho_s^{-1} = \bar{v}^0 + \frac{1}{2} \left(\frac{\partial \bar{v}}{\partial c} \right)^0 c + \dots \quad (25)$$

3.4 Light Scattering Apparatus

The light scattering apparatus is shown schematically in Fig. 1. It is equipped with a data acquisition and processing system, DAPS, by Science Research Systems of Troy (Model DAS 6). Other components include an argon-ion laser with etalon (Lexel Model 85), a He-Ne laser (Spectra-Physics Model 120), a photomultiplier with an S-2 photocathode (ITT, FW-130-RF), a photomultiplier housing (Products for Research, Inc.) and a discriminator amplifier (SSR Instruments Co.). Optical components allow for beam alignment, rotation of the polarization plane of the incident beam (one-half wave plate), beam spreading for total intensity measurements, transfer of an auxillary light beam to the photomultiplier with an optical fiber (Oriel Corp., Model 7167), definition of the scattering volume by slits S_H and S_V , collimation of the accepted rays by pinhole P, selection of the wavelength of the light impinging on the photomultiplier by use of interference filters for fixed or variable bandpass, e.g., Oriel Corp., Model 7155, or fixed band rejection (to

eliminate light with wavelength of the incident beam), and an analyzer to select the polarization of the scattered beam.

In the mode used here, the DAPS, which is based on a Texas Instruments 980B computer, acquires pulses in each of $4,736$ intervals of length $\Delta\tau$, with a deadtime of 25 ns included in each interval; the number of pulses per interval can be large as 2^{15} . The full auto-correlation function $G^{(2)}$ is computed over the primary data base of 2^{12} intervals to give a correlation with up to 512 points spaced at intervals of $\Delta\tau$. Usually, a 16 point correlation was used in this work. After each acquisition cycle, the unnormalized correlation $G^{(2)}(k\Delta\tau)$ and the mean count rate are calculated as

$$G^{(2)}(k\Delta\tau) = \frac{1}{T} \sum_i^T n_i n_{i+k} \quad (26)$$

$$\langle n \rangle = \left(\frac{1}{T} \sum_{i=1}^T n_i \right) \quad (27)$$

where $k = 0, 1, 2, \dots$ and $T=2^{12}$. The acquisition and calculation cycle is repeated M times, and averaged in the form

$$G_M^{(2)}(k\Delta\tau) = \frac{1}{M} \sum_{j=1}^M G_j^{(2)}(k\Delta\tau) \quad (28)$$

$$\langle \langle n \rangle^2 \rangle_M = \frac{1}{M} \sum_{j=1}^M \langle n \rangle_j^2 \quad (29)$$

and the unnormalized factorial moments are calculated over the data base of TM intervals as

$$N^{(r)} = \frac{1}{TM} \sum_{i=1}^{TM} \{n(n-1) \cdots (n-r+1)\}_i \quad (30)$$

$$N^{(1)} = \langle n \rangle \quad (31)$$

The distribution $P(n, \gamma)$ of photon pulses per interval is also computed over the data base of TM intervals. If $P(n, \gamma)$ is the same for each of the M data sets, then $\langle \langle n \rangle^2 \rangle_M$ and $\langle n \rangle^2$ are equal. If the $P(n, \gamma)$ differ (e.g., because of scattering from 'dust' in a few of the M sets), then $\langle \langle n \rangle^2 \rangle_M \geq \langle n \rangle^2$.

Further data processing includes calculation of $g^{(2)}(\tau)$ and $n^{(r)}$. For the former $\langle \langle n \rangle^2 \rangle_M$ is used to give

$$g^{(2)}(k\Delta\tau) = G_M^{(2)}(k\Delta\tau) / \langle \langle n \rangle^2 \rangle_M ; k > 0 \quad (32)$$

$$g^{(2)}(0) = \frac{G_M^{(2)}(0) - \langle n \rangle}{\langle \langle n \rangle^2 \rangle_M} \quad (33)$$

It may be remarked that the use of $\langle \langle n \rangle^2 \rangle_M$ rather than $\langle n \rangle^2$ or $G_M^{(2)}(\infty)$ to normalize $G^{(2)}(\tau)$ is not trivial for realistic data, owing to the effects of noise and drift, etc.⁸ Values of $g^{(2)}(\tau)$ calculated with Eqn. (32) exhibit the expected property that $g^{(2)}(\infty)$ tends to unity, even under conditions for which $\langle \langle n \rangle^2 \rangle_M > \langle n \rangle^2$. An estimate for K_1 is calculated by least-squares fit of $\ln(g^{(2)}(\tau)-1)$ versus τ , using the correlation points for k from 1 to 7. With the algorithm in use in the DAPS, the time Δt per correlation point required to compute

$G^{(2)}(k\Delta\tau)$ is fixed (80 ms) for $\langle n \rangle$ larger than 2, but decreases with decreasing $\langle n \rangle$ for smaller $\langle n \rangle$. Consequently, the efficiency $(1 + C \Delta t / 2^{1/2} \Delta\tau)^{-1}$ varies with $\Delta\tau$, $\langle n \rangle$ and the number C of correlation points calculated, but generally ranges from 0.2 to nearly unity, with values being about 0.8 or greater for typical experiments.

The factorial moments are calculated as

$$n^{(r)} = N^{(r)} / (N^{(1)})^r \quad (34)$$

Usually, $P(n, \gamma)$ is closely given by the approximate two-parameter function:¹⁶

$$P(n, \gamma) = \frac{\Gamma(n+m)}{n! \Gamma(m)} \left(1 + \frac{\langle n \rangle}{m}\right)^{-m} \left(1 + \frac{m}{\langle n \rangle}\right)^{-n} \quad (35)$$

so that

$$n^{(r)} = \frac{m(m+1) \cdots (m+r-1)}{m^r} \quad (36)$$

Examples of comparison of Eqn. (35) with experimental $P(n, \gamma)$ are given in Fig. 2 for several values of $\Delta\tau/\tau_h$. Distortion of $P(n, \gamma)$ by excessive scattering during a few of the sampling intervals can result in values of $n^{(5)}$ far larger than the estimate given by Eqn. (36) with m calculated from $n^{(2)}$, providing a test for the internal consistency of the data. Another test is provided by comparison of $g^{(2)}(0)$ with $n^{(2)}(0)$. These should be equal, but may differ if $P(n, \gamma)$ varies substantially among the M data sets.

The function $f(A)$ is fixed by the detector optics. In the optical system used in this study, $f(A)$ is principally determined by the pinhole P, and is less dependent on slits S_H and S_V . Pinholes from 100 to 1000 μm diameter are used in this study. Typical data for $f(A)$ as a function of the pinhole diameter are given in Fig. 3, along with a theoretical estimate for $f(A)$.⁸

In most of the photon correlation studies reported here, conditions were selected to give $f(A)$ in the range 0.1 - 0.3. If $f(A)$ is much larger, then $\langle n \rangle$ tends to be so small that the time required to acquire sufficient total counts $TM\langle n \rangle$ for acceptable error limits on τ_h is excessive. If $f(A)$ is much smaller, then the precision of the experiment suffers. Theoretical treatment of this problem predicts that such an optimum condition should obtain.⁸ An illustration of the interplay of $f(A)$ and $TM\langle n \rangle$ is given in Fig. 4. In this case, $f(A)$ was varied by variation of the pinhole, and by presence or absence of a lens to focus the incident beam in the scattering cell.

Finally, although not used in this study, we note that the optical fiber may be used to provide light to serve as a local oscillator to mix with the scattered beam to force compliance with Eqns. (18) and (19) (or the equivalents for heterodispersed solutes).

In total intensity experiments, the count rate $\langle n \rangle_s$ of the scattered light is determined with the use of a rotary chopper to modulate the incident intensity, and the DAPS to determine and analyze $G^{(2)}(\tau)$. This permits elimination of the count rate $\langle n \rangle_D$ due to

thermionic emission in the photomultiplier, room light, stray electrical noise, etc., and, in one mode, provides a comparison to the count rate $\langle n \rangle_R$ proportional to the intensity of the incident light. The chopper is comprised of two disks mounted coaxially on the shaft of a 200 RPM geared synchronous motor (300 ms period). The disks are slotted such that in one orientation of the two disks, there are five openings and five shutters of equal length, producing a train of pulses with $(\langle n \rangle_S + \langle n \rangle_D)\tau_S$ counts for duration $\tau_S = 30$ ms alternating with $\langle n \rangle_D\tau_D$ average counts for duration $\tau_D = 30$ ms (e.g., simple on-off chopping at 1000 Hz). In a second orientation, the pulse train is altered to be $(\langle n \rangle_S + \langle n \rangle_D)\tau_S$ for $\tau_S = 95$ ms; $\langle n \rangle_D\tau_D$ for $\tau_D = 95$ ms; $(\langle n \rangle_R + \langle n \rangle_D)\tau_R$ for $\tau_R = 15$ ms and $\langle n \rangle_D\tau_D$ for $\tau_D = 95$ ms, with repetition every $\tau_S + 2\tau_D + \tau_R = 300$ ms. A mirror attached to the disk supplies $\langle n \rangle_R$ by reflecting the incident beam onto an optical fiber (after the beam passes through neutral density filters). As noted above, the optical fiber directs the beam onto the photomultiplier through the detector optics (see Fig. 1). In the first mode, $G^{(2)}(\tau)$ is a triangular function with period $2\tau_S$ and peak-to-peak amplitude $\langle n \rangle_S^2/2$. The slope $\partial G^{(2)}(\tau)/\partial \tau = \langle n \rangle_S^2/2\tau_S$ determined in the range $2.5\tau_S < \tau < 3\tau_S$ is used to compute $\langle n \rangle_S$. In the second mode the values s_1 and s_2 of $\partial G^{(2)}(\tau)/\partial \tau$ determined, respectively, over the range $\tau < \tau_R$ and $\tau_R < \tau < \tau_S$ are used to calculate $\langle n \rangle_S/\langle n \rangle_R = [s_2/(s_1 - s_2)]^{1/2}$. Both of these methods eliminate extraneous photon counts $(\langle n \rangle_D)$, and the latter provide a comparison of the scattered and incident light intensities every 300 ms.

3.5 Light Scattering Methods

The two types of light scattering cells used in this study are illustrated in Fig. 5. Each can be sealed under vacuum or closed with a teflon cap, and centrifuged while suspended by flotation in a centrifuge tube in a swinging-bucket rotor. The larger cell (ca 5 ml) is used for total intensity experiments to permit the use of an incident beam with rectangular cross-section (3 x 1 mm). This permits the use of detector optics to limit the height of the scattered volume accepted to less than the illuminated height to facilitate instrument calibration. The smaller cell (ca 0.8 ml) is used for photon correlation experiments. The small diameter of the cell suppresses convection along the cell axis. This permits selective scattering experiments along the cell axis following centrifugation to determine whether fractionation of the solute occurred during centrifugation, see below. In this study, solutions were filtered into the light scattering cells, which were then sealed under vacuum.

The cells are immersed in a fluid with refractive index close (± 0.02) to that of the scattering fluid. The immersion fluid is held in a cylindrical cell with flat entrance and exit windows (Brice-Phoenix, cylindrical light scattering cell) using teflon rings at the top and bottom of the light scattering cell to position it. The teflon rings and light scattering cell may be translated along the axis of the cylindrical cell to permit measurements of the scattering from different positions as described above. The cylindrical cell is held in a concentric cylinder thermostat, with incident and scattered rays passing through small (6 mm dia) ports.

Calibration methods, corrections for absorption and fluorescence, scattering volume, etc. have been described previously.³ In these experiments, the scattering from a solution of polystyrene in butanone served as a secondary standard. In addition, the scattering from the polystyrene solution was used to align the analyzer in the R_{Hv} mode (by adjustment to give minimum scattering at 90 degree scattering angle).

As discussed above, estimators for $g^{(2)}(\tau, \gamma)$ and $n^{(r)}(\gamma)$, $r = 1-5$, are calculated for each data set as a function of scattering angle θ , usually over the range 30-135 deg. In most cases, the number M of post-autocorrelation averages was adjusted so that the total number of counts $TM\langle n \rangle$ was about 10^6 to calculate $g^{(2)}(\tau, \gamma)$, and 10^5 to calculate $n^{(r)}(\gamma)$. The DAPS provides for automatic scan through θ and $\Delta\tau$ ranges to facilitate these measurements.

Since $g^{(2)}(\tau, \gamma)$ should be unity for all τ in the range used here for fluorescence measurement of $g^{(2)}(\tau, \gamma)$ for fluorescence (e.g., from the polymer solutions under study) provided a convenient means to verify that the incident beam was free of modulation. In one case, this test revealed modulation at about 1500 Hz found to be related to residue in the water lines of the heat exchange for the laser head; this preceded failure caused by leakage of water into the plasma tube. Otherwise, the test showed $g^{(2)}(\tau)$ to be unity within ± 0.004 .

Since solutions of PBT absorb light at the wavelength used in photon correlation studies, it was necessary to demonstrate that this absorption did not affect the estimate of τ_h . In order to

investigate this, $g^{(2)}(\tau)$ was determined for a polystyrene solution in butanone, and for the same solution with an amount of dye (violet red) added to bring the optical density to a level typical of PBT solutions. The incident beam was not focused in the cell, and detector optics were adjusted to give $f(A)$ about 0.2. The estimate for $K_1 h^2$, which was independent of h , was not affected by the dye. If the beam was focused in the cell, then the transmitted incident beam was diffracted into a series of concentric rings with diameter that increased linearly with the incident beam intensity. With more strongly absorbant solutions, these rings can also appear with the unfocused incident beam. Under severe conditions, $g^{(2)}(\tau)$ is distorted by a periodic modulation with a frequency that increases with increasing incident light intensity, see, for example, Fig. 6. These effects, which are attributed to thermal gradient with nearly cylindrical symmetry about the incident beam direction,¹⁷ were avoided in the data reported herein.

3.6 Fluorescence And Absorption Spectroscopy

The fluorescence emission was determined at 90 degree scattering angle using the laser as the incident source, and a square cell (10 x 10. mm) for the solution. The cell was mounted on a stage to permit its translation along the directions of the incident and scattered beams. For this geometry, the ratio of the count rate $\langle n \rangle_{F1}$ for the fluorescent emission to the count rate $\langle n \rangle_{STD}$ for a standard material is

$$(\langle n \rangle_{F1} / \langle n \rangle_{STD})_P = \mu_{\lambda} c K^0 Q(c) \exp[-(\mu_{\lambda} l + \mu_{\lambda'} l') c] S(\mu_{\lambda} c \Delta l) S(\mu_{\lambda'} c \Delta l') \quad (37a)$$

$$S(x) = \frac{\sinh(x/2)}{(x/2)} \quad (37b)$$

where μ_{λ} and $\mu_{\lambda'}$ are the extinction coefficients at the wavelengths λ and λ' of the incident and emitted light, with path lengths l and l' respectively, measured from the center of the scattering volume, Δl is the length of the incident beam accepted by the detector, $\Delta l'$ is the width of the incident beam, K_0 is the quantum efficiency of the fluorescence at infinite dilution (in relative units), and $Q(c)$ accounts for concentration dependent quenching. Use of the translation stage permits evaluation of μ_{λ} and $\mu_{\lambda'}$ by study of $\langle n \rangle_{F1} / \langle n \rangle_{STD}$ as a function of l and l' , and allows extrapolation to the condition $l = l' = 0$ for evaluation of $Q(c)$ and K^0 . For the conditions of interest here, $\mu_{\lambda} c \Delta l / 2$ and $\mu_{\lambda'} c \Delta l' / 2$ are small enough to permit the factors S to be replaced by unity.

The right-angle geometry described above was used for excitation wavelengths such that $\mu_{\lambda} c$ was less than about 0.5 (mm)^{-1} (with a 10 mm cell). Fluorescence measurements were also made with excitation wavelengths such that $\mu_{\lambda} c$ was of order 10^2 (mm)^{-1} . In this case, the incident beam was at an angle of 0-20 degs with the front face of the cell, and the fluorescence emitted back toward the incident beam was detected, such that the acute angle α between the inward incident beam and outward emitted beam was about 20 deg. If α is

zero, then

$$\left(\frac{\langle n \rangle_{F1}}{\langle n \rangle_{STD}}\right)_B = \frac{\mu_\lambda^0 K_0}{\mu_\lambda + \mu_{\lambda'}} Q(c) \{1 - \exp[-(\mu_\lambda + \mu_{\lambda'})Lc]\} \quad (38)$$

where L is the path length from front to rear of the cell (e.g., 10 mm). Since this geometry was used only when $\mu_\lambda c$ was so large that the term in brackets could be replaced by unity, Eqn. (38) provided a useful approximation even though α was not zero.

The emission wavelength was selected by use of an interference filter chosen to match the maximum wavelength of the fluorescence emission. Since this filter prevents light with the incident wavelength from reaching the photomultiplier, the detection scheme with chopping at 1000 Hz (e.g., triangular $G^{(2)}(\tau)$) was employed to measure $\langle n \rangle_{F1}$ and the scattering $\langle n \rangle_{STD}$ from a standard (the latter was measured at the incident wavelength). Since the instrument response was not calibrated over all wavelengths, the quantum efficiency K^0 is only expressed in relative units, e.g. K^0 is the limiting value $(\langle n \rangle_{F1} / \langle n \rangle_{STD}^{\mu_\lambda})_P^0$.

In addition to the determination of μ_λ and $\mu_{\lambda'}$ mentioned above in connection with studies of $Q(c)$, the extinction coefficient was also determined as a function of λ with a Cary 219 spectrophotometer.

TABLE 1
RODLIKE POLYMERS USED IN THIS STUDY

	$[\eta]^{(a)}$ cm^3/g		$[\eta]^{(a)}$ cm^3/g
PBT 31	200	PBO 160-1	20
PBT 43	960	PBO 160-3	38
PBT 72-7	1400	PBO 160-4	75
PBT 72-8	1770	PBO 160-5	170
		PBO 160-8	520
PPTA 2	265	PBO 2	268
		PBO 6	100

(a) Determined in methane sulfonic acid, 25°C.

TABLE 2

ARTICULATED PBT AND PBO COPOLYMERS INVESTIGATED (a)

PBO Copolymers

Sample	n Fraction -Ar-	-Ar-	η_{Inhr} (dl/g)	Sample	n Fraction -Ar-	-Ar-	η_{Inhr} (dl/g)
59894-31	1	I	1.72	292-80	0.10	II	5.24
59894-37-2	0.25	I	1.94	292-86	0.05	II	6.81
59894-45-1	0.25	I	1.99	292-71	0.05	II	6.92
352-4	0.10	I	7.08	292-88	0.10	III	5.44
292-70	0.05	I	6.04	292-96	0.05	III	6.74
292-59	0.08	I	3.57	352-58	0.10	III	5.04
352-54	0.05	I	8.58	352-39	0.05	IV	4.07

PBT Copolymers

352-18	0.10	I	12.02
352-34	0.10	II	4.60
352-28	0.05	II	6.43
352-36	0.10	IV	6.04
352-38	0.05	IV	8.01

(a) See text for notation used to identify -Ar-moieties.

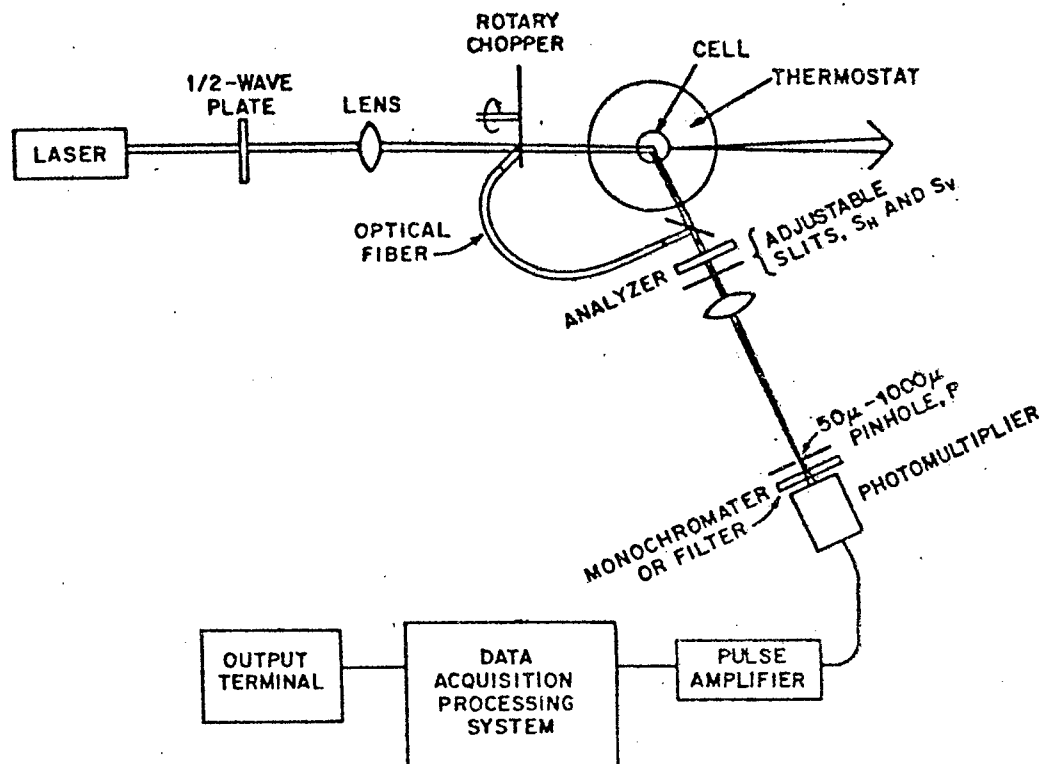


Figure 1 Schematic diagram of light scattering apparatus showing the principal components discussed in the text.

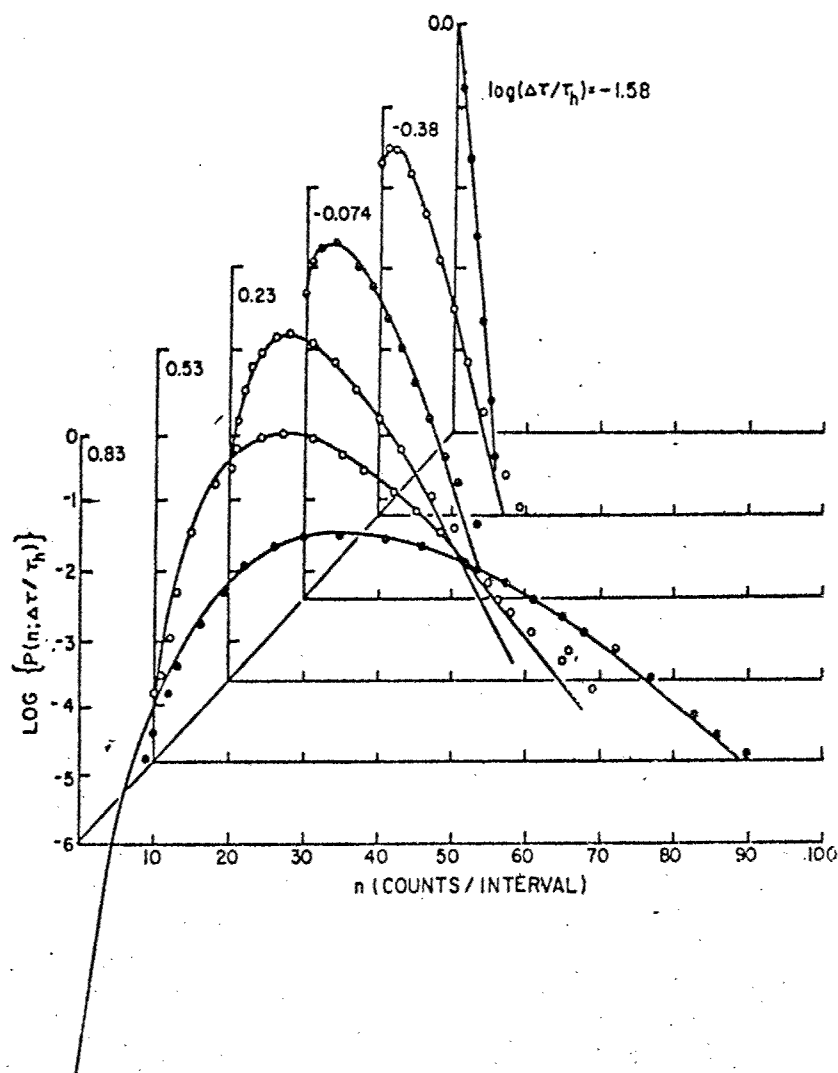


Figure 2 The distribution $P(n, \gamma)$ determined for a polystyrene solution for several values of $\Delta\tau$. Numbers on each curve give $\log \Delta\tau/\tau_h$. The solid curves were constructed with Eqn. (35) using the experimental $n^{(2)}$ to compute $m^{-1} = n^{(2)} - 1$.

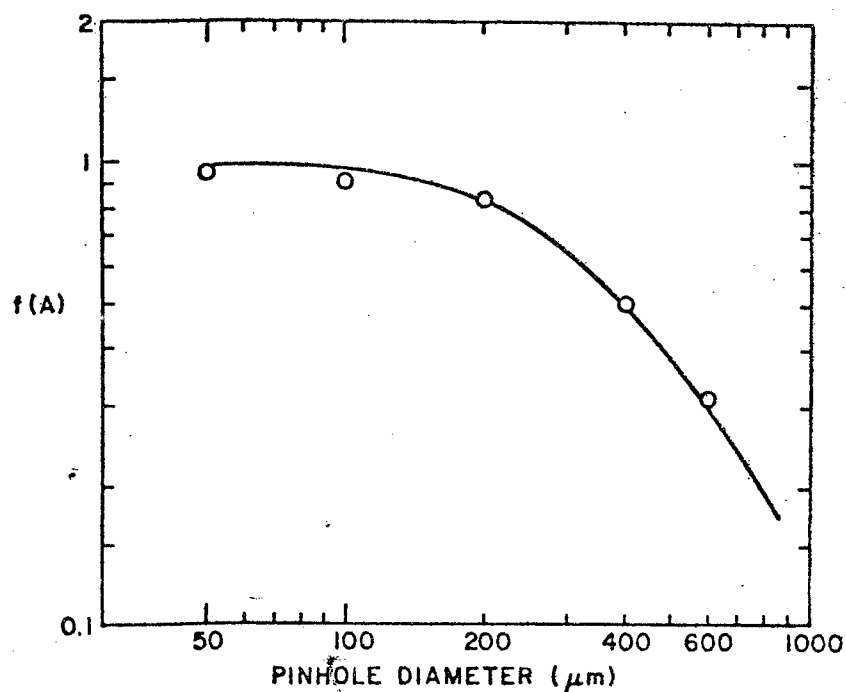


Figure 3 The coherence factor $f(A)$ determined for several values of the pinhole diameter D . The curve is a theoretical estimate, fitted to the data by use of an arbitrary proportionality between D^2 and the coherence area A .

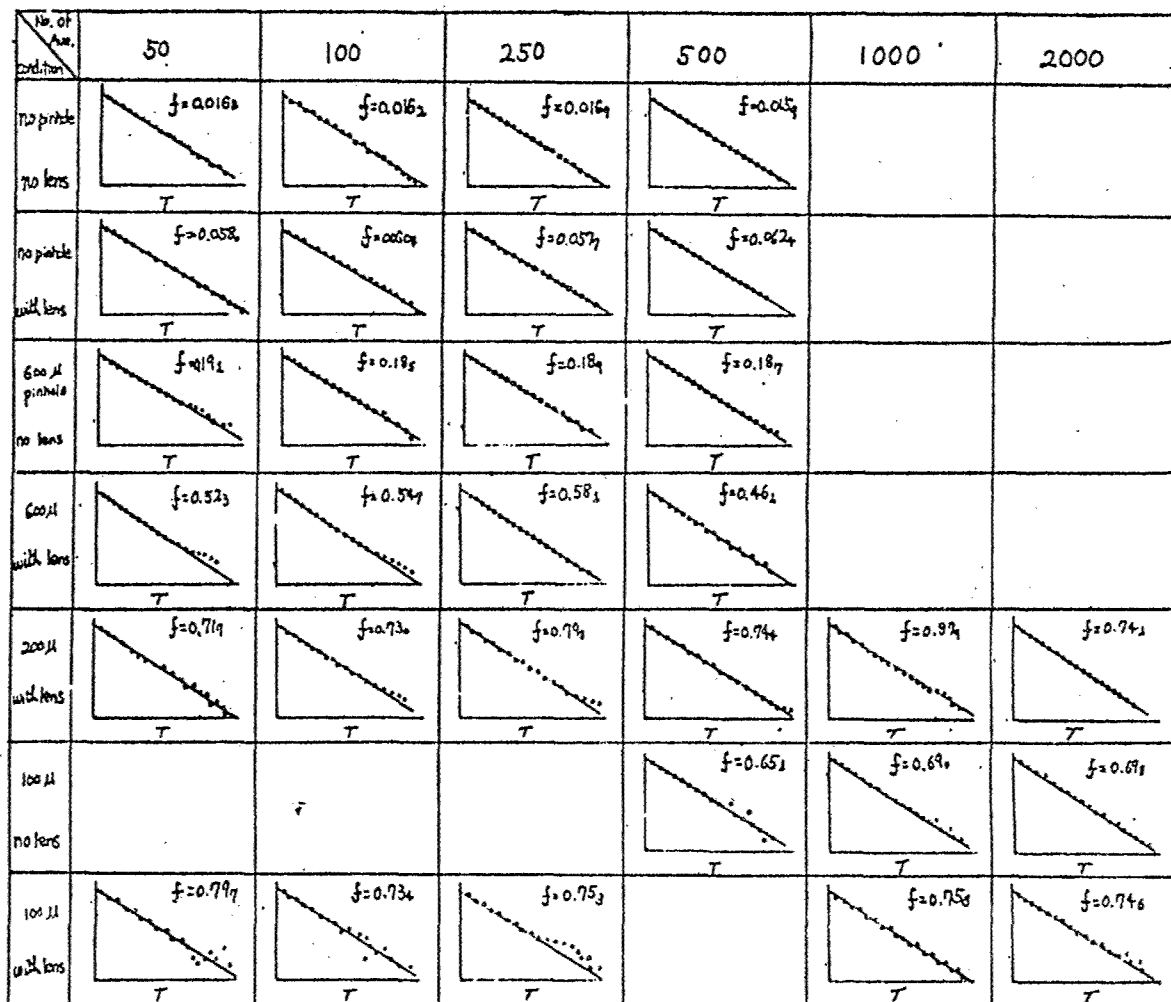


Figure 4 Example of $\log(g^{(2)}(\tau) - 1)$ versus τ for several combinations of pinhole diameter, number of $G^{(2)}(\tau)$ results averaged, and the presence or absence of a focusing lens in the incident beam. The value of $f(A)$ is entered on the diagram.

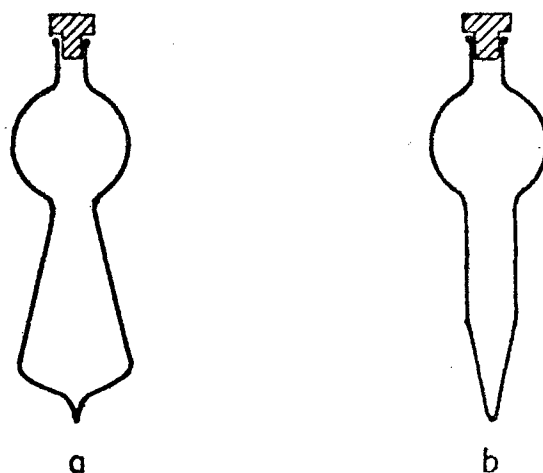


Figure 5 Light scattering cells used for a) total intensity scattering and b) photon correlation scattering.

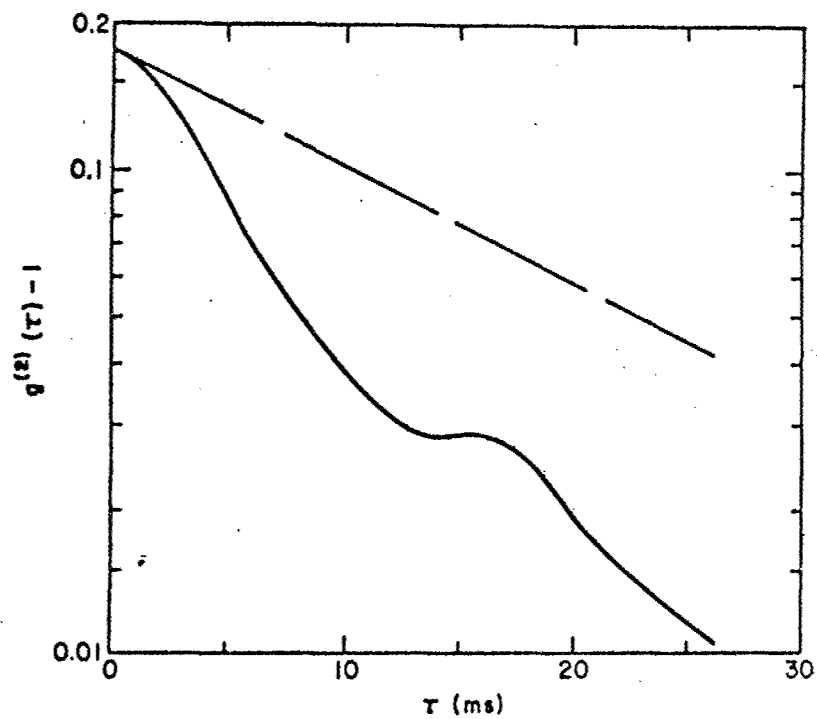
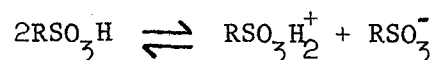


Figure 6 Illustration of modulation effect on $g^{(2)}(\tau)$ caused by excessive heating on absorption of the incident beam; the dashed curve represents $g^{(2)}(\tau)$ for the same material obtained under conditions to suppress the heating effect.

4. RESULTS

4.1 Freezing Point Depression

Values of the melting temperature T_m determined for seven materials are recorded in Table 3. As discussed in reference 7, based on the work of Gillespie,⁵ evaluation of the degree of protonation ν is facilitated if the freezing point depression $\Delta\theta$ is calculated with reference to a hypothetical melting temperature T_m^0 that would obtain if the solvent underwent no process of self-protonation, such as



or other reactions of association and dissociation. For 100 percent sulfuric acid, T_m^0 is 0.254°C below the melting temperature 10.371°C of the acid. The m_i in Eqn. (1) must include all such ions. Thus, Σm_i is given by summation of the molality m_s of the solute with the molality $(\Sigma m_i)_{xs}$ of all other ions present. Since the latter is known, say $(\Sigma m_i)_{xs}^0$ for 100 percent sulfuric acid, changes in $(\Sigma m_i)_{xs}$ reflect the ν ions conjugate to the protonated solute. A graphical method to estimate ν from $(\Sigma m_i)_{xs}$ is given in reference 7. Evaluation of $(\Sigma m_i)_{xs}$ from $\Delta\theta$ requires estimation of the molal osmotic coefficient ϕ :

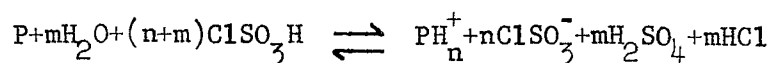
$$(\Sigma m_i)_{xs} = \frac{\Delta\theta}{K_f\phi} - m_s \quad (39)$$

where $\Delta\theta = T_m - T_m^0$ and for 100 percent sulfuric acid, K_f is 6.12, T_m^0 is 10.117°C, and

$$\phi = 1 + \frac{\sum m_i m_i B_{ii}}{\sum m_i} + \dots \quad (40)$$

Possible values of ϕ will be considered below. Estimates of $(\sum m_i)_{xs}$ calculated with ϕ equal to unity are listed in Table 2, and used to estimate the corresponding values of ν listed--for the polymeric solute the degree of protonation is expressed as ν' the number of protons per repeating unit. For the polymeric solute, m_s is so small that it may be neglected on the rhs of Eqn. (39). Thus, for polymeric solutes, the estimate for $(\sum m_i)_{xs}$ is inversely proportional to the ϕ used.

Values of ν' calculated with $\phi = 1$ are in the range 2-4 with the exception of the data for the PBO polymers, for which ν' is calculated to be 8-12. If the large value of ν' is ascribed to a residual low molecular weight impurity that will itself become protonated (e.g., water, which is tenaciously adsorbed by PBO), it is possible to calculate the effect expected on $\Delta\theta$ and ν' (with $\phi = 1$). For example, with PBO 2, the presence of one mole of such an impurity per mole of PBO repeat unit (e.g., 6 weight percent) would reduce ν' to 3. With PBO, it is difficult to reduce the water content below 1-2 percent by heating in a vacuum, which was the method used here to dry the solute. This estimate is based on the HCl evolved when wet PBO is dissolved in chlorosulfonic acid:



The presence of 2% water by weight would reduce v' to 5.2 for PBO-2 and 9.0 for PBO-6. Thus, such an impurity may offer a partial explanation for the large values of v' calculated for PBO.

4.2 Partial Specific Volume

Values of \bar{v} are plotted versus solute concentration c in Fig. 7. It may be seen that \bar{v} is nearly independent of c over the range studied. Extrapolated values of \bar{v}^0 at infinite dilution are listed in Table 4, along with $\partial \ln \bar{v} / \partial c$, which is small and positive. These results indicate that the excess volume of mixing is negative, and increases slightly with increasing c . Furthermore, \bar{v} does not seem to be very dependent on the ionic strength I of the solvent since similar data are obtained with methane sulfonic acid ($I \sim 0.05$) and chlorosulfonic acid ($I \sim 0.002$). The disparity between \bar{v}^0 and v is considerably larger for the polymeric solutes than for the model compounds, see below.

4.3 Fluorescence And Absorption Spectroscopy on PBT Polymers

Samples of PBT 72-7 and 72-8 have identical extinction coefficients over the range 200 to about 450 nm (μ is a maximum for $\lambda = 423$ nm), and for this range, μ is the same for solutions in methane and chlorosulfonic acids. At longer wavelengths, μ is about 10^3 smaller, distinctly different for the two samples, and depends on the solvent. Absorption spectra are shown in Fig. 8a; the extinction

coefficients do not depend on concentration. The fluorescence emission is qualitative similar for 72-7 and 72-8, but differs quantitatively for excitation in the long wavelength region. Uncorrected emission spectra are given in Fig. 8b for excitation at 288, 476, 488 and 514 nm. All were obtained as $(\langle n \rangle_{F1} / \langle n \rangle_{STD})_B$. It is seen that distinct spectra are obtained for excitation at 488 and 514 nm, whereas the spectrum for excitation at 476 nm appears to be that obtained at 288 nm. Similar data were taken with the PBO polymers studied. The spectra in Fig. 9a show that the principal absorption band is the same for all PBO polymers, but that the absorption at long wavelengths decreases with increasing chain length; as with PBT, the extinction coefficients do not depend on concentration. The emission spectra for excitation at 288, 488 and 633 nm are all distinctly different, whereas that for excitation at 514 nm appears to be a mixture of the spectra obtained at 488 and 633 nm. Apparently the chromophores are well isolated electronically, perhaps even on separate moieties corresponding to aggregated species, see below.

The fluorescence for 514 nm excitation was examined in more detail by measurements of $(\langle n \rangle_{F1} / \langle n \rangle_{STD})_P$ as a function of ℓ , ℓ' and c . A typical plot of $(\langle n \rangle_{F1} / \langle n \rangle_{STD}^c)_P$ versus ℓ used to extrapolate to $\ell = 0$ is shown in Fig. 10, and plots of $\ln[(\langle n \rangle_{F1} / \langle n \rangle_{STD}^{\mu_\lambda c})_P]_{\ell = \ell' = 0}$ versus c are given in Fig. 11. Values of μ_λ and $\mu_{\lambda'}$, calculated from $-(\partial(\ln \langle n \rangle_{F1} / \langle n \rangle_{STD})_P / \partial \ell)_{\ell', c}$ and $-(\partial(\ln \langle n \rangle_{F1} / \langle n \rangle_{STD})_P / \partial \ell')_{\ell, c}$, respectively are given in Table 4 for PBT 72-7 and 72-8 along with K^0 equal to $(\langle n \rangle_{F1} / \langle n \rangle_{STD}^{\mu_\lambda c})_P^0$. For convenience, the

concentration dependent quenching was analyzed with Perrin relation:^{18,19}

$$Q(c) = \exp(-K_q c) \quad (41)$$

For small $K_q c$, the constant K_q is equivalent to K'_q in the Stern-Volmer relation¹⁹

$$Q(c) = (1 + K'_q c)^{-1} \quad (42)$$

frequently used to study $Q(c)$. Values of K_q for 72-7 and 72-8 are also listed in Table 5, and data for solutions of PBO are given in Table 6. Similar values of K_q have been reported for solutions of polybenzimidazole in acidic solvents.²⁰

Fluorescence and absorption was also determined for the solutions used for total intensity light scattering. In this case $l = l' = r$, where r is the radius of the cell (7 mm), and K_q is small compared with $(\mu_\lambda + \mu_{\lambda'})r$ (see Table 6). Since fluorescence was measured with an interference filter that attenuated light with wavelength of the scattered light, but had high transmittance for light of other wavelength, $\langle n \rangle_{F1}$ can be represented by the relation

$$(\langle n \rangle_{F1} / \langle n \rangle_{STD})_P = \sum_{\lambda'} P_{\lambda'} \exp(-(\mu_\lambda + \mu_{\lambda'})rc) \sum_i \mu_{\lambda'} K_{O\lambda',i} c_i \quad (43)$$

where $c = \sum c_i$, $\mu = \sum \mu_i c_i / c$ for both μ_λ and $\mu_{\lambda'}$, K_q has been neglected

in comparison with $(\mu_{\lambda} + \mu_{\lambda'})r$, and P_{λ} is the instrument response function (including the response of photomultiplier, interference filter, etc.). Solutions used for light scattering were examined after being filtered into the cell through a fine porous frit, and again after being centrifuged for 24 hours. Usually, $(\langle n \rangle_{F1} / \langle n \rangle_{STD})_P$ increased slightly (about 10%) after centrifugation. As seen from Eqn. (43), interpretation of this result is complex, owing to the several effects that might occur. For the concentrations used, $(\langle n \rangle_{F1} / \langle n \rangle_{STD})_P$ either increased or was not changed by increased c (e.g., Eqn. (43) exhibits an extremum, but at higher c than used here). Thus, the increase must be ascribed to preferential loss of some strongly absorbant species. To simplify, consider only two species, the completely dissolved polymer (2) and a large aggregate (1), with $c_1 \ll c_2$. Then $\langle n \rangle_{F1} / \langle n \rangle_{STD}$ will increase with loss of (1) if

$$\Sigma P_{\lambda} \exp(-\mu_{\lambda'} r c) \{ \mu_{\lambda 1} + \mu_{\lambda' 1} \} r \left[\frac{c_1}{c} + \frac{\mu_{\lambda 2} K_{0 \lambda' 2}}{\mu_{\lambda 1} K_{0 \lambda' 1}} \right] - 1 \} > 0 \quad (44)$$

This will obtain if $\mu_{\lambda 1} + \mu_{\lambda' 1}$ is large enough (even if $K_{0 \lambda' 2}$ is zero). Thus, the observed increase can be ascribed to the loss of strongly absorbant aggregate species.

4.4 Light Scattering On PBT Polymers

4.4.1 Total Intensity Light Scattering

The total R_{Vv} scattering from solutions of PBT 72-7 and 72-8 was examined after one or a combination of treatments including:

- 1) preparation by dilution of a stock solution after the latter was centrifuged for 24 hr (5,000 g);

- 2) filtration through a fine sintered glass frit;
- 3) suspension in an oil bath in an ultrasonic field, at about 50°C;
- 4) centrifugation for 24 hr (5,000 g), in the light scattering cell.

All solutions used for light scattering received at least the second treatment. Plots of $\log R_{Vv}$ vs h^2 given in Fig. 12 show the effects of some of these treatments on samples with concentration about 0.6 mg/ml, which is near the upper limit used in this study. Data in Fig. 12 show substantial difference in the curvature of the scattering envelopes of two filtered solutions, with the data for 72-7 exhibiting extreme curvature at small h indicative of large moities (e.g., the apparent radius of gyration calculated as $(3\partial \ln R_{Vv} / \partial h^2)_{h=0}^{1/2}$ is about 500 nm). The difference between the two samples is lessened by use of precentrifuged stock solution, or by centrifugation of the solution itself. Addition of sonication to the previous three treatments resulted in only modest change in R_{Vv} .

Since the fluorescence emission is comparable to R_{Hv} for excitation with light of 514 nm wavelength, R_{Hv} was measured only with 633 nm wavelength light, for which the fluorescence is much smaller. Data for R_{Vv} and R_{Hv} for solutions of PBT 72-7 and 72-8 that received all four treatments described above are given in Fig. 13. Typically, the effect of centrifugation was much less on R_{Hv} than on R_{Vv} .

The angular data were extrapolated to zero angle in plots of c/R versus h^2 , with neglect of the behavior at small h . This treatment has the effect of suppressing the scattering from the large components

present. Plots of $c/R_{VV}(0)$ and $c/R_{HV}(0)$ versus concentration are given in Fig. 14, and the parameters determined from the data analysis are collected in Table 7. The constant K, given by

$$K = \frac{2}{N_A} \left(\frac{\pi m}{\lambda^2} \frac{\partial n}{\partial c} \right)^2 C(n)$$

was evaluated with $(\partial n / \partial c) = 0.56 \text{ ml/g}$ determined by differential refractometry,¹³ and the refraction coefficient $C(n)$ equal to n^{-2} for the detector optics employed.

4.4.2 Photon Correlation Light Scattering

Both $n^{(2)}(\gamma)$ and $g^{(2)}(\tau)$ were determined for solutions of PBT 72-7 and 72-8 in methane sulfonic acid. Each of the solutions studied was treated by the four methods described above (e.g., precentrifugation of the solution). Illustrative data are shown in Fig. 15 for $n^{(2)}(\gamma)$, and Fig. 16 for $g^{(2)}(\tau)$. It may be noted that the plot of $n^{(2)}-1$ versus $\Delta\tau \sin^2 \theta/2$ forms a single envelope for two values of scattering angle for 72-8, but not for 72-7. This is indicative of extreme polydispersity in 72-7. In order to investigate this effect in more detail, the scattering was studied at two positions in the scattering cell, separated along its length by about 1 cm. These two positions represented regions of different centrifugal field for the solution during centrifugation of the light scattering cell in a swinging-bucket rotor. The results for $\langle \tau_h \rangle_{g(2)} \sin^2 \theta/2$ and $\langle \tau_h \rangle_{n(2)} \sin^2 \theta/2$ obtained in the experiments are given in Table 8. Also listed are values of $g^{(2)}(0)-1$ and $n^{(2)}(0)-1$. For well behaved solutions (e.g., no association, or components with $R_{Gh} > 1$), estimates

of $\langle \tau_h \rangle_g(2)$ and $\langle \tau_h \rangle_n(2)$ would be independent of scattering angle or position in the scattering cell, as would be $g^{(2)}(0)$ and $n^{(2)}(0)$.

Several features may be noted in Table 7, including (1) values of $\langle \tau_h \rangle_n(2)$ and $\langle \tau_h \rangle_g(2)$ tend to be closer with sample 72-8 than with 72-7; (2) $\langle \tau_h \rangle_n(2) \sin^2 \theta / 2$, $\langle \tau_h \rangle_g(2) \sin^2 \theta / 2$, $g^{(2)}(0)$ and $n^{(2)}(0)$ are nearly independent of scattering angle and cell position for 72-8, but vary greatly with these parameters for 72-7; and (3) at a given θ , $\langle \tau_h \rangle_g(2)$ and $\langle \tau_h \rangle_n(2)$ tend to be larger, and $n^{(2)}(0)$ and $g^{(2)}(0)$ to be smaller at the bottom than the top of the cell. Each of these is consistent with the displacement of large moities (larger τ_h) toward the cell bottom during centrifugation, with 72-7 evidently having more of these species present than does 72-8. Sedimentation of polymeric aggregate in methane sulfonic acid solutions is in accord with values of $\Delta\rho/c$ given above.

The low values of $g^{(2)}(0)$ and $n^{(2)}(0)$ observed for scattering at the bottom of position at 45 degree scattering angle (e.g., data for 72-8) suggest that the large moities are nearly immobile, acting as sources for a local oscillator ($\tau_h = \infty$) mixing with the other scattered light. Accordingly, $\langle \tau_h \rangle$ is larger than other values obtained by other conditions. For example, the value observed for $g^{(2)}(0)$ gives $r = 0.3$ for the data on 72-8 at 45 degree and cell bottom if interpreted with Eqn. (19). Use of this estimate in Eqn. (21) reduces $\langle \tau_h \rangle_g(2) \sin^2 \frac{\theta}{2}$ to 0.45 msec, which is closer to the other data for 72-8. It is important that experiments be carried out under optical conditions for which $f(A)$ is known to enable assessments of this type.

Values of $\langle \tau_h \rangle_n^{(2)}$ and $\langle \tau_h \rangle_g^{(2)}$ obtained at the top position of the cell are given in Table 9 for several concentrations of 72-7 and 72-8. Values of $[\langle \tau_h \rangle \sin^2 \frac{\theta}{2}]^{-1}$ are extrapolated to infinite dilution in Fig. 17 for 72-8, using averaged values of $\langle \tau_h \rangle$ obtained from the data on $\langle \tau_h \rangle_n^{(2)}$ on $\langle \tau_h \rangle_g^{(2)}$ in Table 9. The data (at 25°C) extrapolate with positive slope to give $\langle \tau_h \rangle_h^{0,2} = 0.60 \mu s (nm)^{-2}$ or a molecular friction coefficient

$$\Xi^0 = kT \langle \tau_h \rangle_h^{0,2} \quad (45)$$

given by $\Xi^0 / \eta_s = 250 \text{ nm}$ (the solvent viscosity η_s is 0.010 Pa s at 25°C). The data for the lowest concentration are not used in these estimates since $n^{(2)}(0)$ and $g^{(2)}(0)$ were unusually small for that solution; this may indicate that r is less than unity for the scattering from these solutions, which would require a correction to τ_h , as discussed above.

4.5 Investigation Of Articulated Copolymers

4.5.1 Phase Equilibria

Each of the articulated copolymers was examined in a solution with 7-9 weight percent polymer to determine whether the solution was optically isotropic or anisotropic and, if isotropic, whether flow birefringence could be easily developed. The results given in Table 10 show that the tendency to form nematic solutions is variable, and not in a simple relation to the fraction n of the articulated moiety, the structure of the latter, or the inherent viscosity of the polymer. In the following discussion of light scattering on articulated PBO copolymers, it will be

shown that these undergo metastable association similar in some respect to the behavior reported in the previous section for PBT. This behavior may be implicated in the phase equilibria behavior observed.

4.5.2 Size Exclusion Chromatography

Size exclusion chromatography (SEC) has been carried out with two of the articulated PBO copolymers, using an apparatus described elsewhere.¹⁻⁴ The chromatographic data were obtained as an optical density A versus the elution volume V_e . A universal calibration for the column relating V_e with the product $[\eta]M$ of the eluent was then used to compute an SEC-averaged $[\eta]M$:

$$([\eta]M)_{\text{SEC}} = \frac{\sum A_i ([\eta]M)_i}{\sum A_i}$$

to give the results $([\eta]M)_{\text{SEC}}$ equal to 31,000 and 15,000 for polymers 80 and 45-1, respectively. Based on estimates for $[\eta]$, these give the chromatographic averaged molecular weight

$$M_{\text{SEC}} \equiv \frac{([\eta]M)_{\text{SEC}}}{[\eta]}$$

equal to 6,000 and 7,500 for polymer 80 and 45-1, respectively.

4.5.3 Light Scattering Behavior

Although it was hoped that incorporation of comonomers with rotational isomeric state (groups to permit articulation) would improve solubility, characteristics of PBO-type polymers, the light scattering data on dilute solutions reveal considerable interchain association with

the articulated polymers. This is illustrated by the data given in Fig. 18, which shows $\ln R_{VV}$ versus h^2 for filtered solutions in comparison with the same solutions after treated by sonication and centrifugation, as described in section 4.4.1. The results reveal decreased scattering at small h , sometimes coupled with a general lessening of the decrease of R_{VV} with increasing h^2 . These effects reveal the loss of large moieties on the post-filtrations treatment. In addition, as may be seen in Figs. 13 c and d, the magnitude of R_{VV} may also be sharply altered; the results in Fig. 18c are very unusual in that R_{VV} was increased by the post-filtration treatment; this increase in scattering was accompanied by increased fluorescence. Both effects could be accounted for by loss of moieties with large extinction coefficients on the post-filtration treatment.

In fact, fluorescence was large at all incident light wavelengths studied (e.g., 488, 514 and 633 nm). In general, the spectra for $I_{||}$ and I_{+} were similar in shape for a given solution, but differed with wavelength. With $I_{||}$, the scattering dominated the fluorescence at the incident wavelength so that R_{VV} could be determined with reasonable accuracy, but with I_{+} , often R_{Hv} was about equal to I_{+} , making reliable estimation of R_{Hv} difficult or impossible, especially with wavelengths of 488 and 514 nm. Some typical results for I_{+} shown in Fig. 19 illustrate this effect.

The effects of solution clarification treatment revealed in Fig. 17 are shown again in Figs. 20-24 in plots of c/R_{VV} versus h^2 for four polymers in methane sulfonic acid, and one in chlorosulfonic acid. The extrapolated values of $c/R_{VV}(0)$ from such data are plotted against c in Figs. 25-29. In addition, estimates of $c/R_{Hv}(0)$ are also given for two sets of data in Figs. 25b and 26b. Owing to the large contributions of

the fluorescence at the excitation wavelength, it was not possible to obtain data on $c/R_{Hv}(0)$ for solutions studied with 514 nm wavelength. Moreover, with sample 352-4 in chlorosulfonic acid, even the R_{Hv} in comparison with fluorescence scattering with 633 nm light was too small to permit a reliable estimate. Even with samples 292-80 and 352-39, for which $c/R_{Hv}(0)$ is reported with 633 nm incident light; the fluorescence is not negligible. Estimates of $R_{Hv}(0)$ were corrected by a scattering contribution remaining on extrapolation of $R_{Hv}(0)$ versus c to infinite dilution; the origin of this contribution is obscure.

The total intensity light scattering data for the articulated polymers extrapolated to infinite dilution and zero angle are collected in Table 11.

As with the PBT polymers studied, the photon correlation data provide additional insight to the association obtaining in dilute solutions. Values of $n^{(2)}(0)$ and $\langle \tau_h \rangle_{n(2)} \sin^2 \theta/2$ are given for two polymers at four concentrations each in Table 12; the data were collected near the top and bottom of a centrifuged solution, as described in section 4.4.2. The results show that for the two polymers studied, both $n^{(2)}(0)$ and $\langle \tau_h \rangle_{n(2)} \sin^2 \theta/2$ vary with the centrifugal field and, especially near the cell bottom, with scattering angle.

The data in Fig. 30 give $n^{(2)}(\Delta\tau/\tau_h)$ versus $\Delta\tau \times \sin^2 \varphi/2$ for a solution of 292-80, before and after centrifugation. It is evident that the filtered, but uncentrifuged data do not give behavior independent of scattering angle, indicative of extreme size heterogeneity in the sample. The superposition is improved (but not complete) for the same solution after centrifugation. Data in Table 13 give $\langle \tau_h \rangle_{n(2)} \sin^2 \varphi/2$ obtained by

analysis of such data with Eqns. 18 and 20 for several solutions (all calculated with $r=1$). Similarly, data for $\langle \tau_h \rangle_{g(2)} \sin^2 \varphi / 2$ obtained by analysis of $g^{(2)}(\tau)$ with Eqns. 19 and 21 (with $r=1$) are given in Table 14. Neither $\langle \tau_h \rangle_{n(2)} \sin^2 \theta / 2$ or $\langle \tau_h \rangle_{g(2)} \sin^2 \varphi / 2$ are independent of scattering angle as would be expected in the absence of extreme heterogeneity. Moreover, the data are more scattered than similar results with well-behaved materials. In general, it appears that post-filtration centrifugation treatment leads to more uniform results, but does not result in entirely satisfactory data. For sample 292-80, the data extrapolate to give $\langle \tau_h \rangle^0 h^2$ about equal to $2 \mu s (nm)^{-2}$ or a molecular friction coefficient Ξ^0 given by $\Xi^0 / \eta_s = 830 \text{ nm}$ (with $\eta_s = 0.01 \text{ Pa s}$). This value is appreciably larger than that reported above (section 4.4.2) for PBT 72-8.

TABLE 3
DEGREE OF PROTONATION FROM THE FREEZING
POINT DEPRESSION IN 100 PERCENT SULFURIC ACID

Sample	(a) m_s mol/kg	$T_m - T_m^{(s)}$ (°C)	Calculated With $\phi = 1$	
			$(\sum m_i)_{xs}$	(a) ν
PBT Model	0.0117	0.180	0.059	3.1
PBT 31	0.0087	0.097	0.057	3.8
PBT 43	0.0034	0.015	0.044	2.8
PBO Model	0.0140	0.239	0.067	3.2
PBO 2	0.0054	0.132	0.063	7.7
PBO 6	0.0048	0.233	0.080	12.5
PPTA 2	0.0375	0.390	0.105	2.4

(a) Expressed in terms of the repeating unit for polymeric solute.

(b) $T_m^{(s)}$ is the actual freezing temperature 10.371°C of 100 percent sulfuric acid.

TABLE 4

PARTIAL SPECIFIC VOLUME OF PBT, PBO AND

MODEL COMPOUNDS

(25°C)

Solute	Solvent ^(a)	\bar{v}^0 (ml/g)	$v = 1/\rho$ (ml/g)	$\frac{\partial \ln \bar{v}}{\partial c}$ (ml/g)
PBT Model1	MSA	0.63	0.69	12.88
	CSA	0.63	0.69	
PBT 72-8	MSA	0.48	0.69	26.40
	CSA	0.42	0.69	32.14
PBT 72-7	MSA	0.48	0.69	
PBO Model1	MSA	0.62	0.72	
	CSA	0.62	0.72	
PBO 160-8	MSA	0.54	0.72	
	CSA	0.46	0.72	

(a) MSA = methane sulfonic acid

CSA = chlorosulfonic acid

TABLE 5
ABSORPTION AND FLUORESCENCE PARAMETERS FOR PBT

$\lambda_{\text{EXCITATION}} = 514.5 \text{ nm}$

Polymer	Solvent	λ' Emissions (nm)	μ_{λ} ml/mg·mm	$\mu_{\lambda'}$ ml/mg·mm	$K^0(a)$	K_q ml/mg
PBT-2122-72-8	MSA	575	0.016	0.0043	25	0.007
" 7	MSA	575	0.023	0.0095	57	0.015
" 8	CSA	575	0.030	0.019	39	0.22
" 7	CSA	575	0.037	0.010	68	0.42

(a) Quantum efficiency in relative units; i.e. $(\langle n \rangle_{F1} / \langle n \rangle_{STD}^{cl_{\lambda}})_p^0$

TABLE 6

ABSORPTION AND FLUORESCENCE PARAMETERS FOR PBO

 $\lambda_{\text{EXCITATION}} = 514.5 \text{ nm}$

Polymer	$\mu_{\lambda'}$ Emission (nm)	Solvent	μ_{λ} ml/mg mm	$\mu_{\lambda'}$ ml/mg mm	K^q $K^{(a)}$ ml/mg	Solvent	μ_{λ} ml/mg mm	$\mu_{\lambda'}$ ml/mg mm	$K^{(a)}$ $K^{(a)}$ ml/mg	K^q ml/mg
PBO-160/1	576	MSA	1.22	0.87	2.40	1.0	CSA	---	---	---
3	576	MSA	0.62	0.28	0.76	1.2	CSA	---	---	---
4	576	MSA	---	---	---	---	CSA	0.45	0.28	3.56 0.68
5	576	MSA	0.18	0.061	2.22	0.23	CSA	0.21	0.12	3.48 0.44
8	576	MSA	0.087	0.031	4.48	0.27	CSA	0.07	0.034	14 0.33
PBO-160/1	686	MSA	1.22	0.46	1.60	0.96	CSA	---	---	---
3	686	MSA	0.62	0.11	0.90	0.75	CSA	---	---	---
4	686	MSA	---	---	---	---	CSA	0.45	0.12	2.11 0.49
5	686	MSA	0.18	---	---	---	CSA	0.21	0.045	1.38 0.47
8	686	MSA	0.087	---	---	---	CSA	0.07	0.018	---

(a) Quantum efficiency in relative units, i.e., $(\langle n \rangle_{F1} / \langle n \rangle_{STD}^{c_{\mu\lambda}})^0$

TABLE 7

TOTAL INTENSITY LIGHT SCATTERING PARAMETERS FOR PBT

(Methane Sulfonic Acid, 25°C)

Polymer	$10^5 [Kc/R_{Vv}(0)]^0$	$10^5 [Kc/R_{Hv}(0)]^0$	$(\partial \ln(c/R_{Vv}) / \partial h^2)^0$	$(\partial \ln(c/R_{Hv}) / \partial h^2)^0$	$(\partial \ln [c/R_{Vv}(0)]^{1/2} / \partial c)^0$
	Dalton ⁻¹	Dalton ⁻¹	nm ²	nm ²	cm ³ /g
PBT-72-7	2.4	48	810	290	1730
72-8	2.7 ₅	50	620	250	1030

TABLE 8

PHOTON CORRELATION LIGHT SCATTERING DATA
FOR TWO PBT POLYMERS AT TWO POSITIONS IN
LIGHT SCATTERING CELL

(METHANE SULFONIC ACID, 25°C)

Sample	Position In Cell	Scattering Angle	$\langle \tau_h \rangle_g^{(2) \sin^2 \frac{\theta}{2} (a)}$ (msec)	$\langle \tau_h \rangle_n^{(2) \sin^2 \frac{\theta}{2} (b)}$ (msec)	$g^{(2)}(0)-1$	$n^{(2)}(0)-1$
=====						
PBT 72-7 ^(c)	Top	45	0.27	0.31	0.16	0.22
	Bottom	45	--	0.56	--	0.06
	Top	90	0.32	0.21	0.07	0.22
	Bottom	90	0.63	0.85	0.13	0.20
PBT 72-8 ^(c)	Top	45	0.57	0.55	0.18	0.22
	Bottom	45	0.70	0.73	0.10	0.07
	Top	90	0.45	0.55	0.18	0.22
	Bottom	90	0.62	0.55	0.15	0.22

(a) Calculated with Eqn. (21); $r = 1$.

(b) Calculated with Eqn. (20); $r = 1$.

(c) Concentrations 0.61 and 0.63 mg/ml for 72-7 and 72-8, respectively.

TABLE 9
PHOTON CORRELATION LIGHT SCATTERING DATA
FOR TWO PBT POLYMERS
(METHANE SULFONIC ACID, 25°C)

Sample	c (mg/ml)	$\langle \tau_h \rangle_g^{(2)} \sin^2 \frac{\theta^{(a)}}{2}$		$\langle \tau_h \rangle_n^{(2)} \sin^2 \frac{\theta^{(b)}}{2}$		$n^{(2)}(0)-1$
		$\theta = 45$	$\theta = 90$	$\theta = 45$	$\theta = 90$	
		(m s e c)				
PBT-72-7	0.118	--	--	0.23	0.23	0.12
	0.209	--	--	0.24	--	0.13
	0.364	0.26	0.31	0.26	0.18	0.15
	0.614	0.16	--	0.17	0.12	0.12
PBT-72-8	0.099	0.55	0.59	0.62	0.52	0.15
	0.183	0.45	0.31	0.49	0.41	0.25
	0.332	0.40	0.44	0.40	0.36	0.20
	0.631	--	0.39	0.31	0.31	0.25

(a) Calculated with Eqn. (21); $r = 1$.

(b) Calculated with Eqn. (20); $r = 1$.

TABLE 10

PHASE EQUILIBRIA DATA FOR SOLUTIONS IN METHANE SULFONIC ACID

Sample	n Fraction -Ar-	-Ar-	η_{inh} (dl/g)	100W ₂	Isotropic for T > 100°C	Easily Developed Flow Birefringence	Nematic at 25°C	Biphasic Temp. Range
PBO POLYMERS								
31	1	I	1.72	8.4	✓			
37-2	0.25	I	1.94	7.9	✓			
45-1	0.25	I	1.99	8.3	✓			
352-4	0.10	I	7.08	8.0	✓	✓		
292-70	0.05	I	6.04	7.4	✓			
292-59	0.05	I	3.57	8.8			✓	58-65
352-54	0.05	I	8.58	8.6		No	Homogeneous Solution	
				5.0	✓	✓		
292-80	0.10	II	5.24	7.8	✓			
292-86	0.05	II	6.81	9.7		No	Homogeneous Solution	
292-71	0.05	II	6.92	7.3	✓	✓		
292-88	0.10	III	5.44	7.9	✓			
292-96	0.05	III	6.74	7.0	✓	✓		
352-58	0.10	III	5.04	7.4	✓	✓		
352-39	0.05	IV	4.07	7.6 _(a)	✓	✓		
352-39	0.05	IV	4.07	6.4			✓	
PBT POLYMERS								
352-18	0.10	I	12.02	7.4		No	Homogeneous Solution	
				4.7	✓	✓		
352-34	0.10	II	4.60	7.2				96-119
352-28	0.05	II	6.43	7.1	✓	✓	✓	
352-36	0.10	IV	6.04	7.4			✓	98-118
352-38	0.05	IV	8.01	7.5			✓	99-127

a) chlorosulfonic acid solution

TABLE 11

TOTAL INTENSITY LIGHT SCATTERING
PARAMETERS FOR ARTICULATED PBO POLYMERS^(a)

Polymer	Comonomer (%)	Solvent	$10^5 [K_c/R_{V_V}(0)]^0$ dalton ⁻¹	$10^5 [K_c/R_{H_V}(0)]^0$ dalton ⁻¹	$(\partial n / \partial c / R_{V_V}) \partial h^2$ ⁰ nm ²	$(\partial n [c/R_{V_V}(0)]^{1/2} / \partial c)$ ⁰ cm ³ /g
292-80	II (10)	MSA	0.65	17	6,000	1,650
292-96	III (5)	MSA	$325 \times \frac{K_{514}}{K_{633}}$			
352-39	IV (5)	MSA	0.025	40	2,400	26,500
352-4	I (10)	MSA	$200 \times \frac{K_{514}}{K_{633}}$			
352-4	I (10)	CSA	1.58		2,600	2,220

(a) All data calculated with $(\partial n / \partial c)$ for PBO.

TABLE 12

PHOTON CORRELATION LIGHT SCATTERING DATA FOR
TWO ARTICULATED PBO POLYMERS AT TWO POSITIONS
IN LIGHT SCATTERING CELL

(METHANE SULFONIC ACID, 15.5°C)

Sample	Concentration	Position in cell	$\theta = 45^\circ$			$\theta = 90^\circ$		
			$n^{(2)}(0) - 1$	$\langle \tau_h \rangle_n^{(2)} \sin^2 \frac{\theta}{2}$	$n^{(2)}(0) - 1$	$\langle \tau_h \rangle_n^{(2)} \sin^2 \frac{\theta}{2}$	$n^{(2)}(0) - 1$	$\langle \tau_h \rangle_n^{(2)} \sin^2 \frac{\theta}{2}$
292-80	0.0099	top	0.13	1.07	0.12	1.36	0.12	1.36
		bottom	0.23	0.92	0.03	2.07	0.03	2.07
	0.0250	top	0.20	1.30	0.20	0.84	0.20	0.84
		bottom	0.40	0.32	0.08	1.25	0.08	1.25
292-96	0.0400	top	0.25	0.79	0.25	0.62	0.25	0.62
		bottom	0.45	1.15	--	--	--	--
	0.0511	top	0.20	0.72	0.20	0.87	0.20	0.87
		bottom	0.20	0.68	0.10	0.70	0.10	0.70
292-96	0.0092	top	0.06	1.50	0.09	1.80	0.09	1.80
		bottom	0.35	0.27	0.18	1.09	0.18	1.09
	0.0236	top	0.34	1.90	0.08	0.51	0.08	0.51
		bottom	0.42	0.27	0.15	0.77	0.15	0.77
292-96	0.0389	top	0.18	0.93	0.18	0.81	0.18	0.81
		bottom	0.40	0.30	0.25	1.22	0.25	1.22
	0.0487	top	0.20	1.00	0.20	1.25	0.20	1.25
		bottom	0.18	0.20	0.16	1.05	0.16	1.05

TABLE 13a
PHOTON CORRELATION LIGHT SCATTERING DATA
FOR ARTICULATED PBO POLYMER 292-80
(METHANE SULFONIC ACID)

C (mg/ml)	Solution Treatment	Scattering Angle						
		45	60	75	90	105	120	135
			$\langle \tau_h \rangle_n$	$(2) \sin^2 \frac{\theta}{2}$			(ms)	
0.099	Filtered ^(a) &	1.07	1.30	1.32	1.36	0.09	0.09	--
0.250	Centrifuged	1.30	1.50	1.08	0.84	0.89	1.13	1.38
0.400		0.79	0.69	0.69	0.62	0.62	0.47	--
0.511		0.72	0.66	0.66	0.87	0.73	0.86	1.35
0.099	Filtered ^(b)	2.30	1.95	1.95	2.65	1.20	--	--
0.250		1.35	1.05	1.18	0.81	2.93	--	--
0.400		1.55	1.05	1.15	0.87	0.66	2.35	1.85
0.511		2.15	3.30	3.25	4.20	6.00	--	--

(a) Light scattering at 15°C.

(b) Light scattering at 25°C.

TABLE 13b

PHOTON CORRELATION LIGHT SCATTERING DATA
FOR ARTICULATED PBO POLYMER 292-96
(METHANE SULFONIC ACID)

C (mg/ml)	Solution Treatment	Scattering Angle						
		45	60	75	90	105	120 (ms)	135
$\langle \tau_h \rangle_{n(2)} \sin^2 \frac{\theta}{2}$								
0.092	Filtered ^(a)	1.50	1.70	0.86	1.80	1.30	2.80	--
0.236	& Centrifuged	1.90	1.16	3.25	0.52	0.65	1.42	1.13
0.389		0.93	0.85	0.85	0.81	2.55	3.25	1.25
0.487		1.00	0.94	1.13	1.25	2.00	--	--
0.092	Filtered ^(b)	1.65	--	2.45	5.55	5.55	8.6	9.8
0.0236		--	3.8	0.53	0.71	0.54	1.13	--
0.389		4.6	--	1.70	1.68	1.25	1.80	3.30
0.487		--	5.9	4.4	4.7	4.5	6.4	8.6

(a) Light scattering at 15°C.

(b) Light scattering at 25°C.

TABLE 13c
PHOTON CORRELATION LIGHT SCATTERING DATA
FOR ARTICULATED PBO POLYMER 352-4
(METHANE SULFONIC ACID)

C (mg/ml)	Solution Treatment	Scattering Angle						
		45	60	75	90	105	120	135
		$\langle \tau_h \rangle_n (2) \sin^2 \frac{\theta}{2}$					(ms)	
=====								
0.376	Filtered ^(a) & Centrifuged	1.23	1.35	1.33	1.55	2.20	3.50	--
0.097	Filtered ^(b)	4.15	3.10	2.50	2.00	2.45	--	--
0.246		0.46	--	--	0.36	--	--	2.23
0.376		2.30	1.58	1.25	1.56	--	2.30	--
0.498		0.83	0.77	0.73	--	0.84	1.25	2.65

(a) Light scattering at 15°C.

(b) Light scattering at 25°C.

TABLE 14a

PHOTON CORRELATION LIGHT SCATTERING DATA
FOR ARTICULATED PBO POLYMER 292-80

(METHANE SULFONIC ACID)

C	Solution Treatment	Scattering Angle						
		45	60	75	90	105	120	135
			$\langle \tau_h \rangle_g$	$(2) \sin^2 \frac{\theta}{2}$			(ms)	
0.099	Filtration (a)	1.47	0.85	0.93	1.06	1.74	0.53	0.92
0.250	& Centrifugation	1.39	1.82	1.68	1.78	--	--	--
0.400		0.81	0.91	0.75	0.80	0.72	0.67	0.49
0.511		0.76	0.62	0.59	0.45	0.41	0.64	0.87
0.099	Filtration (b)	0.46	1.66	1.07	0.36	1.19	0.89	--
0.250		0.77	0.62	0.57	0.61	0.95	0.46	0.48
0.400		0.77	0.57	0.46	0.56	0.64	0.59	2.13
0.511		--	4.61	5.61	2.74	1.79	2.59	1.39

(a) Light scattering at 15°C.

(b) Light scattering at 25°C.

TABLE 14b

PHOTON CORRELATION LIGHT SCATTERING DATA
 FOR ARTICULATED PBO POLYMER 292-96
 (METHANE SULFONIC ACID)

C	Solution Treatment	Scattering Angle						
		45	60	75	90	105	120 (ms)	135
		$\langle \tau_h \rangle_g (2) \sin^2 \frac{\theta}{2}$						
0.236	Filtered ^(a) & Centrifuged	0.95	0.94	0.85	0.73	0.79	1.36	1.47
0.092	Filtered ^(b)	1.21	1.43	1.15	3.58	1.45	2.80	1.81
0.236		--	--	0.18	0.43	0.10	0.26	0.52
0.489		2.29	1.78	1.97	1.56	11.5	0.53	0.61

(a) Light scattering at 15°C.

(b) Light scattering at 25°C.

TABLE 14c
PHOTON CORRELATION LIGHT SCATTERING DATA
FOR ARTICULATED PBO POLYMER 352-4
(CHLOROSULFONIC ACID, 25°C)

C	Solution Treatment	Scattering Angle						
		45	60	75	90	105	120 (ms)	135
		$\langle \tau_h \rangle_g (2) \sin^2 \frac{\theta}{2}$						
0.092	Filtration	2.06	1.71	1.23	--	--	--	--
0.246		0.45	0.50	--	0.34	--	--	0.92
0.376		0.97	0.18	0.52	0.56	0.66	0.51	0.53
0.498		0.40	7.46	0.20	0.62	0.59	0.58	0.57

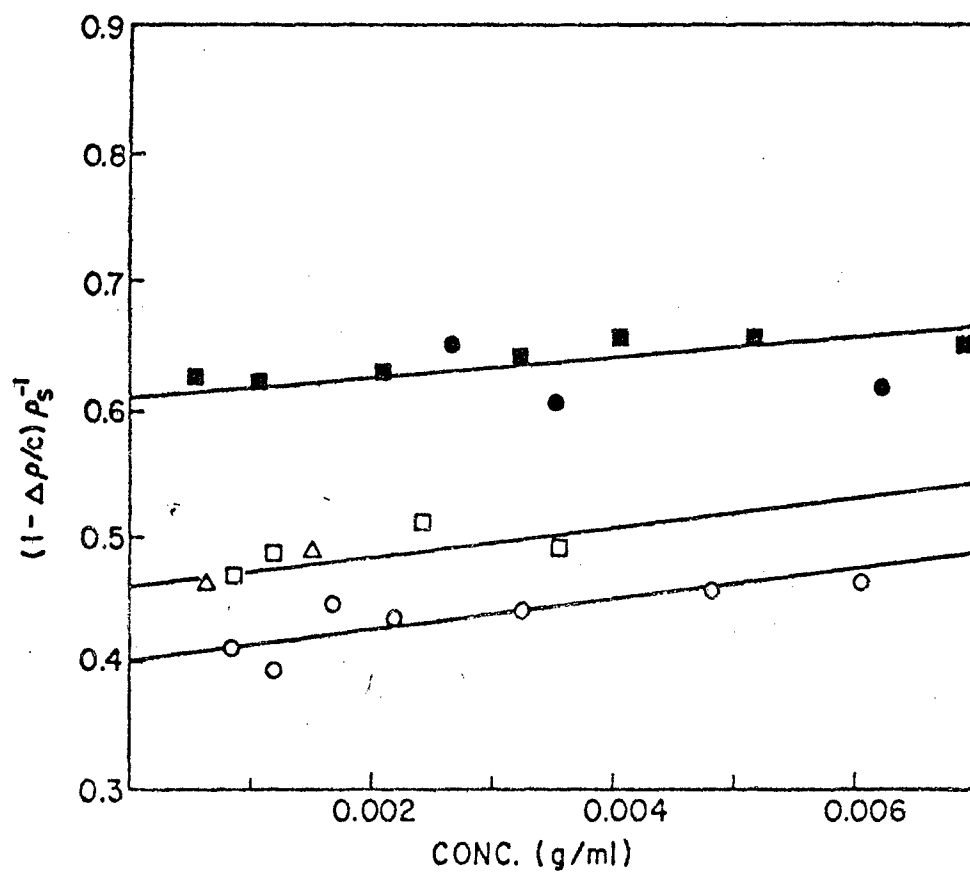


Figure 7 The partial specific volume $(1 - \Delta\rho/c)\rho_s^{-1}$ versus solute concentration for PBT 72-8 in CSA, O, and MSA, \square ; PBT 72-7 in MSA, Δ ; and PBT model in CSA, \bullet and MSA, \blacksquare . Here MSA and CSA are methane and chlorosulfonic acids, respectively.

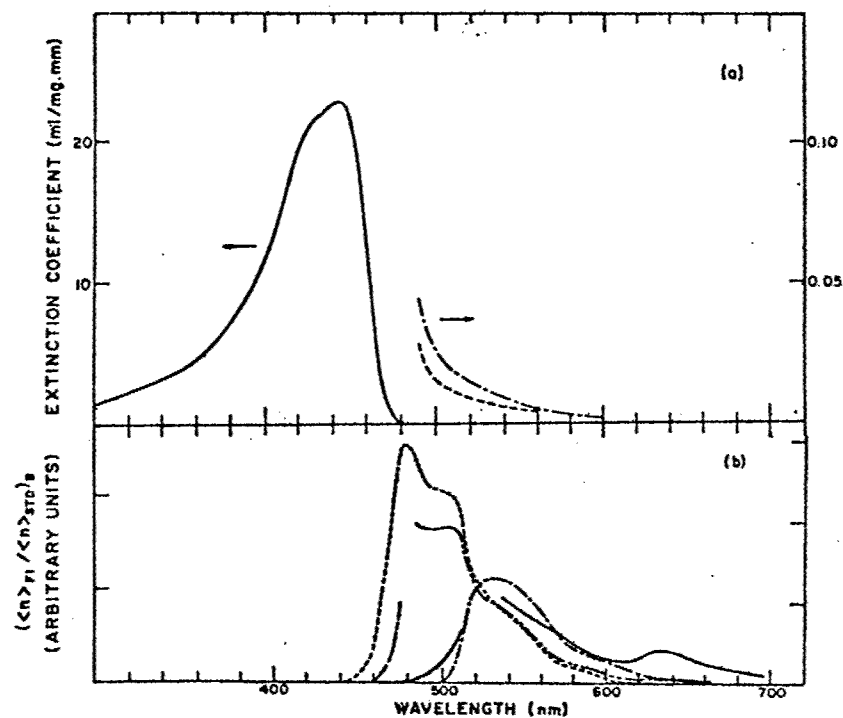


Figure 8 a) Extinction coefficient for PBT 72-7 and 72-8 in solution in methane sulfonic acid:— 72-7 and 72-8; ---, 72-8; and — — — 72-7.

b) $\langle n \rangle_{F1} / \langle n \rangle_{STD,B}$ for PBT 72-7 or 72-8 for four excitation wavelengths; ---, 268; — — —, 476; — — —, 488; —, 514 nm.

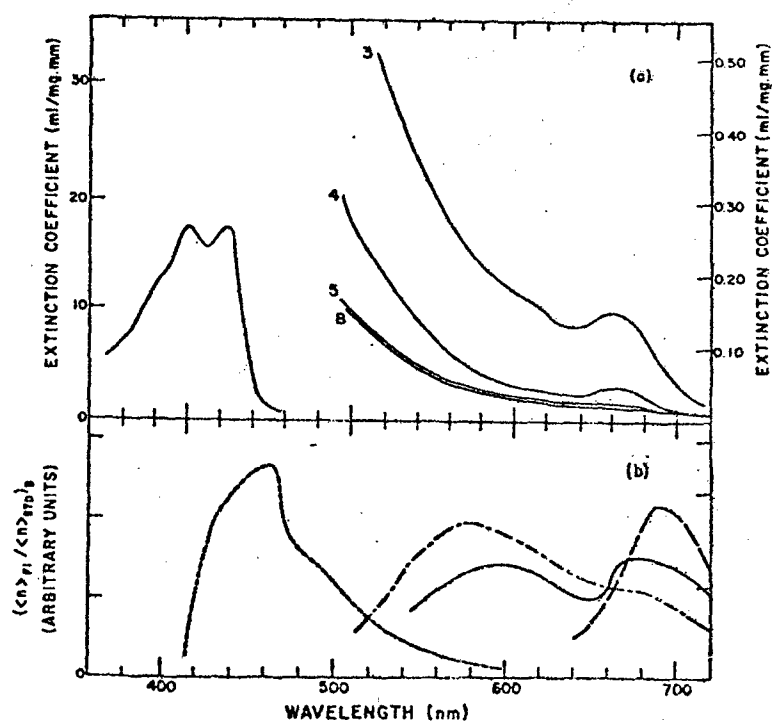


Figure 9 a) Extinction coefficient for PBO in solution in methane sulfonic acid: spectrum below 450 nm is for all PBO samples, whereas the numerals identify the PBO 160 samples for longer wavelength.

b) $(\langle n \rangle_{F1} / \langle n \rangle_{STD})_B$ for PBO samples for four excitation wavelengths; ---, 288; -.-.-, 488; —, 514; and 633 nm, ---.

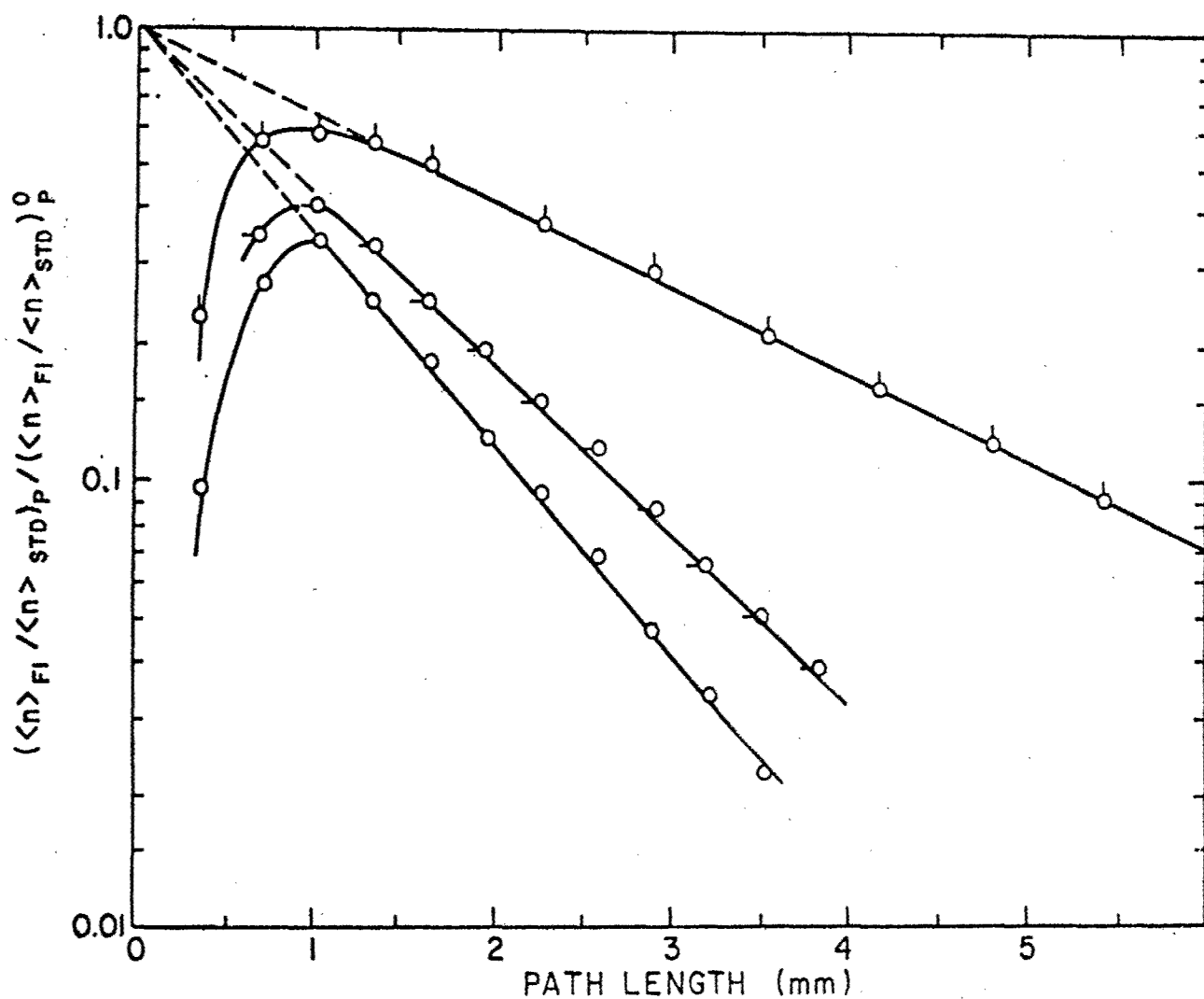


Figure 10 Example of a plot of $\log \left(\frac{\langle n \rangle_{F1} / \langle n \rangle_{STD}^P}{\langle n \rangle_{F1} / \langle n \rangle_{STD}^P} \right)^0$ versus path length for PBO 160-1 ($c = 1.04$ g/ml) for three wavelengths: 514, 0; 575, -0; and 686 nm, 0. Below 1 mm path length the illuminated volume of solution decreases.

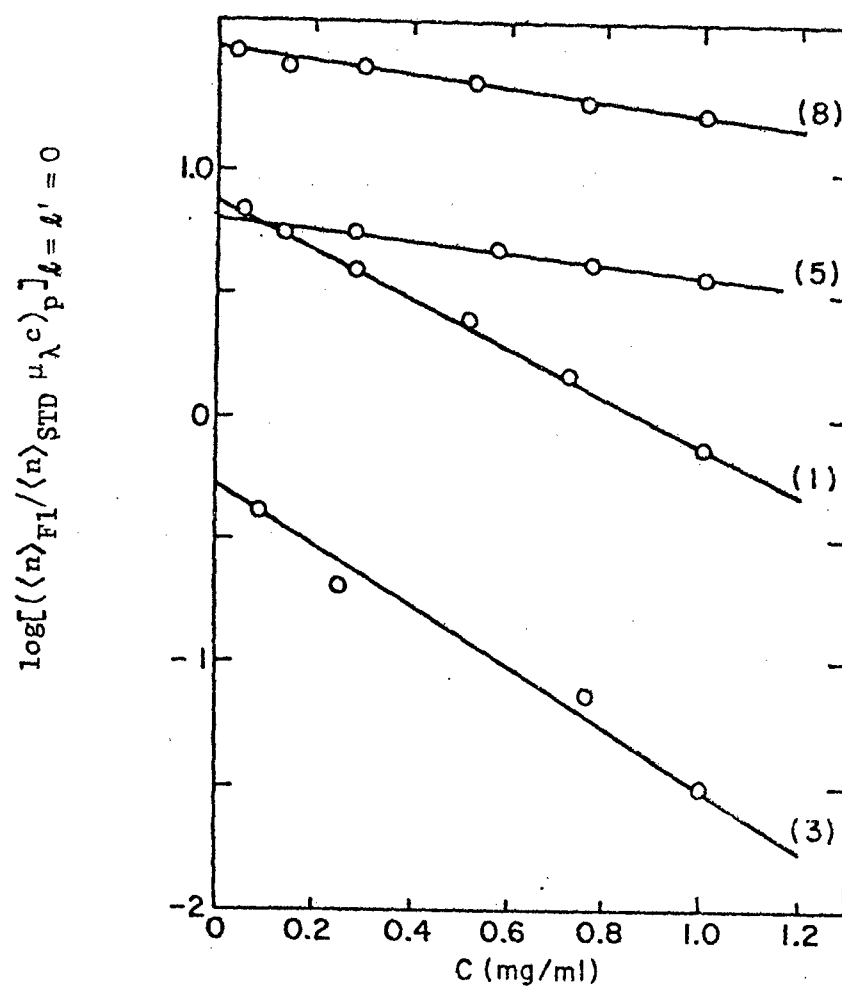


Figure 11 Examples of plot of $\log[(\langle n \rangle_{F1} / \langle n \rangle_{STD} \mu_{\lambda}^c)_p]_{\ell=\ell'=0}$ versus c used to evaluate the quenching parameter K_q . Data are for PBO 160 series number given on the figure.

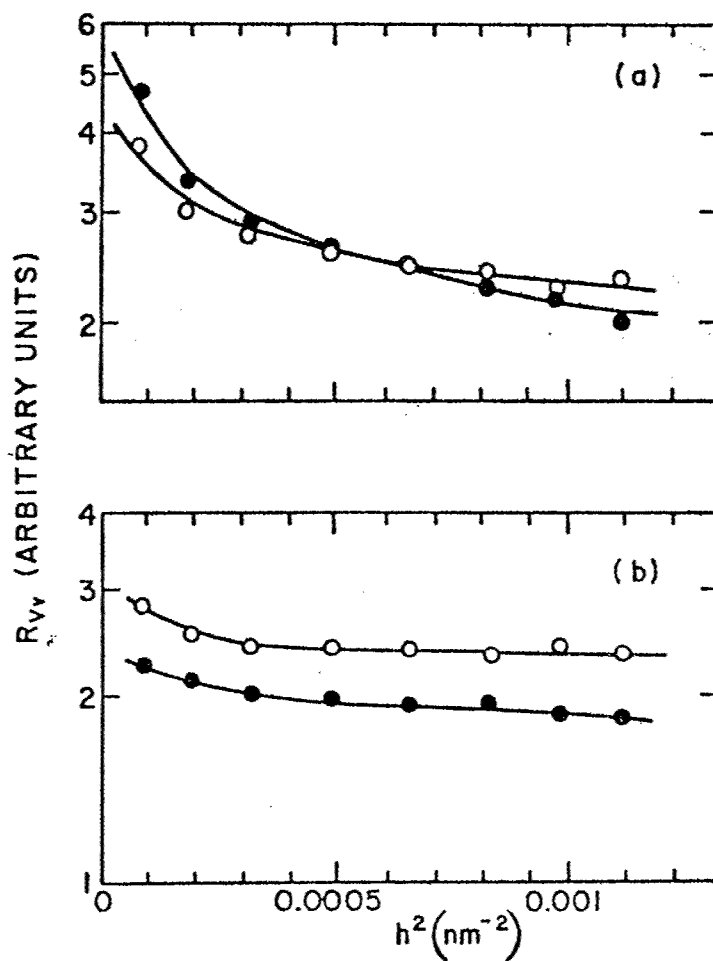


Figure 12 Examples of $\log R_v/c$ versus h^2 for solutions of PBT 72-7, ● ($c = 0.614 \text{ mg/ml}$) and 72-8, ○ ($c = 0.631 \text{ mg/ml}$) in methanesulfonic acid: a) precentrifuged stock solution, diluted and filtered into light scattering cell; b) as in a), but also centrifuged in the cell after the filtration.

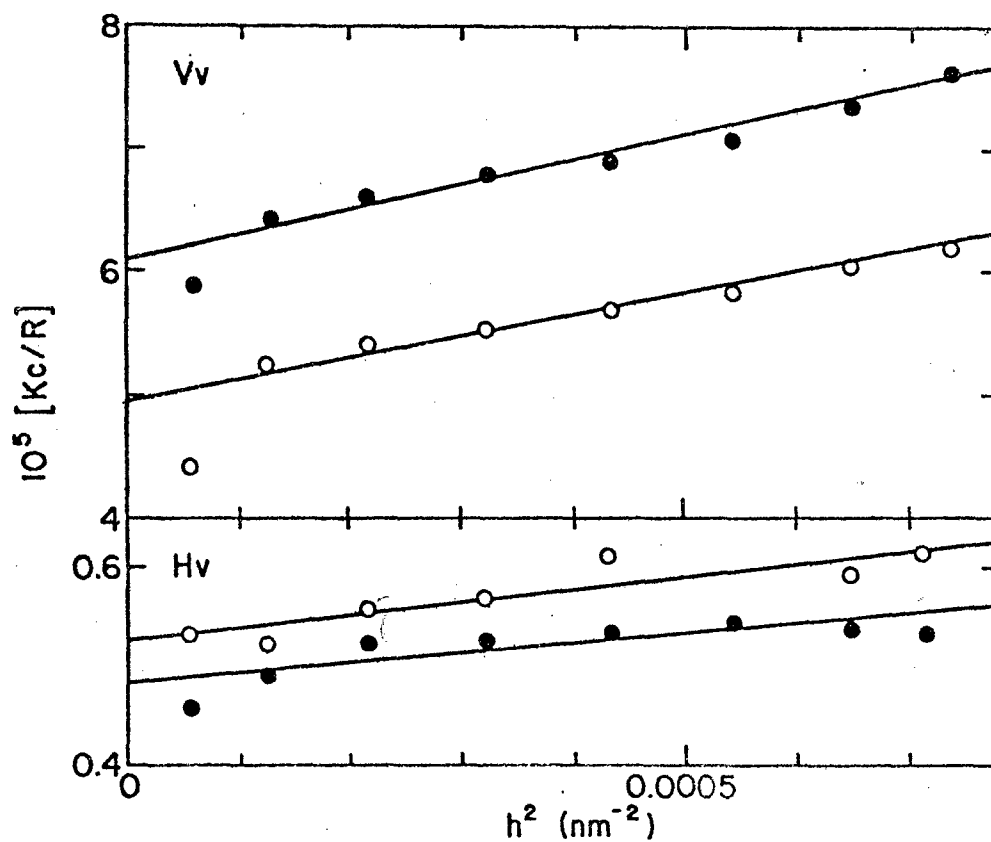


Figure 13 Examples of (c/R_{Vv}) and (c/R_{Hv}) versus h^2 for PBT 72-7, ● ($c = 0.364$ mg/ml) and 72-8, ○ ($c = 0.332$ mg/ml) for solutions treated by all four methods of clarification discussed in the text.

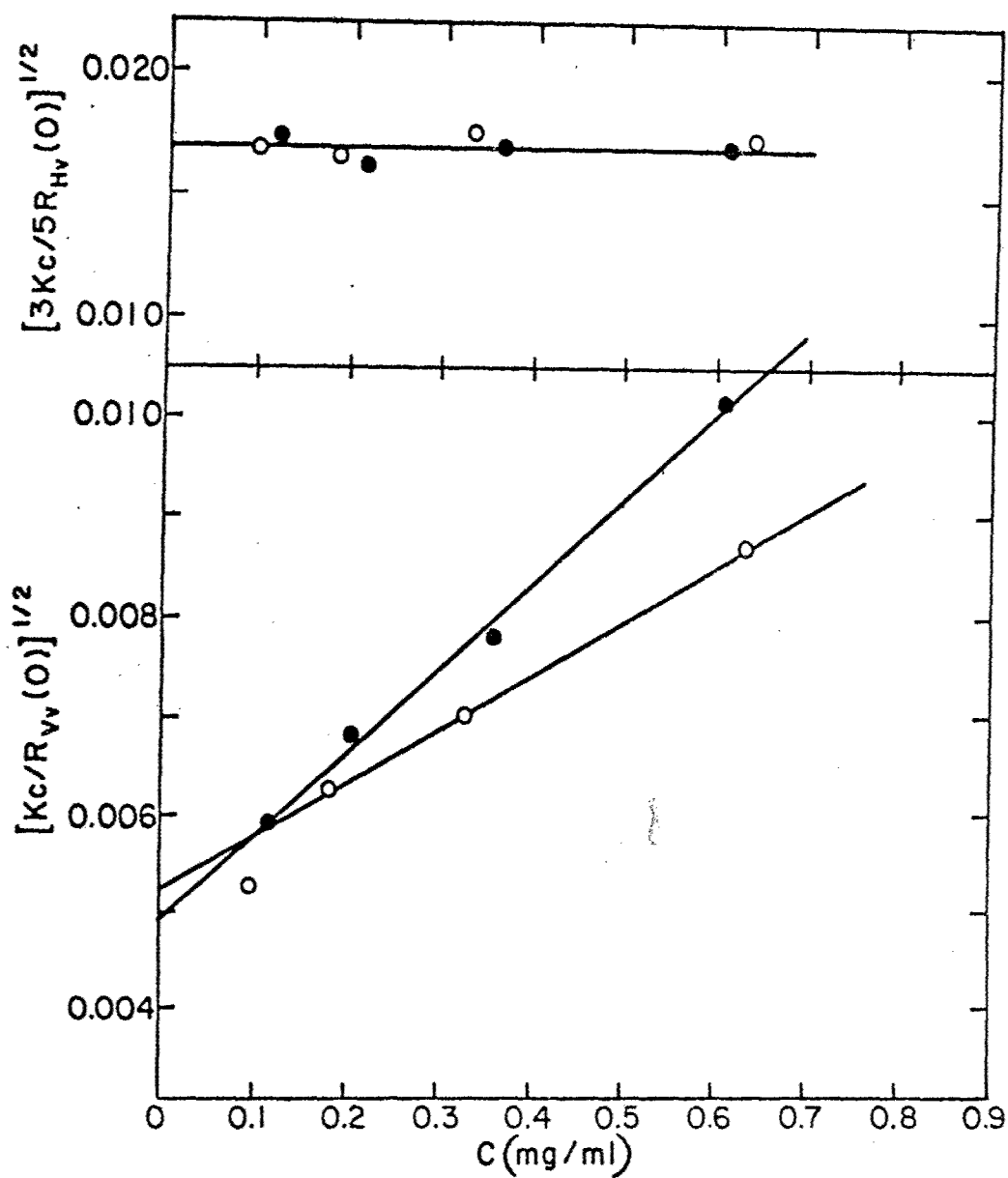


Figure 14 Plots of $[Kc/R_{vv}(0)]^{1/2}$ and $[Kc/R_{Hv}(0)]^{1/2}$ versus c for PBT 72-7, ● and 72-8, ○ for solutions in methanesulfonic acid.

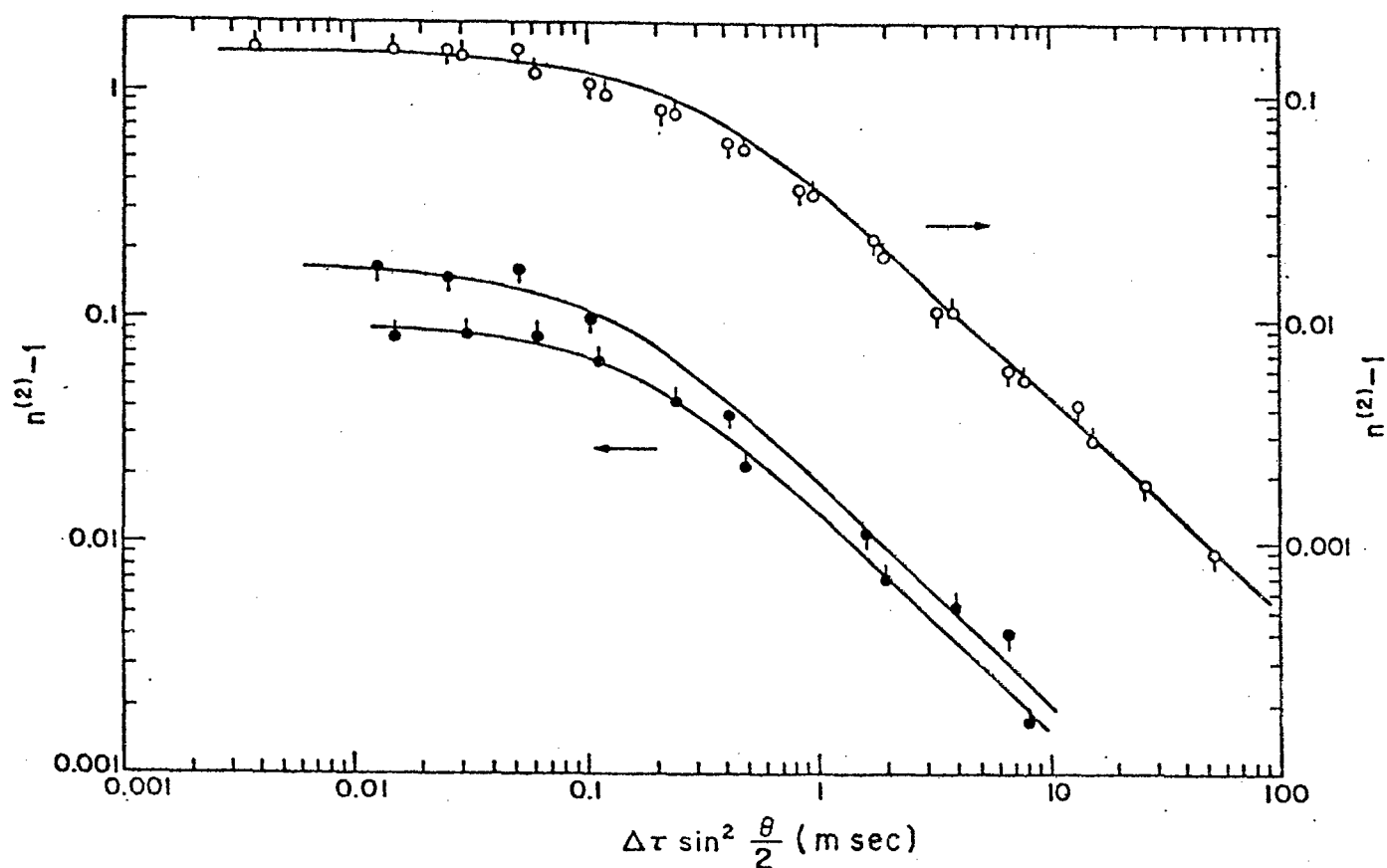


Figure 15 Bilogarithmic plots of $n^{(2)}(\gamma) - 1$ versus $h^2 \Delta \tau$ for PBT 72-7, ● ($c = 0.36 \text{ mg/ml}$) and 72-8, O ($c = 0.33 \text{ g/ml}$), for 45 and 90 degree scattering angle (pips up and down, respectively). The curves represent Eqn. 8 and 11.

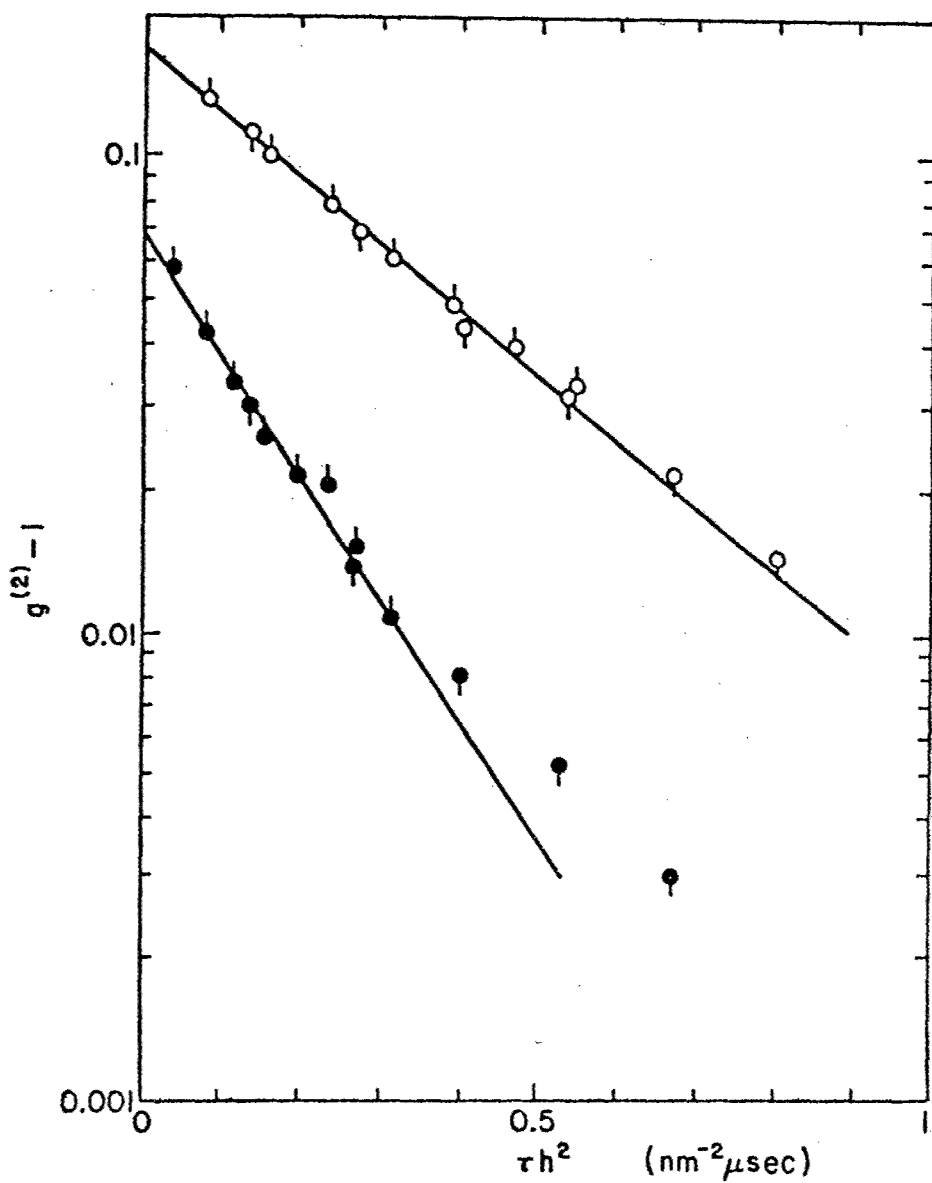


Figure 16 Plots of $\ln(g^{(2)}(\tau)-1)$ versus $h^2 \tau$ for PET 72-7, ● ($c=0.36$ mg/ml) and 72-8, ○ ($c=0.33$ mg/ml), for 45 and 90 degree scattering angle (pips up and down, respectively).

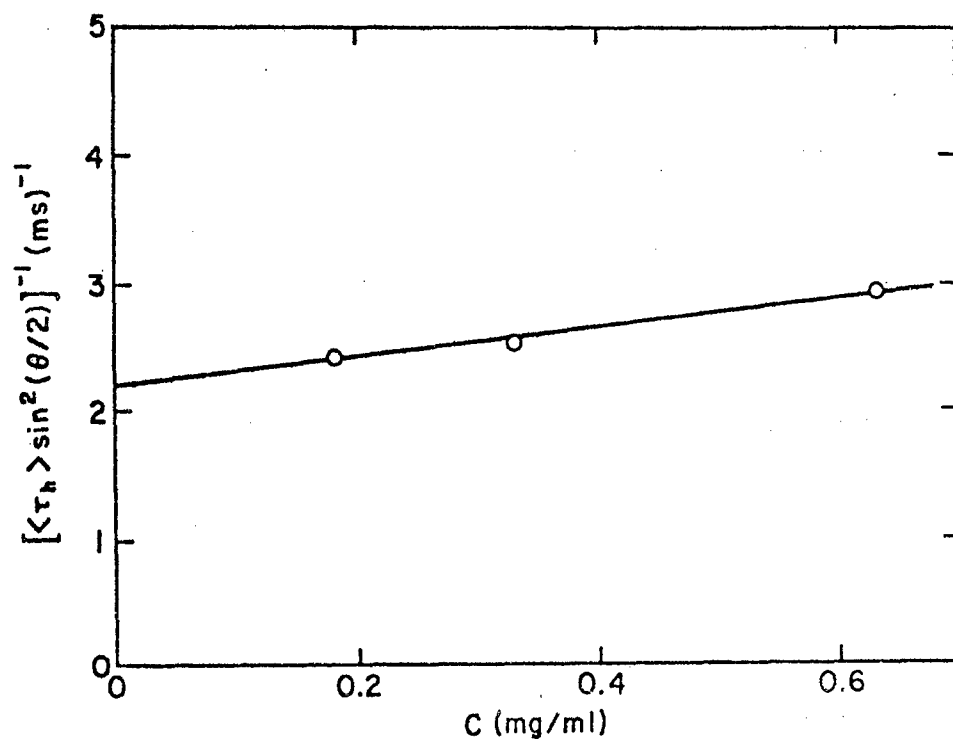


Figure 17 Plots of $[\langle \tau_h \rangle \sin^2(\theta/2)]^{-1}$ versus c for solutions of PBT 72-8 in methane sulfonic acid.

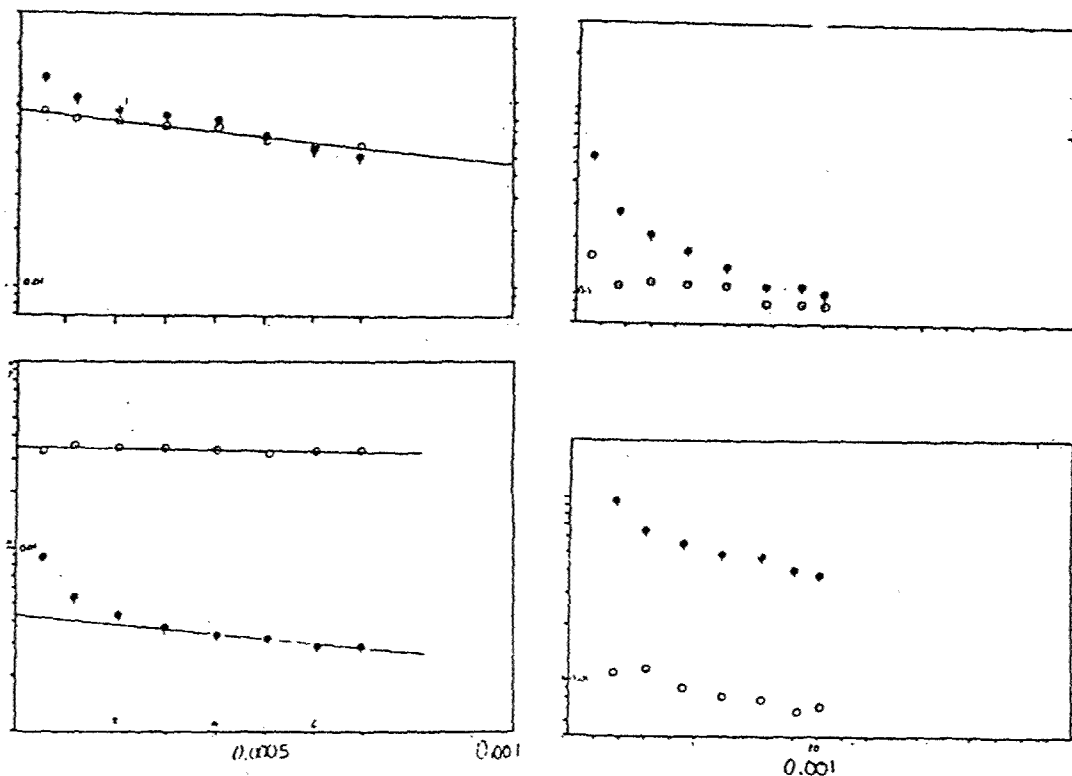


Figure 18

Examples of $\ln R_V$ versus h^2 for solutions of articulated PBO copolymers ($c \sim 0.5 - 0.6$ mg/ml). In each case the sample treatment is designated as filtered, ●, or filtered and centrifuged, ○: a) 292-80 in MSA, 633 nm; b) 292-96 in MSA, 514 nm; c) 352-4 in CSA, 633 nm; and d) 352-4 in MSA, 514 nm.

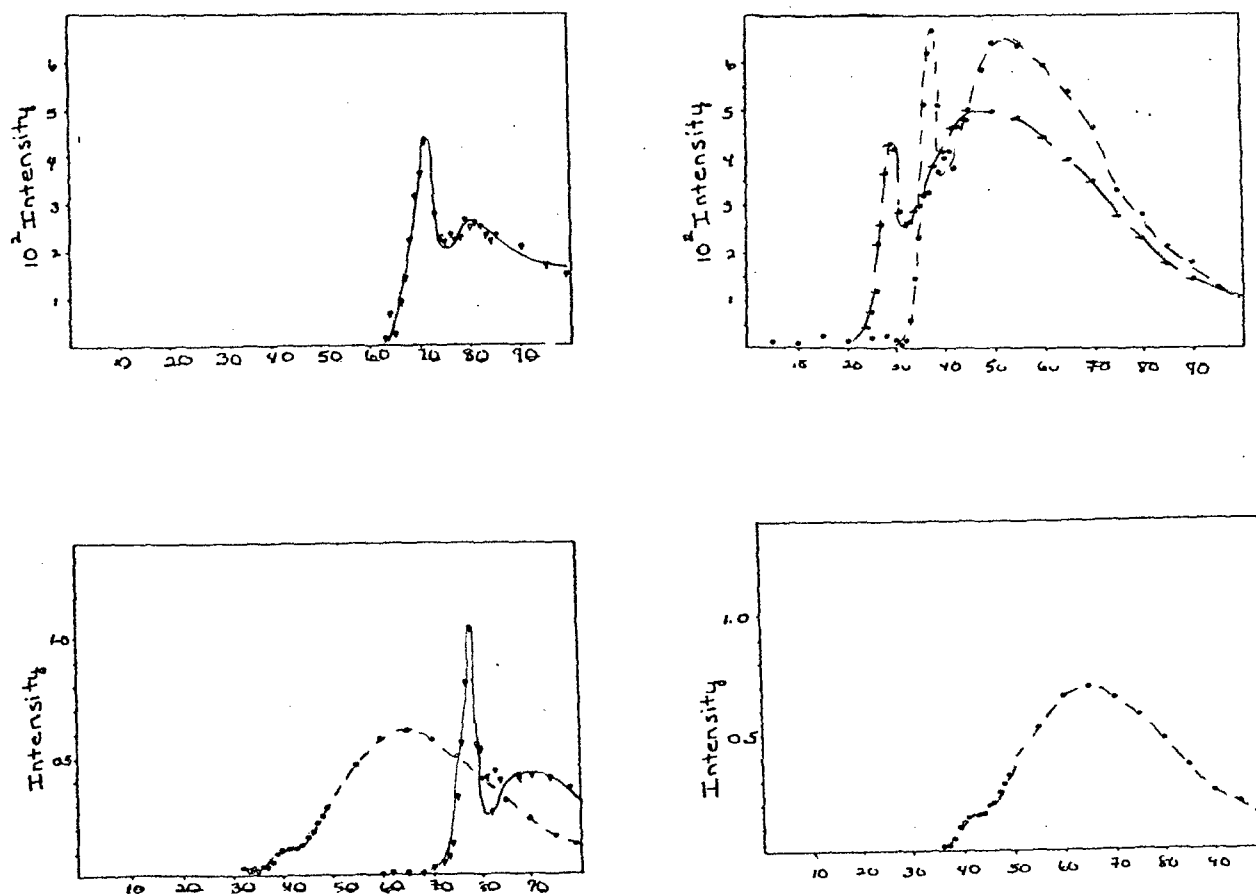
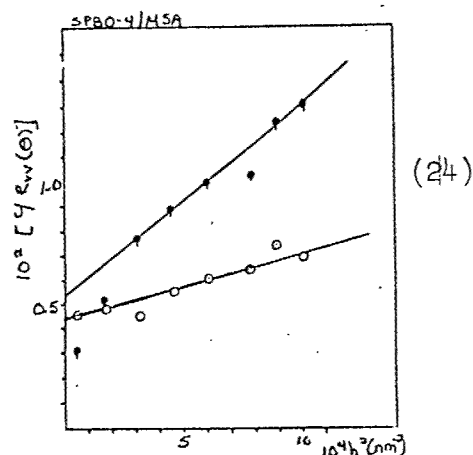
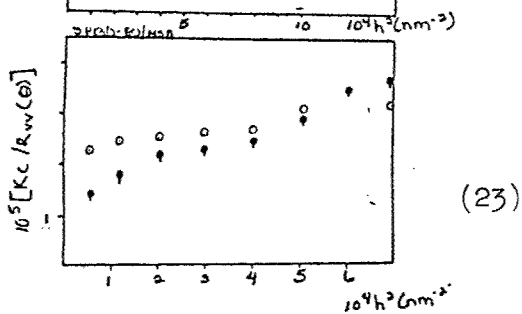
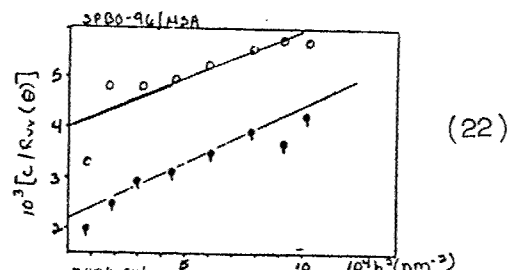
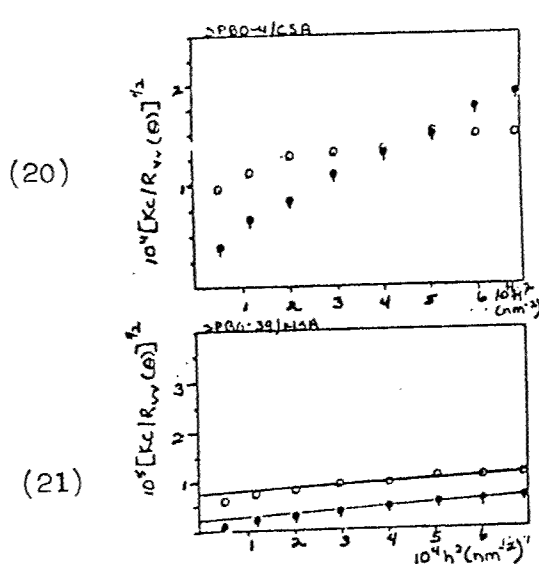


Figure 19

Examples of I_+ fluorescence spectra for solutions of articulated PBO copolymers ($c \sim 0.4 - 0.6$ mg/ml). Excitation wavelengths are 388, — —; 514, ----, or 633 nm, — · —. In each case the R_{Hv} scattering may be seen superposed on I_+ at the excitation wavelength, and intensities are normalized by the peak value of R_{Hv} : a) 292-80 in MSA; b) 292-96 in MSA; c) 352-4 in CSA; and d) 352-4 in MSA.



- Figure 20 Example of Kc/R_{VV} versus h^2 for 292-80 in MSA; 633 nm.
Symbols as in Fig. 18.
- Figure 21 Example of Kc/R_{VV} versus h^2 for 292-96 in MSA; 514 nm.
Symbols as in Fig. 18.
- Figure 22 Example of Kc/R_{VV} versus h^2 for 352-39 in MSA; 633 nm.
Symbols as in Fig. 18.
- Figure 23 Example of Kc/R_{VV} versus h^2 for 352-4 in CSA; 633 nm.
Symbols as in Fig. 18.
- Figure 24 Example of Kc/R_{VV} versus h^2 for 352-4 in MSA; 514 nm.
Symbols as in Fig. 18.

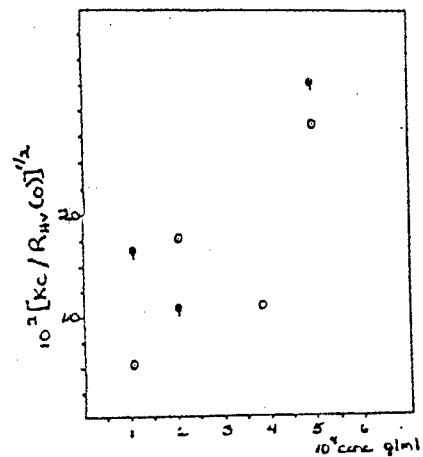
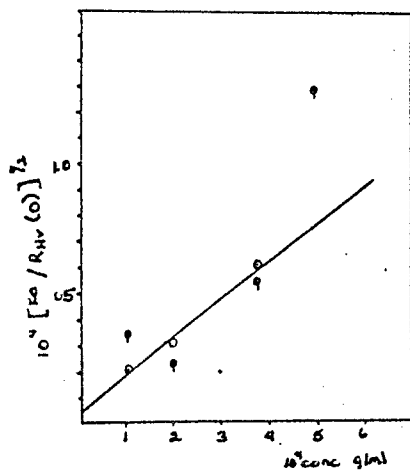
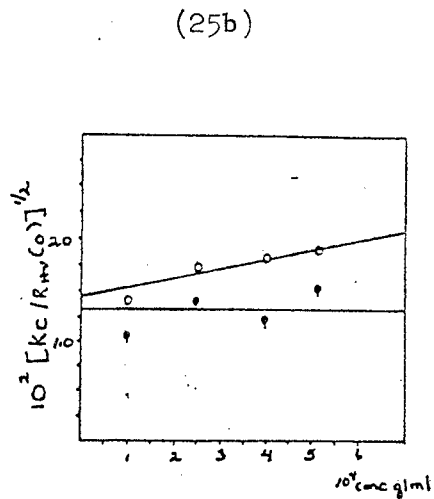
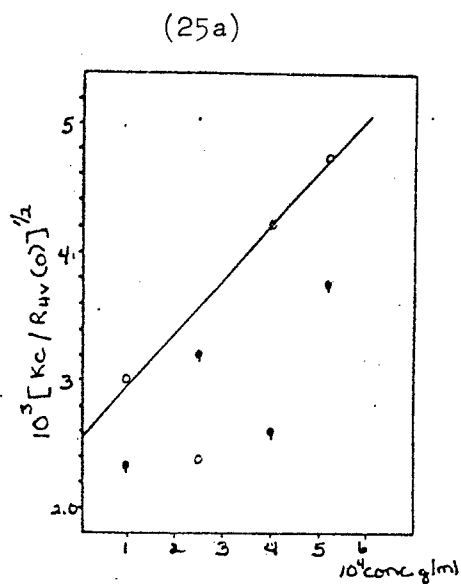
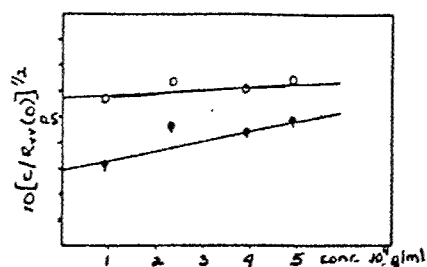
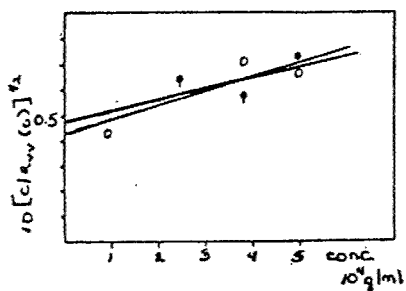


Figure 25 Plots of $(Kc/R(0))^{1/2}$ versus concentration for 292-80 in MSA; 633 nm: a) R_{VV} data and b) R_{HV} data. Symbols as in Fig. 18.

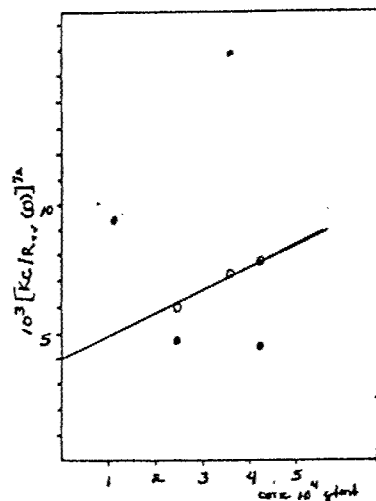
Figure 26 Plots of $(Kc/R(0))^{1/2}$ versus concentration for 352-39 in MSA; 633 nm: a) R_{VV} data and b) R_{HV} data. Symbols as in Fig. 18.



(27)



(28)



(29)

- Figure 27 Plots of $(Kc/R_{VV}(0))^{1/2}$ versus concentration for 292-96 in MSA; 514 nm. Symbols as in Fig. 18.
- Figure 28 Plots of $(Kc/R_{VV}(0))^{1/2}$ versus concentration for 352-4 in CSA; 633 nm. Symbols as in Fig. 18.
- Figure 29 Plots of $(Kc/R_{VV}(0))^{1/2}$ versus concentration for 352-4 in MSA; 514 nm. Symbols as in Fig. 18.

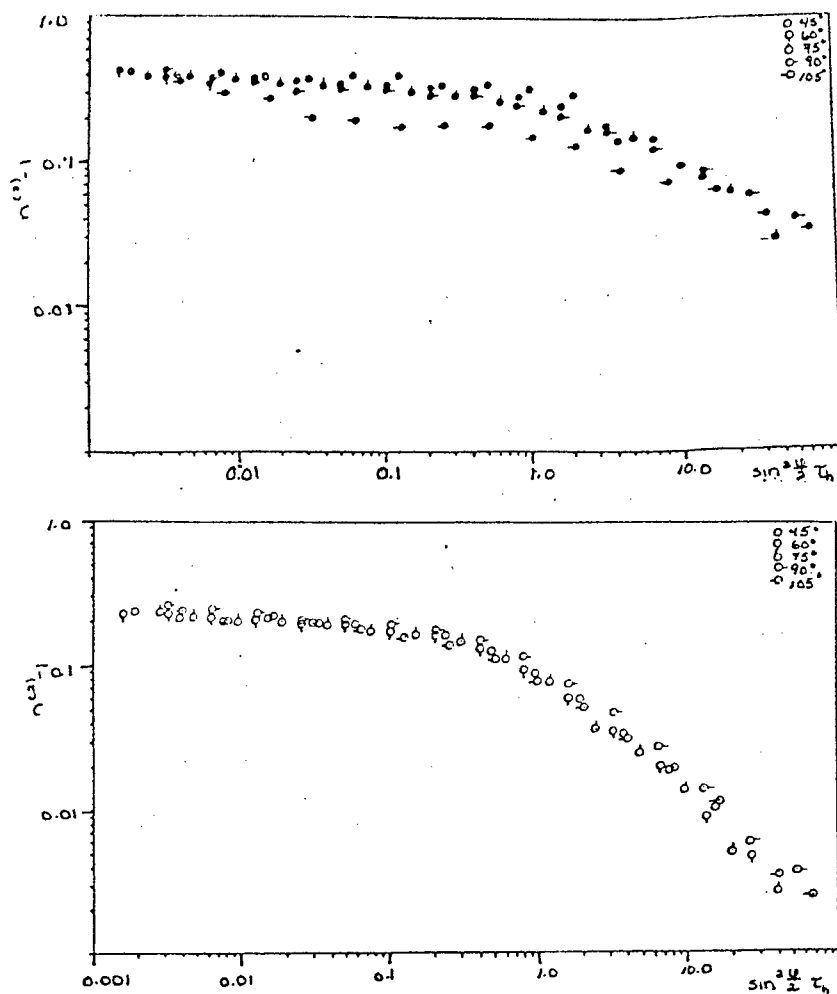


Figure 30 Plots of $n^{(2)}(\Delta\tau/\tau_h)$ versus $\Delta\tau \times \sin^2 \psi/2$ for a solution of 292-80 in MSA ($c = 0.10$ mg/ml). Filled and unfilled symbols as in Fig. 18. Angles indicated as no pip, 45° ; pip down, 60° ; pip up, 75° ; pip right, 90° ; and pip left, 105° .

5. DISCUSSION

5.1 Cryoscopy and Densitometry

Neither the density or the freezing point depression of solutions of PBT are especially sensitive to the state of aggregation. As discussed above with polymeric solutes, the latter is dominated by the conjugate ions from protonation of the solute. The data in Table 3, calculated with $\phi = 1$, indicate that both PBT and its model compound carry 3-4 protons per repeating unit. A similar result obtains for PPTA and the model compound of PBO. As discussed above, the degree of protonation listed for PBO in Table 3 may be too large. Use of $\phi = 1$ for the polymeric solute appears to be justified, even though the interaction terms B_{12} and B_{22} (expressed in molar concentration units) may be large. Thus, if it is assumed that the contributions in Eqn. (40) may be separated into terms with interactions among small molecules, (1), and large molecules, (2), then

$$\phi = 1 + [B_{11} + (m_2/m_1)B_{12} + (m_2/m_1)^2 B_{22}] \frac{m_1}{(1+m_2/m_1)} \quad (46)$$

Since M is about 10^4 for the polymers studied m_2/m_1 is of order 10^{-3} and consequently, $1-\phi \sim -B_{11}m_1$, even though, for example, $m_2 B_{22} = A_2 Mc$ may be relatively large, e.g., 1-2 (see below). Thus, $1-\phi$ is expected to be nearly unity (e.g., 0.8-1), and approximated by the Debye-Huckel relation.⁷ A similar conclusion can be based on treatments discussed by Manning⁶ for which ϕ is found to depend on the ratio ξ of the Bjerrum screening length $e^2/\epsilon kT$ (ϵ is the dielectric constant of the solvent) to the

charge spacing b on the macroion (e.g., $b = L/\nu$). With neglect of the interaction terms among macroions, Manning finds a result for $(m_1^2 B_{11} + m_1 m_2 B_{12}) / (m_1 + m_2)$ that can be put in the form

$$1 - \phi = \psi(\xi) X (X + 2)^{-1} \quad (47)$$

where $2\psi(\xi)$ is ξ if $\xi < 1$ and $2 - \xi^{-1}$ if $\xi > 1$, and X is $\nu' m'_2 / m_1$ in the present case (primes referring to quantities expressed in moles of repeating units of the macroions). The values of ν' calculated with $\phi = 1$ give $\xi \sim 2$ for PBT, and estimates of ϕ with Eqn. (47) are found to be nearly unity, as expected.

The considerable protonation of PBT, PBO and PPTA in strong sulfonic acids is probably crucial for their solubility in these reagents. The intermolecular electrostatic repulsion acts to compensate for the low entropy of disorientation inherent in the dissolution of rodlike chains.²¹

The partial specific volume is somewhat less than the specific volume for the model compounds of PBO and PBT in the two sulfonic acids used, but this effect is much greater with PBT and PBO. Since \bar{v} is not very dependent on concentration, it is of interest to consider the chain diameter calculated from the relation:

$$d = 2(M_L \bar{v}^0 / \pi N_A)^{1/2} \quad (48)$$

For PBT in methane sulfonic acid, this gives the reasonable estimate

$d = 0.47$ nm. The variation of \bar{v}^0 between methane and chlorosulfonic acids indicates that this geometric interpretation may be too simple through neglect of electrostatic interactions. It may be noted that d so calculated is smaller (0.44 nm) in chlorosulfonic acid, which has the smaller ionic strength and longer electrostatic interaction lengths. Similarly, d calculated with \bar{v} replaced by f_v in Eqn. (48) tends to be greater than these estimates for reasonable estimates of the packing efficiency f , (e.g., f is $\pi/2\sqrt{3}$ and for close packed parallel arrays of the rods in hexagonal or rectangular packing, respectively, with $d = 0.49$ nm for the latter).

5.2 Light Scattering Behavior For PBT Polymers

The range of the electrostatic interaction among PBT chains in solution may be characterized by a thermodynamic diameter d_T calculated from A_2 by use of the relations:²²

$$A_2 = A_2^0 [1 - b_1(L/\rho)\zeta + \dots] \quad (49a)$$

$$A_2^0 = \frac{\pi N_A d_T^2}{4M_L} \quad (49b)$$

$$\zeta = M^2 A_2^0 / 4\pi^{3/2} N_A R_G^3 \sim \frac{d_T}{L} \frac{3}{2} \sqrt{\frac{3}{\pi}} \quad (49c)$$

Since $b_1(L/\rho) \ll b_1 = 2.865$ for small L/ρ (e.g., b_1 is zero for $L/\rho = 0$), and because ζ is less than 0.1, $A_2 \sim A_2^0$. With A_2 calculated from Eqn. (2):

$$A_2 = \frac{1 + \frac{4}{5} \delta^2}{M} [\partial \ln(Kc/R_{VV}(0))^{1/2} / \partial c]^0 \quad (50)$$

and $\delta = 0.5$, $M = 12,000$ (see below), the data for PBT 72-8 in methane sulfonic acid give $d_T = 11$ nm. This is surprisingly large, but demonstrates the long-range nature of the intermolecular electrostatic interactions. Indeed, d_T is even larger with solutions in chlorosulfonic acid, which has a lower ionic strength, making it very difficult or impossible to carry out reliable extrapolations to infinite dilution.^{13,23}

The values of $[\eta]$ (in cm^3/g), Ξ^0/η_s , and the data in Table 7 can be used to obtain several estimates of the average contour length of the rodlike chain by use of the relations²⁴

$$R_G^2 = L^2 W(L/\rho)/12 \quad (51)$$

$$R_H = \Xi^0 / 6\pi\eta_s = L/2H(L/\rho, L/d_H) \quad (52)$$

$$M[\eta] = \pi N_A R_G^2 R_H(L/\rho, L/d_H) F^{-1}(L/d_H) \quad (53)$$

Here,

$$\lim_{L/\rho \rightarrow 0} W(L/\rho) = 1 - \frac{1}{5} (L/\rho) + \frac{1}{30} (L/\rho)^2 - \dots \quad (54)$$

$$\lim_{L/\rho < 2} H(L/\rho, L/d_H) = H(L/d_H) \sim 1.887 (L/d_H)^{0.2} \quad (55)$$

$$F(L/d_H) \sim 0.745 H(L/d_H) \quad (56)$$

where the power law approximations are useful for L/d_H in the range 30 to 3,000.¹ Corresponding estimates of the contour lengths may be calculated as

$$L_\eta = \left\{ \frac{2^4 M_L [\eta]}{\pi N_A L^{0.2}} \frac{F}{W} \right\}^{\frac{1}{1.8}} \quad (57)$$

$$L_H = \left\{ \frac{H H^0}{3 \pi \eta_s L^{0.2}} \right\}^{1.25} \quad (58)$$

$$L_{G,H} = \{28(\partial \ell_m(c/R_{Hv})/\partial h^2)^0/W\}^{1/2} \quad (59)$$

$$L_{G,V} = \{36 J(\delta)(\partial \ell_m(c/R_{Vv})/\partial h^2)^0/W\}^{1/2} \quad (60)$$

$$L_H = 5(R_{Hv}(0)/Kc)^0/3\delta^2 M_L \quad (61)$$

$$L_V = (R_{Vv}(0)/Kc)^0/(1 + \frac{4}{5} \delta^2) M_L \quad (62)$$

Since L/ρ is small (rodlike limit), F , W and H can be evaluated by the approximations given above, and L becomes the length of the rodlike chain. In this case, for polydispersed samples, the relations

$$L_W(L_Z/L_W)^{4/9} \sim L_\eta \quad (63)$$

$$L_W = L_V = L_H \quad (64)$$

$$(L_Z L_{Z+1})^{1/2} = L_{G,H} = L_{G,V} \sim L_{\Xi} \quad (65)$$

provide representation in terms of well-defined averages of L .

Values of L_η , L_{Ξ} and $L_{G,H}$ given in Table 15 do not depend on δ , and the entries for $L_{G,V}$ and L_V do not vary too much with δ for small δ ; the entries listed were calculated with the rodlike limits for F, W and H. Since $J(\delta) \geq 1$, it can be seen that $L_{G,H}$ is less than $L_{G,V}$ for any estimate of δ , indicating that $L_{G,V}$ reflects residual association. For PBT 72-8, $L_{G,H}$ is also smaller than L_{Ξ} , the latter being about equal to L_V (calculated with a reasonable estimate for δ , see below). The larger values of $L_{G,V}$ and L_{Ξ} in comparison with $L_{G,H}$ are discussed further below.

Two methods to estimate δ are available:¹³

- (1) Use of the depolarization $\rho_V^0 = (c/R_{V_V}(0))^0 / (c/R_{H_V}(0))^0$ and Eqns. (2) and (3) which give

$$\rho_V^0 = \frac{3\delta^2}{5+4\delta^2};$$

- (2) Use of the R_{H_V} data alone in the form $\delta^2 = (\delta^2 L_H / L_{G,H}) (L_Z / L_W) (L_{Z+1} / L_Z)^{1/2}$, which requires an estimate for

the molecular polydispersity to compute δ . The former gives δ equal to 0.28 and 0.33 for 72-8 and 72-7, respectively, whereas the latter gives $\delta = 0.50$ for both, based on reasonable estimates for the polydispersity¹⁰ ($L_Z/L_W = 1.4$ and $L_{Z+1}/L_Z = 1.2$). The larger value of δ obtained by use of only the R_{Hv} scattering data is in accord with the disproportionately large effects of association on $(c/R_{Vv}(0))^0$ as compared with $(c/R_{Hv}(0))^0$ that have precedence with other optically anisotropic polymers, both flexible and rodlike.¹⁻⁴ One manifestation of this behavior, also found here for PBT 72-7 and 72-8, is the greater effect of centrifugation on R_{Vv} as compared with R_{Hv} . Such effects indicate that the polarizability tensors of the rodlike components of the aggregates are orientationally independent, which is reasonable. For this reason, the estimate $\delta \sim 0.5$ is believed to be the more reliable. This relatively large δ is only possible if L/ρ is small, in accord with the expected rodlike structure of PBT.

If the R_{Vv} scattering is affected by residual association, then the use of Eqns. (60) and (62) to obtain estimates for L is not meaningful. For example for 72-8, comparison of M_w calculated as $5(R_{Hv}(0)/Kc)^0/3\delta^2 = 12,000$ and M_w calculated as $(R_{Vv}(0)/Kc)^0/(1+4\delta^2/5) = 30,000$ (both with $\delta = 0.50$) presumably differ since the latter includes the effect of association, with about 2-3 molecules per aggregate on a weight average. Similarly, Eqn. (60) cannot be used to relate R_G to L , unless the aggregates are formed by parallel arrays of the rodlike chains. If the latter is assumed, then comparisons of $L_{\overline{H}}$ and $L_{G,H}$ show that the aggregation increases the average length of the population. Aggregation with the chains in nearly parallel arrays is in accord with the observations, and represents a reasonable stable form of association.

The effects of association on the light scattering data on PBT 72-8 solutions discussed above are less pronounced than those with PBT 72-7. As pointed out in the preceding, the R_{VV} and photon correlation light scattering data were more severely altered by centrifugation for 72-7 than for 72-8. Moreover, the photon correlation data for 72-7 gave values of $n^{(2)}(0)$ and $g^{(2)}(0)$ too small for the optical arrangement used (see Table 9), suggesting that $r < 1$, consistent with the presence of large moities, with very large τ_h . Nonetheless, $\langle \tau_h \rangle$ is only about half the value found for 72-8 when measured near the top of a cell after centrifugation (see Tables 8. and 9). Estimates of $\langle \tau_h \rangle$ near the bottom of such a cell are larger, but $\langle \tau_h \rangle h^2$ is not independent of h , indicative of extreme heterogeneity. This behavior indicates that the longer chains among the population are selectively sedimented during centrifugation of 72-7 (in contrast with 72-8), showing that these are involved in the aggregate structures that affect the light scattering data. The aggregates are not so large that they fully sediment to the cell bottom, even after centrifugation for 24 hr (5,000 g), but they are sufficiently large and numerous to have a marked effect on the light scattering behavior.

The effect of the aggregates on $[\eta]$ is also complex. As seen in Table 15, L_η calculated with Eqn. (57), and the rodlike limits for F and W , is somewhat larger than $L_{G,H}$ and L_E for 72-8, and differs between 72-8 and 72-7. Unlike the treatment of light scattering data, it is not possible to remove some of the effects of the aggregates by data treatment methods (e.g., neglect of the R_{VV} data for small angles, etc.

The specific viscosity η_{sp} is a sum over the product of the number of moities per unit volume v_i and the intrinsic viscosity $[\eta]_i^{(v)}$ expressed as volume per number of moities ($[\eta]_i^{(v)} = M_i[\eta]_i/N_A$)

$$[\eta] = \lim_{c \rightarrow 0} \eta_{sp}/c = \frac{\sum [\eta]_i^{(v)} v_i}{c} \quad (66)$$

Association can alter both $[\eta]_i^{(v)}$ and v_i . For example, for a rodlike chain,

$$[\eta]^{(v)} = \frac{\pi}{24} L^3 F^{-1}(L/d_H) \quad (67)$$

Since F depends only weakly on d_H , association with the rodlike molecules in parallel arrays (no change in L) will have little effect on $[\eta]^{(v)}$, but will greatly decrease $[\eta]$ as fewer moities will contribute to the sum in Eqn. (66); (essentially, M_L for the aggregate is enhanced, thereby decreasing $[\eta]$). If the parallel aggregates have larger L , then $[\eta]$ could be increased; effects of this type have been calculated for dimers of rodlike molecules for specific geometries.²⁵ (Of course, other forms of aggregation with more complex effects can be envisioned). With a polydispersed sample, formation of aggregates with the chains in parallel array might not cause a large increase in the average L . Thus, the difference in $[\eta]$ (and hence L_η in Table 15) for 72-8 and 72-7 might reflect increased fraction of parallel aggregates for 72-7; in fact, the decrease in L_η is quantitative in

accord with the increase in L_V .

A working model for the association of PBT chains can be postulated on the basis of these observations. A substantial fraction of the chains appear to be bound in aggregates with the chains held in approximately parallel array, with 2-3 chains per aggregate. These aggregates are probably metastable, and may preferentially involve the longer chains. A much smaller fraction of the chains are involved in larger aggregates, perhaps with ill-defined shape. These large aggregates are far more prevalent in 72-7 than in 72-8, and are responsible for pronounced effects on the R_{VV} and photon correlation scatterings.

The difference in the aggregation of PBT 72-7 and 72-8 may be attributed to the nature of the solvation of PBT in polyphosphoric acid and methane sulfonic acid. At the conditions of the polymerization, PPA is an oligomer²⁶ (DP of about 5), and probably complexes with the growing PBT to have the effect of short branches. During precipitation in water, these are hydrolyzed and removed as the polymer precipitates, but they could suppress parallel close packing of the rodlike chains during the precipitation process by steric effects. This protection is not available when the polymer is precipitated from methane sulfonic acid, the difference possibly giving rise in the latter case to the formation of metastable aggregates in larger number and size. Since these are apparently not easily dissociated, the implications are clear if solutions are to be processed into well oriented solids.

5.3 Light Scattering Behavior For Articulated PBO Copolymers

Both total intensity and photon correlation light scattering data reveal the presence of aggregated material in the four articulated PBO copolymers studied, e.g., 352-4, 292-80, 292-96, and 352-39, having comonomers with structure I, II, III, and IV, respectively. None of them showed nematic behavior in methane sulfonic acid (e.g., Table 10), although two, 292-96 and 352-39, developed marked flow birefringence. The extreme variation of R_{VV} and $\langle \tau_h \rangle$ on solution treatment (e.g., filtration and centrifugation history) shows that at least the filtered, but uncentrifuged solution contains rather large aggregate moieties. The small estimate for $[Kc/R_{VV}(0)]^0$ given in Table 11 for the centrifuged solutions suggests that even these are not free of aggregated material. Although R_{HV} was usually much less than R_{VV} , with solutions of 352-4 in chlorosulfonic acid, R_{HV} was very large for the filtered solution, but decreased to nearly zero after centrifugation. The latter behavior indicates that the large (aggregated) moieties were at least partially ordered in this system.

With polymer 292-80, values of $[Kc/R_{VV}(0)]^0$, Ξ^0/η_s and $(\partial \ln c / R_{VV} / \partial h^2)^0$ all indicate a very large species, even for the centrifuged solution; the value of $[Kc/R_{HV}(0)]^0$ indicates a low degree of order in the dominant scattering species. Since $[R_{VV}(0)/Kc]^0$ is twenty times M_w estimated by SEC (see section 4.5.2), it seems certain that the light scattering data are skewed by the presence of an aggregate species. This aggregation may also prevent attainment of proper data on phase equilibria. Although $[Kc/R_{HV}(0)]^0$ is considerably larger than $[Kc/R_{VV}(0)]^0$, it is still too small to be consistent with a completely dissociated molecule with

a completely dissociated molecule with $M_w = 8,000$. For example, these two values would give $\delta > 1$ (see Eqn. 3), which is not possible; a mitigating effect might be our use of $\partial n / \partial c$ for PBO instead of the copolymer. The data could be consistent with aggregates in a semi-parallel array, such that some enhancement of $M\delta$ for the aggregate occurs, along with much more marked enhancement of M , Ξ^0 , and R_G . For example, with sample 292-80, an aggregate species with about 20 molecules trapped in an array with an ellipsoidal shape. If treated by this model, the data on R_G and Ξ^0 / η_s combines to give an aggregate with a major to minor axis ratio of 500, and a major axis some 3000 nm long (and only 6 nm wide). Such an asymmetric structure implies near parallelism of the aggregated molecules, perhaps giving rise to the apparently large $M\delta$ mentioned above.

A similar situation appears to obtain with the other polymers studied; incomplete SEC prevents a detailed analysis at this time. Nonetheless, it appears that the articulated PBO polymers studied are each aggregated, even at the low concentrations used in light scattering. This circumstance does not augur well for the attainment of well developed flow induced orientation in more concentrated solutions, and it is suggested that further work on articulated PBO copolymers be replaced by work on articulated PBT copolymers. The observation of nematic solutions for several of the PBT copolymers studied (see Table 10) is consistent with this recommendation.

5.4 Fluorescence And Absorption Spectroscopy On PBT Polymers

Several features of the fluorescence and absorption behavior of solutions of PBT 72-7 and 72-8 are noteworthy in connection with the association detected for these two polymers.

- 1) μ tends to be larger for 72-7 than for 72-8 in the long wavelength portion of the spectrum ($\lambda > 480$ nm), with the difference greater for solutions in methane sulfonic acid than those in chlorosulfonic acid;
- 2) the apparent quantum yield K^0 is greater for solutions of 72-7 than for those of 72-8;
- 3) values of K_q are ten-fold greater for solutions in chlorosulfonic acid than for those in methane sulfonic acid, and K_q is greater for 72-7 than for 72-8;
- 4) generally, $(\langle n \rangle_{F1} / \langle n \rangle_{STD})_p$ is increased slightly on centrifugation.

The failure to observe fluorescence emission for which $\langle n \rangle_{F1} / \langle n \rangle_{STD}^c$ increased with increasing c (negative K_q) to accompany the quenched fluorescence (positive K_q) suggests that excimer or exciplex formation is not implicated in the observed quenching of the fluorescence emitted on excitation at 514 nm. The constant K_q is equal to the product $k_q \tau_E$ of the lifetime τ_E of the excited state and the rate constant k_q for the process by which the excited state decays to the ground state and emits the fluorescent radiation. An estimate of 1-5 ns was obtained for τ_E by measurement of the fluorescence decay following excitation by a light pulse. Consequently, k_q is of order $10^{11} \text{ l mol}^{-1} \text{ s}^{-1}$, which is far too large for a diffusion-controlled quenching rate constant for collision of the rodlike chains.

This is further evidence that excimer or exciplex formation is not implicated in the quenching. The large values of K_q observed can be accounted for by non-radiative columbic interaction between the excited species and another moiety with smaller (or zero) K^0 . The data are consistent with the assumption that the aggregated species is both more absorbant and fluorescent for excitation at 514 nm (e.g., larger μ and K^0) than is the fully dissolved polymer, with quenching caused by columbic interaction between the excited aggregated species and the individual chain. The increased K^0 could be caused by decreased quenching by collision with solvent for chains deep within the aggregate species, by small differences in the population of rotational isomers of isolated chains completely dissolved, in comparison with chains held in aggregate structures in parallel array, or by an altered electronic structure of the chains in the aggregate. The difference between K_q in methane sulfonic acid and chlorosulfonic acid is in accord with the role of a columbic interaction. As mentioned above, the increase in $(\langle n \rangle_{F1} / \langle n \rangle_{STD})_P$ on centrifugation is consistent with the removal of a strongly absorbing fluorescent species, providing further support for implication of the aggregated species in the fluorescence behavior.

Similar behavior is found with the data in Table 5 for the series of PBO polymers, but these data are not amenable to complete interpretation since several factors may affect K^0 and K_q among the samples. For example, both may depend on chain length, irrespective of any association. Thus, the marked decrease of K^0 observed for

160-3 in comparison with 160-1 may reflect the effects of end groups in the lower molecular weight 160-1. On the other hand, the increase in K^0 observed with further increase in chain length may reflect increased association with increased chain length. The difference among K^0 for samples 160-4 and 5 for emission at 576 and 686 nm indicates distinct emitting species, perhaps related to the aggregate structures present. With M estimated from $M_L \eta$ using Eqn. (57), values of K_q range from 1 to $2 \times 10^{12} \text{ L mol}^{-1} \text{ s}^{-1}$ for the data in methane sulfonic acid, if τ_c is taken to be 2 ns. Thus, as with PBT, K_q is in the range expected for nonradiative columbic interactions. Since a quantitative model for the effects of association on K^0 and K_q is lacking, we can only conclude that the fluorescence data on PBO are in accord with the postulate that chain length dependent association of PBO obtains in both methane and chlorosulfonic acids, but cannot use the data to specify the degree of association.

TABLE 15
APPARENT CONTOUR LENGTHS
FOR TWO PBT POLYMERS ^(a)

	Polymer	
	72-8	72-7
L_{η}	135 ^(b) _{nm}	120 ^(b) _{nm}
L_{Ξ}	130 ^(b)	60 ^(b)
$L_{G,H}$	85	90
$J^{-1/2}(\delta) L_{G,V}$	150	170
$L_{G,V}$	190 ^(c)	250 ^(c)
$\delta^2 L_H$	15	16
L_H	55 ^(c)	60 ^(c)
$(1 + \frac{4}{5} \delta^2) L_V$	165	190
L_V	135 ^(c)	150 ^(c)

(a) Calculated with the rodlike limites for H, F and W.

(b) Calculated with $d_H = 1$ nm.

(c) Calculated for $\delta = 0.5$.

6. CONCLUSIONS

Total intensity and photon correlation light scattering on a PBT polymer show it to be rodlike, with length $L_w = 55$ nm. The data also reveal that the polymer is associated, even at very high dilution, probably in metastable aggregates. The differences found among the properties of solutions of PBT 72-7 and 72-8 show that at least some aspects of the aggregation are influenced by the processing history of the polymer (in accord with the metastable nature of the aggregates). The repulsive electrostatic interactions resulting from the extensive protonation of PBT in the strong sulfonic acids used as solvents is probably essential for its dissolution. More short-ranged interactions resulting from solvation by nonelectrolytes with solubility parameter close to PBT do not effect dissolution, even though they may be adsorbed in considerable concentration in some cases.²⁷ Similar behavior has also been reported for coil-like heterocyclic polymers.⁴

The difficulty of complete dissolution of the metastable aggregates does not imply that the attractive interactions responsible for their formation are unusually large. Even dispersion forces would result in an appreciable attractive interaction when summed over the length of rodlike chains held in (nearly) parallel array. The nearly planar rodlike configuration available to PBT and PBO may increase the stability of such aggregate structures, but similar problems of metastable association have been reported, for example, for cellulose esters (which do not have a rodlike conformation in

dilute solution). It can be expected that polymers with a helicoidal conformation with overall rodlike structure may also be subject to the formation of metastable intermolecular aggregates. As may be seen by the preceding discussion, the presence of such aggregation may not be evident on the basis of one physical measurement (e.g., only the R_{Vv} total intensity scattering, etc.).

II. RHEOLOGICAL AND RHEO-OPTICAL STUDIES ON SOLUTIONS OF PBT

S. Venkatraman, Y. Einaga, and G.C. Berry

1. INTRODUCTION

Some rheological and rheo-optical properties of PBT solutions will be discussed in the following. In the next section, rheological properties of a solution of PBT in polyphosphoric acid (PPA) will be discussed; the data cover the temperature range 28 to 145°C. The results show that the rheological properties studied are relatively insensitive to temperature over the span 90 to 145°C. In subsequent sections, both transient and steady-state rheological and rheo-optical properties are reported for solutions of PBT in methane sulfonic acid (MSA). The results reveal that the onset of nonlinear behavior depends both on the rate of deformation relative to a solution time constant τ_c (see below) and the total strain imposed on the sample. The relation of τ_c to time constants observed for stress and birefringence relaxation following steady-state flow will also be discussed.

2. RELATIONS FOR RHEOLOGICAL AND RHEO-OPTICAL ANALYSIS

The relations needed to analyze the rheological and rheo-optical data discussed in subsequent sections are given in here for convenience. Experiments to be discussed include:

- 1) Creep and recovery
- 2) Response to a sinusoidal deformation
- 3) Stress-growth at constant shear rate
- 4) Steady-state flow
- 5) Steady-state flow birefringence
- 6) Stress relaxation
- 7) Birefringence relaxation

For small stress levels, the linear creep compliance $J_0(t)$ can be expressed in the form²⁸

$$J_0(t) = R_0(t) + t/\eta_0 \quad (68)$$

where η_0 is the viscosity and $R_0(t)$ is the linear recoverable compliance, with the value

$$R_0 = \lim_{t \rightarrow \infty} R_0(t) \quad (69)$$

being the steady-state linear recoverable compliance. The components $J'(\omega)$ and $J''(\omega)$ of the frequency dependent complex compliance are related to $R_0(t)$ and η_0 by the expressions

$$J'(\omega) = R_0 - \omega \int_0^{\infty} [R_0 - R_0(t)] \sin(\omega t) dt \quad (70)$$

$$J''(\omega) = (\omega\eta_0)^{-1} + \omega \int_{-\infty}^{\infty} [R_0 - R_0(t)] \cos(\omega t) dt \quad (71)$$

such that

$$\lim_{\omega \rightarrow 0} J'(\omega) = R_0 \quad (72)$$

$$\lim_{\omega \rightarrow 0} [\omega J''(\omega)]^{-1} = \eta_0 \quad (73)$$

Alternatively, the components $\eta'(\omega)$ and $\eta''(\omega)$ of the complex viscosity can be defined in terms of $J'(\omega)$ and $J''(\omega)$ by the relations

$$\eta' = [\omega J''(1 + \tan^2 \delta)]^{-1} \quad (74)$$

$$\eta'' = [\omega J'(1 + \tan^{-2} \delta)]^{-1} \quad (75)$$

where $\delta = J''/J'$. For some materials, the steady-state viscosity η_κ at shear rate κ is approximately given by

$$\eta_\kappa \approx [\eta'(\omega)^2 + \eta''(\omega)^2]_{\omega=\kappa}^{1/2} \approx \eta'(\omega)|_{\omega=\kappa} \quad (76)$$

Steady-state of properties to be considered here include the limiting values at low shear rate of the viscosity η_0 , the linear steady-state recoverable compliance R_0 (often denoted J_e^0), and the intrinsic birefringence Δn_∞ . In addition to these parameters, we will also be interested in the following functions, involving ratios of steady-state

properties at rate of strain κ divided by an appropriate limiting value:

$$\eta_{\kappa}/\eta_0 = Q(\tau_c \kappa) \quad (77)$$

$$R_{\kappa}/R_0 = P(\tau_c \kappa) \quad (78)$$

$$\Delta n/\Delta n_{\infty} = M(\tau_c \kappa) \quad (79)$$

Here, η_{κ} is the ratio σ/κ of the shear stress σ to the shear rate κ measured in steady-state flow, R_{κ} is the ratio γ_R/η_{κ} of the ultimate recoverable strain γ_R following cessation of steady-state flow to the stress imposed during the flow, and Δn is the difference in the principal components of the refractive index ellipsoid of the solution; Δn increases from 0 to Δn_{∞} as $\tau_c \kappa$ increases from zero. The characteristic time τ_c is given by

$$\tau_c = \eta_0 R_0 \quad (80)$$

With the systems studied in this part, it is possible to determine each of the limiting parameters η_0 and R_0 , so that the functions Q and P in Eqns. 77 and 78 are well defined. For solutions with φ about equal to or larger than φ_c , this is not always possible.

Although we will not report data on the first normal stress difference $N_{\kappa}^{(1)}$, it will be convenient to refer to the function

$$S_{\kappa} = \frac{N_{\kappa}^{(1)}}{2(\eta_{\kappa} \kappa)^2} \quad (81)$$

and its limiting value S_0 at small κ , and to define the ratio

$$S_{\kappa}/S_0 = N(\tau_c \kappa) \quad (82)$$

Of course, for simple fluids,²⁹ $S_0 = R_0$. On the other hand, there is no reason to believe that P and N are equal for all $\tau_c \kappa$, see below.

In Eqns. 77, 78 and 82 Q , P and N have been written as explicit functions of the reduced shear rate $\tau_c \kappa$. Experimental studies on solutions of flexible chain polymers,³⁰ and theoretical studies³¹ have shown that $\tau_c \kappa$ is a useful and natural variable to use in expressing the dependence of Q , P and N on κ . For example, for many materials, the functions so defined are independent of temperature. In addition, it has been found that for a given solute, Q and P are often nearly independent of ϕ over a wide range. Of course, deviation from this behavior must be expected for large $\tau_c \kappa$, in the so called "upper Newtonian" range for which, for example, Q exhibits a plateau value that depends on ϕ . For flexible chain polymers, Q is unity for small $\tau_c \kappa$, and crosses over to a decreasing function of $\tau_c \kappa$ for $\tau_c \kappa$ in the range of unity. Similarly, P is unity for small $\tau_c \kappa$, but the behavior for large $\tau_c \kappa$ is less easily summarized. Typically, with increasing κ , P decreases from its limiting value for very small $\tau_c \kappa$ for polymers with a broad distribution of molecular weight, but may depend only weakly on $\tau_c \kappa$ for polymers with a narrow molecular weight distribution.

The function M depends on the distribution of molecular orientations with the flow direction, and the usual relations are based on an assumed coincidence of the principal directions of the stress and

refractive index ellipsoids; this approximation is termed the stress-optical law. Thus, for shear flow, the difference Δp of the two principal stresses in the flow plane is related to the shear stress $\eta_c \dot{\gamma}$ and the first normal stress difference N_1 by the expressions (see, for example, ref. 32, section 1.2)

$$\Delta p \sin 2\chi' = 2 \eta_c \dot{\gamma} \quad (83)$$

$$\cot 2 \chi' = S_1 \eta_c \dot{\gamma} \quad (84)$$

where χ' is the angle between the flow direction and a principle stress axis in the flow plane (chosen so that $\chi' \leq \pi/4$). The stress-optical law assumes that

$$\Delta n / \Delta p = C \quad (85a)$$

$$\chi = \chi' \quad (85b)$$

where χ is the extinction angle locating the cross of isocline (i.e., the locus of minimum intensity in the flow plane) defining the angle in the flow plane between the flow direction and a principal axis of the refractive index ellipsoid ($\chi \leq \pi/4$). Coleman and coworkers³³ have demonstrated that these relations are expected to apply for simple fluids in the limit of what are termed "slow flows", for which the limiting relations at small $\tau_c \dot{\gamma}$ obtain:

$$\Delta n = 2 C \eta_0 \dot{\gamma} / \sin 2\chi \quad (86)$$

$$\cot 2 \chi = S_0 \eta_0 \dot{\gamma} \quad (87)$$

They also find that the stress-optical law cannot be generally assumed for larger $\tau_c \dot{\gamma}$. Nonetheless, experience has frequently shown that

Eqns. (86) and (87) can be used with constant C even for $\tau_c \kappa$ large enough that $Q < 1$, if modified by substitution of η_0 and S_0 by η_κ and S_κ , respectively (e.g. examples cited in section 1.4 of reference 32). Equations (87) and (88) so modified give Δn implicitly as a function of $\tau_c \kappa$ using Eqns. (77) and (78), see below.

The preceding discussion, with Eqns. (69-87) is concerned with steady-state rheological or rheo-optical properties. In the following, some transient measurements will also be reported. For small applied stress σ , Eqn. (68) defines the transient creep behavior, one example of the transient measurements to be reported. More generally, the creep compliance $J_\sigma(t)$ defined by

$$J_\sigma(t) = \gamma_\sigma(t)/\sigma \quad (88)$$

where $\gamma_\sigma(t)$ is the strain at time t following imposition of shear stress σ will be given; of course $J_\sigma(t)$ reduces to $J_0(t)$ for very small σ , see below. The transient stress-growth behavior will also be described in terms of the transient viscosity $\eta_\kappa(t)$ defined by

$$\eta_\kappa(t) = \sigma(t)/\kappa \quad (89)$$

where $\sigma(t)$ is the stress measured after time t following imposition of shear deformation at shear rate κ . For the linear viscoelastic range, $\eta(t)$ is related to the distribution of relaxation time τ_i :

$$\eta(t) = \sum_i G_i \tau_i [1 - \exp(-t/\tau_i)] \quad (90)$$

where G_i are the moduli increments associated with each τ_i . In two extreme limits,

$$\lim_{t \rightarrow 0} \eta(t) = \eta(0) = t \sum_i G_i \quad (91)$$

$$\lim_{t \rightarrow \infty} \eta(t) = \eta(\infty) = \sum_i G_i \tau_i = \eta_0 \quad (92)$$

providing a means to compute an averaged relaxation time:

$$\tau_N = \frac{\sum_i G_i \tau_i}{\sum_i G_i} \quad (93)$$

for comparison with τ_c , which is given by

$$\tau_c = R_0 \eta_0 = \frac{\sum_i G_i \tau_i^2}{\sum_i G_i \tau_i} \quad (94)$$

The ratio τ_c/τ_N provides a measure of the breadth of the distribution of relaxation times.

Relaxation of the stress or birefringence following steady flow provides an additional measure of the distribution. For a linear viscoelastic fluid,

$$\sigma(t) = \sum_i G_i \exp(-t/\tau_i) \quad (95)$$

$$\Delta n(t) = \sum_i n_i \exp(-t/\lambda_i) \quad (96)$$

where one would expect similar values of τ_i and λ_i .

3. EXPERIMENTAL METHODS

The cone and plate rheometer used to determine the steady-state viscosity and recoverable compliance as functions of shear rate has been described in detail elsewhere.³⁴ The instrument employs an inert cone and plate, a wire-suspended cone mounted coaxially with a drag-cup torque transducer, and a plate that may be rotated at precisely controlled angular velocity Ω . The drag-cup transducer generates the restoring torque M required to hold the cone stationary in steady-state flow. In recovery measurements, both M and Ω are set equal to zero, and the rotational angle φ_R of the cone in recovery is determined. The viscosity and the shear rate are calculated with the usual relations for cone and plate deformation with torque M and angular velocity Ω of the plate relative to the cone^{35a}:

$$\eta_k = \sigma / \dot{\gamma} \quad (97)$$

$$\sigma = 3M / 2\pi r^3 \quad (98)$$

$$\dot{\gamma} = \Omega / \Theta \quad (99)$$

Here Θ is the angle between the cone and plate, and r is the radius of the cone. The recoverable compliance is calculated from the ultimate recoverable strain γ_R determined by the ultimate angular recovery φ_R following cessation of steady-state flow under shear stress:

$$R_{\dot{\gamma}} = \gamma_R / \sigma \quad (100)$$

$$\gamma_R = \varphi_R / \Theta \quad (101)$$

As with previous experiments,^{30a} a positive pressure of dry nitrogen is maintained in the rheometer to inhibit contamination of the solution by moisture, but in addition, the cone-plate assembly is surrounded by a glass ring dipped into an oil-filled trough to seal the test solution. Mineral oil, dried by contact with sulfuric acid is used in the trough. The presence of the oil did not add significantly to the measured torque M , and had no effect on ϕ_R .

Flow birefringence measurements were made with either a parallel plate apparatus or a concentric cylinder device. With the former, the lower plate is rotated with angular velocity Ω , while the upper plate is stationary. In this arrangement, the shear rate varies linearly with the distance from the center of rotation, and inversely with the separation h of the plates:^{35b}

$$\kappa = (r/h) \Omega \quad (102)$$

A light beam was directed perpendicular to the plane of the plate (the so-called 1-3 plane, where 1 is the flow direction, and 2 is the direction of gradient)³² for measurement. Optical measurements were performed with an analyzer placed with its transmission axis at angle β to that of a polarizer placed in the incident beam. Since the birefringence under study is relatively large, it was sufficient to use schlieren grade glass windows for the plates, and polaroid polarizers. The birefringence Δn_{13} was determined by one of two methods. In one method, a polarized beam from

a He-Ne laser is transmitted through an area of diameter $d = 1.5$ mm with its center located at radial position r and azimuthal angle α measured from the transmission axis of the analyzer. With γ the angle between the axis of the polarizer and the unique axis (n_1) of the refractive index ellipsoid, the transmission T is given by^{36,37}

$$T = \frac{1}{2} \sin^2 \frac{\delta}{2} (1 - \cos 4\gamma) \quad (103)$$

for $\beta = \pi/2$, where δ is the retardation

$$\delta = 2\pi h \Delta n_{13} / \lambda \quad (104)$$

(δ in radian) with λ the wavelength of the incident light in a vacuum.

According to Eqn.(103), T is zero when γ is $m \pi/2$, $m = 0, 1, 2$ or 3 . For birefringence in the 1-3 plane, one expects³⁸ an extinction isocline ($T = 0$) for azimuthal angles $\alpha = m \pi/2$, $m = 0, 1, 2$, or 3 , as is observed with the solutions under study, so that $\cos 4\gamma = \cos 4\alpha$. When δ is equal to 2π , T is zero for all α , so that an extinction circle is observed. To determine δ for δ not equal to 2π , γ is set to $\pi/4$, and the transmission is monitored by the responses G_κ and G_0 of a photodiode placed above the analyzer, with $\beta = \pi/2$ for the sample in flow and $\beta = \pi/2 - \epsilon$ for the quiescent fluid, respectively, to give

$$\sin^2(\delta/2) = (G_\kappa/G_0) \sin^2 \epsilon \quad (105)$$

from which δ may be determined. In another method sometimes used to determine δ , a quarter wave plate is placed between the fluid and the analyzer, oriented with its slow direction parallel to the transmission axis of the polarizer. Under these conditions, the transmission is given by

$$T = \cos^2 \beta + \frac{1}{2} \sin 2\beta \sin 2\gamma - \frac{1}{2} \cos 2\beta \sin^2 \frac{\delta}{2} (1 - \cos 4\gamma) \quad (106)$$

With $\delta - 2\beta = \pi$, Eqn.(106) exhibits two-fold symmetry:

$$T_{\delta - 2\beta = \pi} = \frac{1}{2} + \frac{1}{2} \cos \delta (1 - \sin^2 2\gamma) - \frac{1}{2} [\sin^2 \delta \sin 2\delta + \cos^2 \delta \sin^2 2\gamma] \quad (107)$$

Consequently, adjustment of β to an angle that results in a two-fold symmetric pattern with extinction for $\gamma = \pi/4$ and $3\pi/4$ provides a means to determine δ .

With the photometric method to determine δ , the coordinates r and α are set by translation of the incident beam by a mirror mounted on an x-y stage. A circular diaphragm centered at the r, α position above the fluid serves to reduce stray light contribution to G. The laser is mounted so that the plane of polarization forms a dihedral angle of 45 degrees with the plane of the positioning mirror. The polarization of the incident beam is adjusted by a half-wave plate placed between the mirror and the sample. The light beam is modulated at 400 Hz by a mechanical chopper, and the output from the transducer is monitored with a Hewlett-Packard Model 501 Wave

Analyzer tuned to the modulation frequency. This procedure eliminates contributions from room light. The angles β and ϵ are adjusted to within 0.5 degrees, which is satisfactory for our purpose.

When using the quarter wave plate to determine δ , the sample is illuminated with a collimated beam from a zirconium arc lamp. The angle β is reproducible to within 0.2 degrees for this measurement. Comparisons of δ determined by the two methods used here agreed within 0.05 radians.

The value of δ is used to calculate the birefringence Δn_{13} with Eqn. (104). According to Philippoff³⁸, the observed birefringence Δn_{13} is related to the difference Δn of the principal components of the refractive index ellipsoid through the equation

$$\Delta n = \frac{\Delta n_{13} - \Delta n_{23}}{\cos 2\chi} = \Delta n_{12} \quad (108)$$

where the birefringence Δn_{23} in the 2-3 plane is usually very small, and Δn_{12} is the birefringence in the 1-2 plane. The strong absorption of light by the solutions under study prohibits direct measurement of Δn_{12} , for example, by Couette flow, which is the more usual method to study birefringence.³² Relatively few examples of birefringence measurements in the 1-3 plane exist.³⁹

With use of the concentric cylinder geometry, measurements are made in the 1-2 plane so that χ is given directly by the orientation of the cross of isocline and the measured birefringence is Δn_{12} . Owing

to the large extinction of visible light by PBT solutions, the concentric cylinder geometry with its long path length was useful only with dilute solutions. For these solutions, χ is essentially $\pi/4$. The birefringence was determined by use of a quarter-wave plate to find the conditions for two-fold symmetry of the isocline, as given by Eqn. (107).

Measurements of $J'(\omega)$ and $J''(\omega)$ were carried out with a Rheometrics model 7200 rheometer, over the range 0.01 to 12 radian/sec. The sample was protected from contamination by moisture by use of an oil-seal around the sample chamber and a slow purge by dry nitrogen.

4. VISCOELASTIC MEASUREMENTS ON PBT IN POLYPHOSPHORIC ACID SOLUTION

The components $J'(\omega)$ and $J''(\omega)$ of the complex compliance were determined as a function of frequency ω over the range 0.01 to 12 radian/sec for a solution of PBT in PPA, weight fraction polymer 0.10, as received from Celanese Research Corp (sample code 2895-32). It may be seen that J' , J'' and η' is relatively insensitive to temperature over the frequency range studied for temperatures from 90 to 145°C. It is likely that differences do exist at lower frequencies. Reduction of the temperature to 28°C results in a ten-fold increase in η' , and a concomitant decrease in J' and J'' . It seems likely that little advantage will accrue to the use of temperature in excess of 100°C in processing pressures required, etc. In fact, the use of higher temperatures is accompanied by foaming of the PPA solution by unknown causes.

Creep and recovery experiments were also carried out with the PPA solution of PBT. The data showed that the solution exhibits viscous flow, even for smaller stress levels than those used with the dynamic mechanical analysis. Data for the creep and recovery at 92°C given in Fig. 32 give a viscosity of about 2×10^6 poise at a shear rate of $6 \times 10^{-5} \text{ sec}^{-1}$. An apparent time constant τ_c of 2,000 sec is obtained from the product of the viscosity and the recoverable compliance. Thus the shear rate $\kappa \sim \tau_c^{-1}$ that must be exceeded to develop orientation is very low, in accord with the data on $\eta'(\omega) \sim \eta_\kappa$, which shows that $\eta'(\omega)$ has not attained its limiting value of η_0 at low ω over the range studied.

Ribbons were formed with the solution of PBT in PPA using methods described in part III of this report. These were supplied to Professor E. L. Thomas, University of Massachusetts, for evaluation.

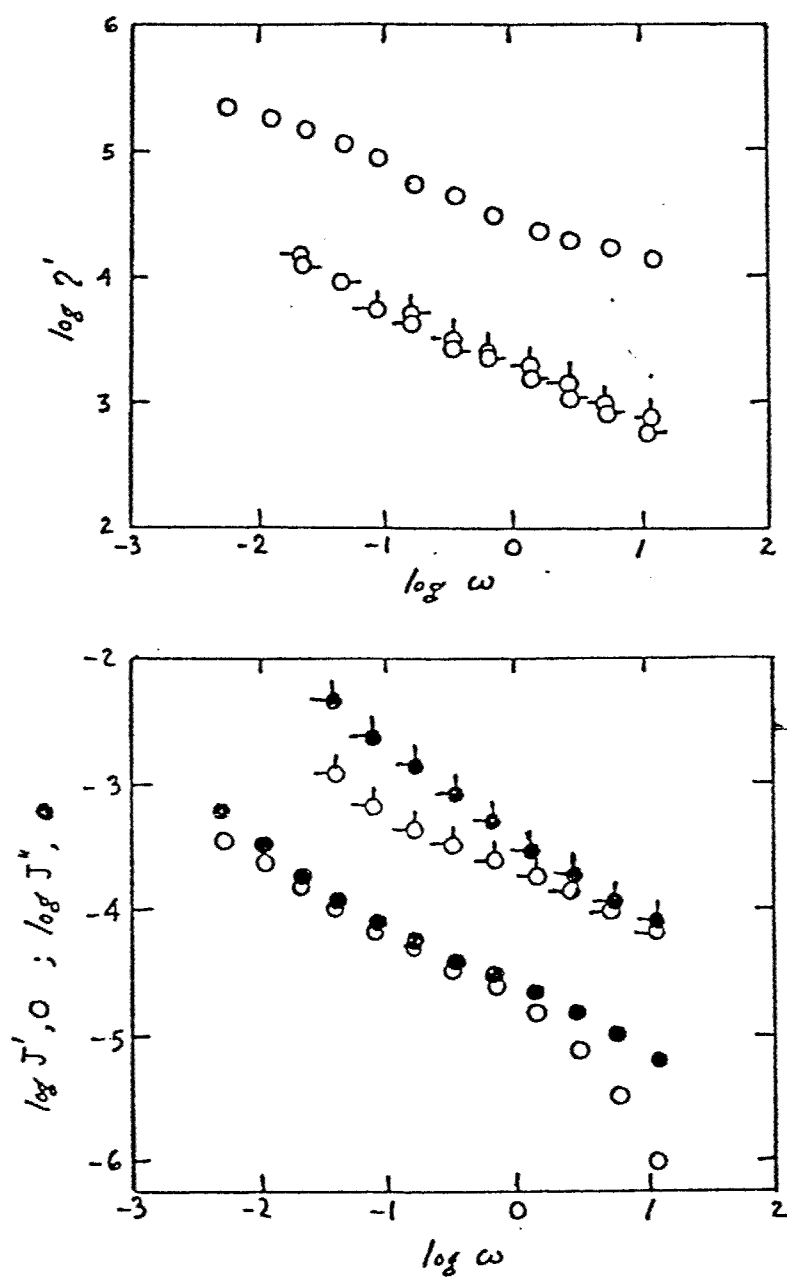


Figure 31 η' , J' and J'' versus frequency ω for a solution of PBT in PPA (10% polymer by weight). The data are for temperature of 28°C (no pips); 89°C (pips left); 102°C (pips up); and 145°C (pips right).

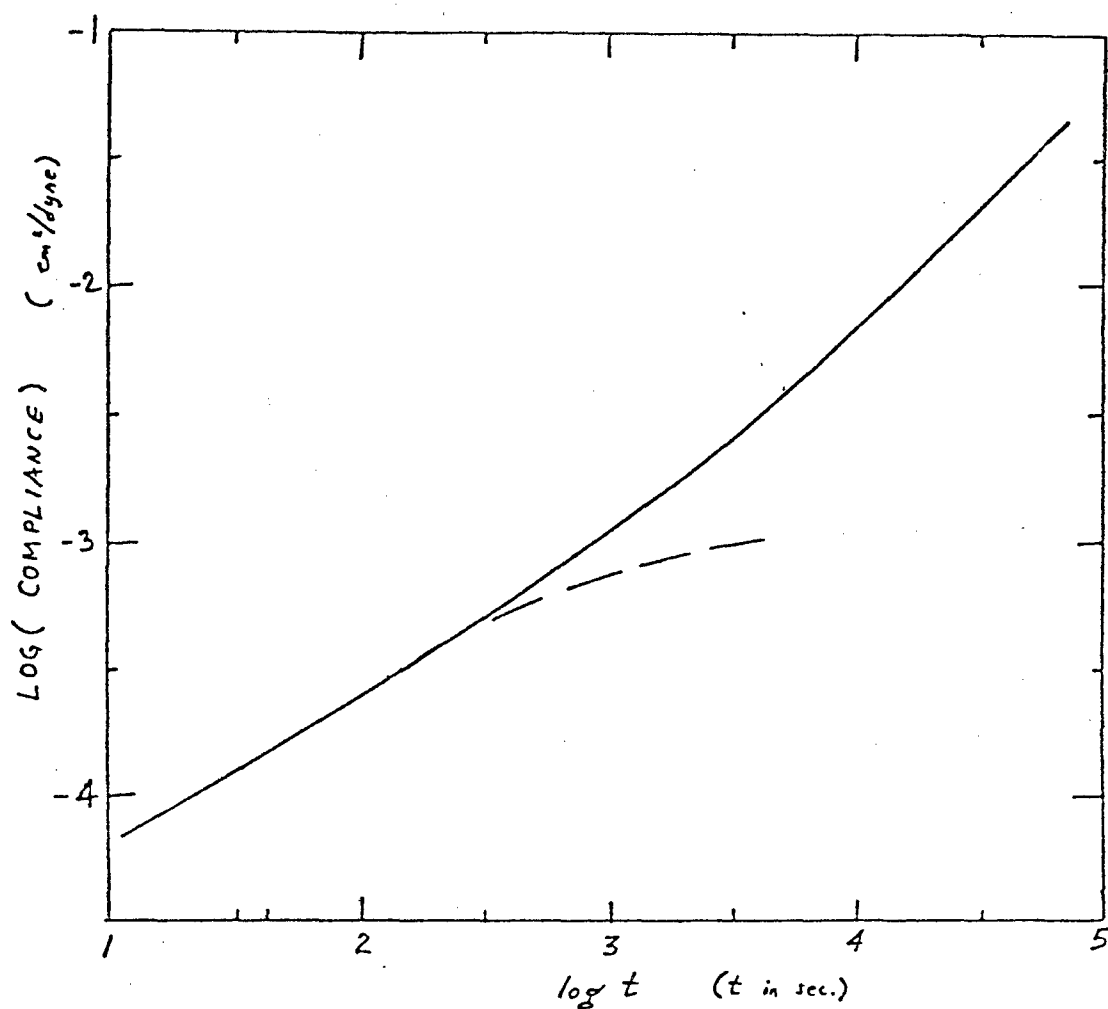


Figure 32 Creep — and recoverable — — compliance for a solution of PBT in PPA (10% polymer by weight), temperature 91.5°C.

5. RHEOLOGICAL AND RHEO-OPTICAL MEASUREMENTS ON PBT IN METHANE SULFONIC ACID SOLUTION

Rheological and rheo-optical measurements have been carried out with solutions of PBT-53 in methane sulfonic acid (MSA). The rodlike polymer has a weight average contour length L_w of 120 nm, and undergoes a phase transition from optically isotropic to anisotropic solution as shown in Fig. 33. Also shown in Fig. 33 are the temperature-concentration combinations used in the rheological or rheo-optical studies. As may be seen in Fig. 33, the concentration ϕ_c for the formation of a stable nematic phase is temperature dependent.

5.1 Steady-State Behavior

5.1.1 Viscosity And Recoverable Compliance

Plots of η_κ/η_0 and R_κ/R_0 v/s κ for the three solutions are shown in Figs. 34-35. The 2.55% solution is well below the critical concentration required for a phase transition to an ordered solution. The 3.23% solution, isotropic at rest at room temperature, is expected to change to a biphasic or nematic solution on cooling. The 4.27% solution is ordered at rest at 25°C, and does not undergo a transition to a disordered solution, over the range 120°C < T < 0°C. The flow curves of these solutions are representative of the three different kinds of behavior, I, II and II, already discussed at length in previous report.⁴⁰ The apparently anomalous behavior of the nematic solution is due actually to an experimental limitation, as discussed below.

The behavior of the isotropic solutions (100w₂ equal to 2.55 at all temperatures studied, and 3.23 at 60°C, see Fig. 33) conforms closely to

the pattern observed previously in this laboratory,⁴⁰ and will not be discussed in detail. Both functions Q and P are unity at low $\tau_c \kappa$, and decrease with increasing $\tau_c \kappa$, both being universal functions $\tau_c \kappa$ over the range of temperature and concentrations studied. The former is fitted reasonably well by a calculation given by Cohen⁴¹ based on modification of a theoretical treatment by Doi and Edwards.⁴² No comprehensive theory is available for P as a function of $\tau_c \kappa$, but it is known that for $\tau_c \kappa$ less than about 10, P often is similar to $R_0(t)/R_0$ evaluated at $t = \kappa^{-1}$, revealing the fundamental relation of P to the linear relaxation spectrum in this range of $\tau_c \kappa$.

The solution with $100w_2 = 3.23$ is close to the biphasic range at 43°C , and is nematic below 30°C . As seen in Fig. 35, the behavior of Q at low $\tau_c \kappa$ reveals the proximity to the biphasic range at 43°C , possibly due to flow induced phase transition. The data for P versus $\tau_c \kappa$ do not reduce as well to a single curve as is observed for the solution with $100w_2 = 2.55$, possibly due to the effects of the phase transition, but are close to the behavior observed for the lower concentration solutions. By contrast, for the fully nematic solution with $100w_w = 4.27$, the shift in P reflects a basic change in the distribution of relaxation times; a change that is only slightly reflected in Q , which is still similar to the behavior for the isotropic solutions (see Fig. 36). In previous work,⁴⁰ Q has been found to increase with decreasing $\tau_c \kappa$ following a plateau near $\tau_c \kappa = 1$. The behavior at low $\tau_c \kappa < \text{ca } 0.01$ has been attributed to domain structure in the nematic fluid. The failure to find such behavior in Fig. 36 may be due to the lack of data at low $\tau_c \kappa$, or may indicate that the domain structure of the solution studied was less well-defined than

usual.

Values of R_0 , η_0 and τ_c are given in Table 16 for the three solutions described above, along with similar data for three other solutions in the same range of concentration, and four solutions with much lower concentrations. The former were obtained by creep and recovery, and the latter from measurements of $J'(\omega)$ and $J''(\omega)$ at low ω through application of Eqns. (70-73).

The theoretical model of Doi and Edwards mentioned above also yields the Rouse-like result

$$R_0 = 5M/3\rho w_2 RT \quad (109)$$

for isotropic solutions with low concentration (using the relation $R_0 = S_0$), with ρ the density. The data for the four solutions with $100w_2$ in the range 0.15 to 0.35 are in accord with the inverse concentration dependence given by Eqn. (109), but give $w_2 R_0 = 10^{-5} \text{ cm}^2/\text{dyn}$ in comparison with $1.2 \times 10^{-6} \text{ cm}^2/\text{dyn}$ calculated with Eqn. (109) for PBT-53. Reasons for this discrepancy may include molecular weight polydispersity, or the effects of intermolecular association.

The dependence of η_0 and R_0 on w_2 for the solutions with $100w_2 > 2$ is similar to that reported in detail elsewhere.⁴⁰

5.1.2 Flow Birefringence

The steady-state flow birefringence has been studied for six optically isotropic solutions. Values of τ_c were also determined by independent measurements. For four solutions, with $100w_2$ equal to 2.55, 2.80, 2.94 and 3.17, Δn_{13} was determined at several temperatures (10 to

TABLE 16

RHEOLOGICAL DATA FOR PBT-53 IN METHANE SULFONIC ACID

$100 w_2$	T	η_0	$10^3 R_0$	$10^5 w_2 R_0$	τ_c
0.145	24	1.45	7.0 ^(a)	1.02	0.0102
0.208	24	3.45	4.7	0.98	0.0163
0.282	24	5.8	3.72	1.05	0.0216
0.350	24	7.45	2.96	1.04	0.0225
2.55	12.5	3.2×10^4	2.0	5.10	64
	23	2.2	1.8		40
	30	1.32	1.7 ^(b)		22
	40	0.91	1.6 ^(b)		15
	60	0.43	1.5		6.5
2.80	40	3.45	1.4	3.92	48
	60	1.74	1.27		20
2.94	21	8.0	2.0	5.9	152
	40	3.48	1.65		58
3.17	40	10.2	1.75	5.5	180
	60	3.0	1.70		51
3.23	10	11	3.0	8.1	330
	19.5	5.6	2.5		140
	43	23	2.0		46
	60	1.1	2.0		22
4.27	10.5	15	3.0	12.8	450
	23	11.4	3.0		340
	43	7.0	3.0		210

(a) Estimated from $w_2 R_0 = 10^{-5}$ based on data for $100 w_2$ equal to 0.208, 0.282, and 0.350.

(b) Estimated as $R_0 = \tau_c / \eta_0$ using η_0 and τ_c from flow curves.

60°C) using the parallel plate geometry, and as mentioned in the preceding τ_c was calculated from R_0 and η_0 determined by creep and recovery measurements. For three other solutions, with $100w_2$ equal to 0.145, 0.208 and 0.282, Δn_{12} was determined at 24°C using the concentric cylinder geometry, and τ_c was calculated from R_0 and η_0 determined from $J'(\omega)$ and $J''(\omega)$ at small $\tau_c \omega$ (see Eqns. 70-73). With the lower concentration solutions, χ was essentially $\pi/4$ over the range of κ studied. Values of R_0 , η_0 and the resultant τ_c are given in Table 15.

In correlations of data in the nonlinear response range, Eqns. (86) and (87) are often rewritten with η_0 and S_0 replaced by η_κ and S_κ , respectively, to approximate the effects of nonlinear behavior in the birefringence.³² These substitutions give

$$\Delta n_{13} \sim 2C'R_0^{-1}NQ(\tau_c \kappa)^2 \quad (110)$$

with

$$C' = C(\cot 2\chi)/S_\kappa \eta_\kappa \kappa \quad (111)$$

and for small $\tau_c \kappa$, for which χ is essentially $\pi/4$,

$$\Delta n_{12} \sim 2C'R_0^{-1}Q(\tau_c \kappa) \quad (112)$$

It appears that C' so defined is often independent of κ , even for $\tau_c \kappa$ greater than unity.⁴³

Bilogarithmic plots of $\Delta n_{13}c/(\tau_c\chi)^2$ and $\Delta n_{12}c/\tau_c\chi$ versus $\tau_c\chi$ are given in Fig. 37, where c is the solute concentration (g/ml). The results show that a) $\tau_c\chi$ is a useful parameter to correlate the data over the range of concentration and temperature examined, and b) that the limiting behavior of $\Delta n_{12}/\tau_c\chi$ (or $\Delta n_{13}/(\tau_c\chi)^2$) is not reached until $\tau_c\chi < 0.2$. Since neither χ nor N were determined in this study, we have examined a variation of Eqn. (110-112) given by

$$\Delta n_{13} = 2C''R_0^{-1}PQ^2(\tau_c\chi)^2 \quad (113)$$

where

$$\Delta n_{12} = 2C''R_0^{-1}Q\tau_c\chi \quad (114)$$

$$C'' = C'N/P \quad (115)$$

is expected to equal C as $P = N$ and $C' = C$ and Eqn. (114) is to be used only for $\chi \approx \pi/4$. Although N and P need not be equivalent for large $\tau_c\chi$, they should approach each other for small $\tau_c\chi$, so that C' and C should be equal, at least for small $\tau_c\chi$. The bilogarithmic plot of $\Delta n_{13}/cPQ^2(\tau_c\chi)^2$ shown in Fig. 37 reveals that $2C''(R_0c)^{-1}$ tends to a constant for $\tau_c\chi$ greater than about unity. For smaller $\tau_c\chi$, $2C''(R_0c)^{-1}$ increases with decreasing $\tau_c\chi$ in the range studied reaching a limiting value about two-fold smaller for $\tau_c\chi < 0.02$.

Since normal stress data are not available, we do not know whether deviation of C'' from C is related to failure of Eqns. (110-114) or to deviation of N from P . Most experiments designed to evaluate C'

have been confined to the range $\tau_c \kappa > 1$, owing to the difficulty of measuring small normal forces. In that range, C' measured here is nearly constant, but smaller than its value for $\tau_c \kappa < 1$. In the latter range, the limiting value of $\Delta n_{13}/c(\tau_c \kappa)^2$ (or $\Delta n_{12}/c \tau_c \kappa$) is 0.09 ml/g. It is of interest to compare this estimate with the result expected for a dilute solution of rodlike molecules, for which⁴⁴

$$\lim_{\substack{\tau_c \kappa = 0 \\ c = 0}} \Delta n/c = (2/5)(\Delta n_\infty/c)\tau_c \kappa \quad (116)$$

where $\Delta n_\infty/c$ is given by

$$\Delta n_\infty/c = 3 \underline{\delta} (\partial n/\partial c) \quad (117)$$

with $\underline{\delta}$ and $(\partial n/\partial c)$ the molecular anisotropy and refractive index increment, respectively, of the polymer in solution. The latter may be expressed in terms of the principal refractive indices n_1 and n_2 through the parameters

$$4\pi g_i = \frac{n_i^2 - n_s^2}{1 + (n_i^2 - n_s^2)L_i/4\pi n_s^2} \quad (118)$$

as

$$\underline{\delta} = (g_1 - g_2)/(g_1 + 2g_2) \quad (119)$$

$$(\partial n/\partial c) = (2\pi/3n_s)(g_1 + 2g_2)\bar{v} \quad (120)$$

Here n_s is the solvent refractive index, \bar{v} is the partial specific volume of solute, and the form factor L_1 is given by $L_1 = 0$ and $L_2 = 2\pi$ for rods. Values of $\bar{\delta}$ and $\partial n/\partial c$ are 0.6 and 0.55 ml/g, respectively for PBT in methane sulfonic acid,⁴⁵ and, apparently, $n_1 \approx n_2 \approx n_3$. These data give $\Delta n_\infty/c$ equal to 1.0 ml/g for PBT in methane sulfonic acid, or 0.4 ml/g for the limiting value of $\Delta n_{13}/c(\tau_c \kappa)^2$ or $\Delta n_{12}/c\tau_c \kappa$, in comparison with the observed value of 0.009 ml/g. It may be noted, however, that the observed value of $\Delta n_\infty/c$ is inversely proportional to the estimate for τ_c , which in turn is proportional to R_0 and that the behavior of these quantities for small w_2 is strongly weighted in the estimate of $\Delta n_\infty/c$. It was noted above that R_0 was ten-fold larger than expected theoretically. It may be that this same discrepancy is reflected in the reduced value of $\Delta n_\infty/c$ in comparison with the estimate expected with Eqn. (115).

In any case, the behavior displayed in Fig. 37 shows that appreciable orientation is induced in shear flow for $\tau_c \kappa > 1$, with a useful approximation to Δn_{12} being given by the relations

$$\Delta n_{12} = 2C''R_0^{-1}Q\tau_c \kappa / \sin 2\chi \quad (121)$$

$$\Delta n_{13} = 2C'R_0^{-1}Q\tau_c \kappa \cot 2\chi \quad (122)$$

$$\cot 2\chi = PQ\tau_c \kappa \quad (123)$$

It may be noted that $\sin 2\chi$ calculated with Eqn. (121) does not vary too much with $\tau_c \kappa$; e.g.,

$$\sin 2\chi = [1 + \cot^2 2\chi]^{-1/2} \quad (124)$$

increases from 1 to 1.4 over the range of $\tau_c \chi$ studied for the data shown in Fig. 37. An estimate for the orientation is

$$\Delta n_{12}/\Delta n_{\infty} = \frac{3\langle \cos^2 \theta \rangle - 1}{2} \quad (125)$$

where θ is the angle between the rod axis and the flow direction. In this case, $\langle \cos^2 \theta \rangle$ is given by

$$\frac{3\langle \cos^2 \theta \rangle - 1}{2} = \frac{\Delta n_{12}}{\Delta n_{\infty}} \frac{[1 + (PQ\tau_c \chi)^2]^{1/2}}{PQ\tau_c \chi} \quad (126)$$

For example, for $\tau_c \chi = 30$, the data in Fig. 37 give $\langle \cos^2 \theta \rangle$ equal to 0.989 or $\arccos[\langle \cos^2 \theta \rangle^{1/2}]$ equal to 6 deg, showing that orientation in flow is well developed at easily accessible $\tau_c \chi$.

5.2 Creep And Stress-Growth Behavior

According to Eqns. (91) and (92), the stress-growth behavior for deformation at constant χ can be used to define a time constant τ_N , provided measurements are carried out in the linear response range ($\tau_c \chi \ll 1$). Values of τ_N so determined are plotted as a function of τ_c in Fig. 38. The data show that for the isotropic and nematic solutions examined, τ_c/τ_N is approximately independent of concentration c and equal to 7. This is surprising in two respects: 1) it might have

been anticipated that τ_c/τ_N would differ for isotropic and nematic solutions, and 2) the ratio $\tau_c/\tau_N = 7$ is about 2-3 times larger than the value usually found with flexible chain polymers. The latter result may be implicated in the deviations noted above in comparison of experimental and theoretical values of R_0 and $\Delta n_\infty/c$.

The creep compliance $J_\sigma(t)$ is given for several levels of the applied stress in Figs. 39 and 40 for isotropic and nematic solutions. These curves are plotted as the time-dependent strain $\gamma(t)$ divided by the stress σ against t/τ_c . As may be seen in Figs. 39 and 40, data for $J(t)$ coincide at low values of t for all σ . For low values of σ , the curves are identical at all t . As σ increases, the curves deviate and the value of $\gamma(t)$ ($= \sigma J(t)$) at which deviation starts to occur is called the critical strain γ^* . This parameter has been shown experimentally to be independent of σ for solutions of flexible chain polymers.^{30b} In those studies, it was found that γ^* is proportional to c^{-1} . The data in Fig. 41 show that a similar relation obtains with the PBT solutions, with $\gamma^* = 3.4/c$. As will be shown elsewhere,⁴⁶ γ^* can be related to the moments

$$\tau^{(l)} = \frac{\sum G_i \tau_i^{l+1}}{\sum G_i \tau_i^l} \quad (127)$$

of the distribution of relaxation times, (e.g., $\tau_c = \tau^{(2)}$ and $\tau_N = \tau^{(1)}$) so that the inverse dependence of γ^* on concentration reflects variation of the distribution with c , even though $\tau_c/\tau_N = \tau^{(2)}/\tau^{(1)}$ is nearly independent of c as shown above.

This critical strain γ^* has a significance in the processing of these solutions into film and fibers. In order to achieve a reasonable degree of orientation, the solution has to be subjected to a strain greater than γ^* . In other words, the product of the shear rate $\dot{\gamma}$, and the time of its imposition t has to be greater than γ^* to obtain a well oriented solution in flow.

With flexible chain polymers, the stress-growth behavior for deformation at constant $\dot{\gamma}$ with $\tau_c \dot{\gamma} > 1$ displays two features related to γ^* :

- 1) $\eta(t) = \sigma(t)/\dot{\gamma}$ is independent of $\dot{\gamma}$ for all $t < t_d$,
where $\dot{\gamma} t_d \approx \text{constant}$, and
- 2) for large enough $\dot{\gamma}$, $\eta(t)$ exhibits a maximum for
 $t = t_m$, such that $\dot{\gamma} t_m \approx \text{constant}$.

For flexible chain polymers, $\dot{\gamma} t_m/2 \sim \dot{\gamma} t_d \sim \gamma^*$.⁴⁶

These features are noted for the stress-growth data given in Fig. 42 for a nematic PBT solution. Values of t_d and t_m are plotted as functions of $\dot{\gamma}$ in Figs. 43 and 44, respectively, for three different solutions. The results in Fig. 43 show that $\dot{\gamma} t_d \sim \gamma^*$. The values of $\gamma_M^* = \dot{\gamma} t_m$ obtained from Fig. 44 are included in Fig. 41, where it is seen that $\gamma_M^* \sim 2\gamma^*$, as is often observed with flexible chain polymers. These results indicate that for PBT solutions, the important parameter γ^* can be estimated from γ_M^* to complement the creep behavior, which requires the use of special rheometers not widely available.

5.3 Stress And Flow Birefringence Relaxation

The loss of birefringence after steady-state flow is directly related to relaxation of the flow induced orientation. This is obviously

of considerable interest in the processing of these solutions into oriented films and fibers. The relaxation of the birefringence after steady-state flow can be monitored using the intensity method with a strip-chart recorder attached to the detector.

A semilogarithmic plot of the ratio of the transient birefringence to the steady-state value $\frac{\Delta n(t)}{\Delta n_0}$ results in curves such as that shown in Fig. 45. Using a method commonly employed in the analysis of stress relaxation of flexible polymer solutions,¹⁴ the relaxation curve can be approximated by a sum of discrete exponentials to obtain relaxation times and their corresponding weights, as defined by Eqn. (96). This same procedure is applied even in the range for nonlinear behavior, even though Eqn. (96) is formally intended only for linear response, and stress relaxation data are similarly treated. The results for a PBT solution at 21°C (100w₂ = 2.94) for which $\tau_c = 152$ s and $\tau_N = 32$ s are given in Table 17.

It may be noted that $\lambda^{(2)}/\lambda^{(1)}$ is generally smaller than $\tau^{(2)}/\tau^{(1)}$ for the stress relaxation, and that both experiments have appreciable fractions of a rapidly relaxing component (e.g., τ_3 and λ_3). The relative contribution of this fast component increases with increasing τ_c . The rotational diffusion time constant τ_R^0 for a rodlike chain in a very dilute solution is given by¹⁴⁷

$$\tau_R^0 = \frac{15}{4} \frac{M[\eta]\eta_s}{RT} \quad (128)$$

where η_s is the solvent viscosity (0.1 p for MSA at 25°C) and $[\eta]$ is

the intrinsic viscosity (1400 ml/g for PBT-53). For PBT-53, τ_R^0 is calculated to be 2 ms, much less than the fastest relaxation times reported in Table 17. This is in contrast with a suggestion of Doi and Edwards^{42b} that well oriented solutions should exhibit a fast relaxation with time constant of about equal to τ_R^0 since the orientation reduces intermolecular contacts. If relaxation occurs on time of order τ_R^0 , it appears that its contribution to the overall relaxation is small for the solution studied here. The implications for maintaining a well oriented solution following solution processing are clear-coagulation must take place on a time scale of order $10^4 \tau_R^0$, or 1-10 sec for PBT in methane sulfonic acid.

TABLE 17
RELAXATION TIME CONSTANTS OBSERVED
FOR A PBT-53 SOLUTION (a)

Stress Relaxation ^(b)								
$\tau_c \kappa$	G_1	τ_1 (sec)	G_2	τ_2 (sec)	G_3	τ_3 (sec)	$\tau^{(1)}$	$\tau^{(2)}$
0.763	0.24	208	0.33	48	0.42	(7)	69	163
1.92	0.14	208	0.36	48	0.50	7.0	50	138
3.83	0.10 ₅	174	0.35	41	0.54 ₅	8.7	37	103
7.63	0.04	232	0.27 ₅	46	0.68 ₅	7.8	27	102

Δn_{13} Relaxation ^(c)								
$\tau_c \kappa$	n_1	λ_1 (sec)	n_2 (sec)	λ_2 (sec)	n_3 (sec)	λ_3 (sec)	$\lambda^{(1)}$	$\lambda^{(2)}$
6.92	0.61	122	0.30	23	0.09	10	82	112
10.38	0.42	135	0.36	28	0.22	5.2	68	117
12.94	0.35	138	0.34	24	0.31	4.0	58	120
28.27	0.25	131	0.30	23	0.40	4.3	44	108
56.85	0.16	123	0.19	23	0.65	3.9	27	95

(a) $100w_2 = 2.94$, temperature equal to 21°C , $\tau_c = 152_5$

(b) G_i are normalized by the steady-state stress

(c) n_i are normalized by the steady-state birefringence

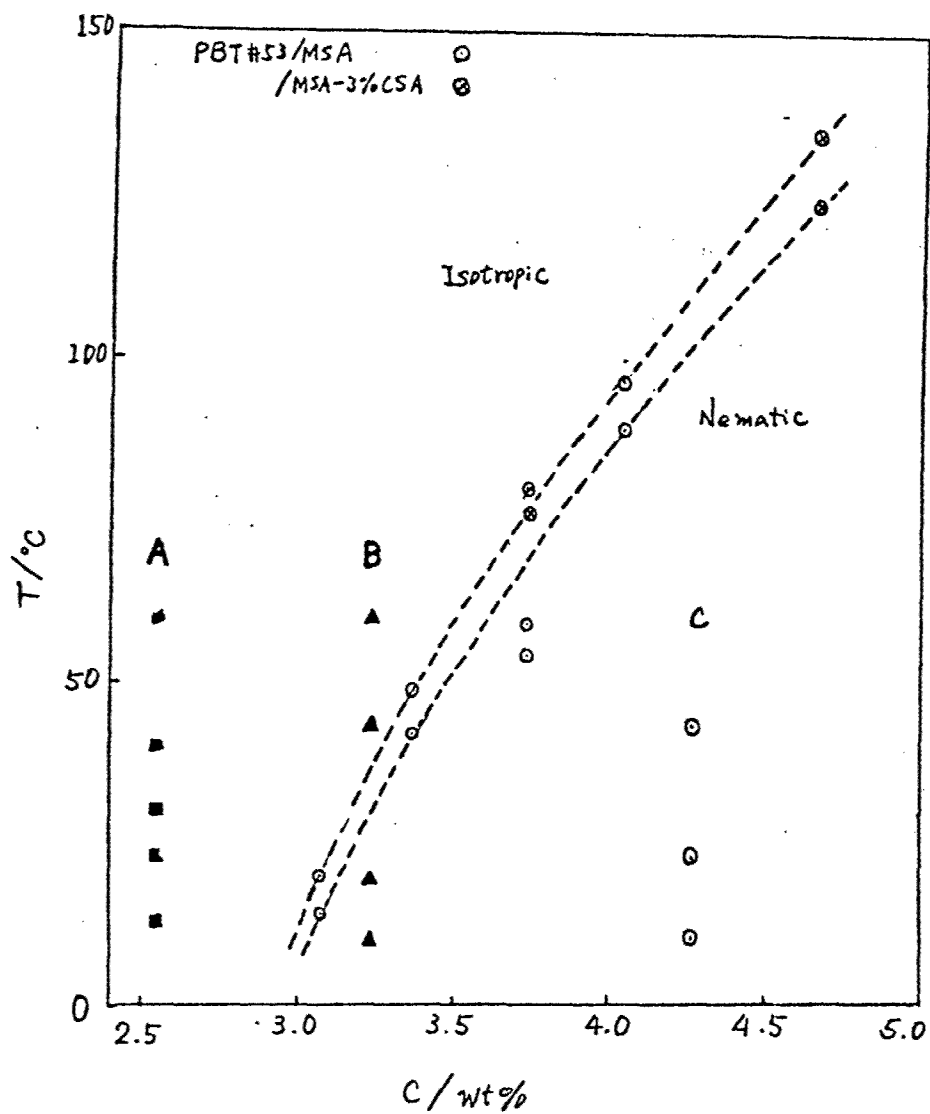


Figure 33

Phase diagram for PBT 53 in methane sulfonic acid, O, and MSA plus 3% chlorosulfonic acid, \otimes .

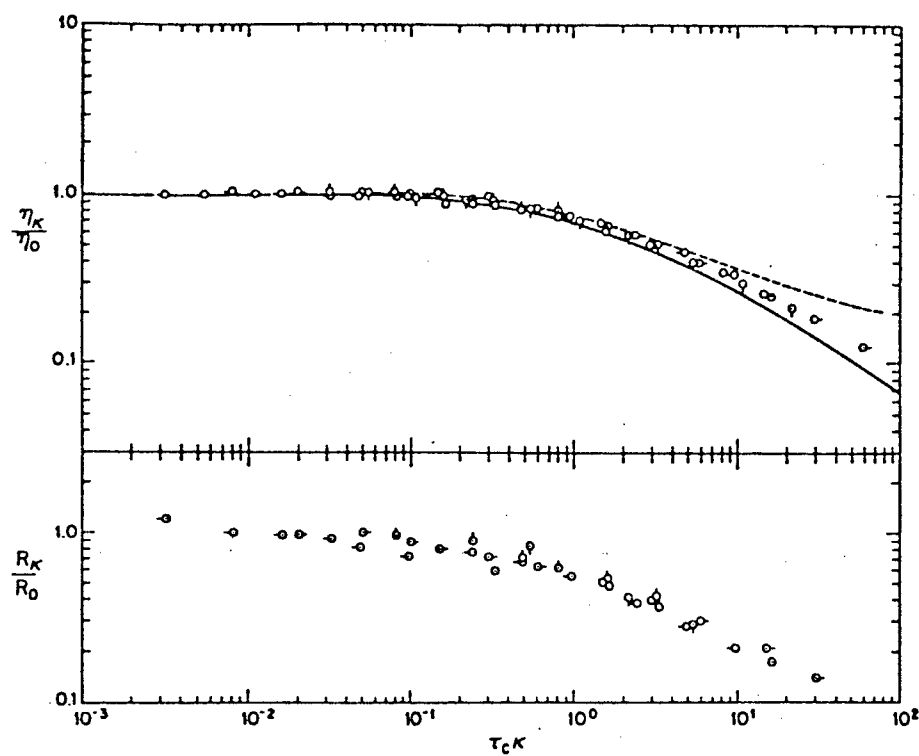


Figure 34

Plot of η_κ/η_0 and R_κ/R_0 for an isotropic (2.55 wt %) solution of PBT.

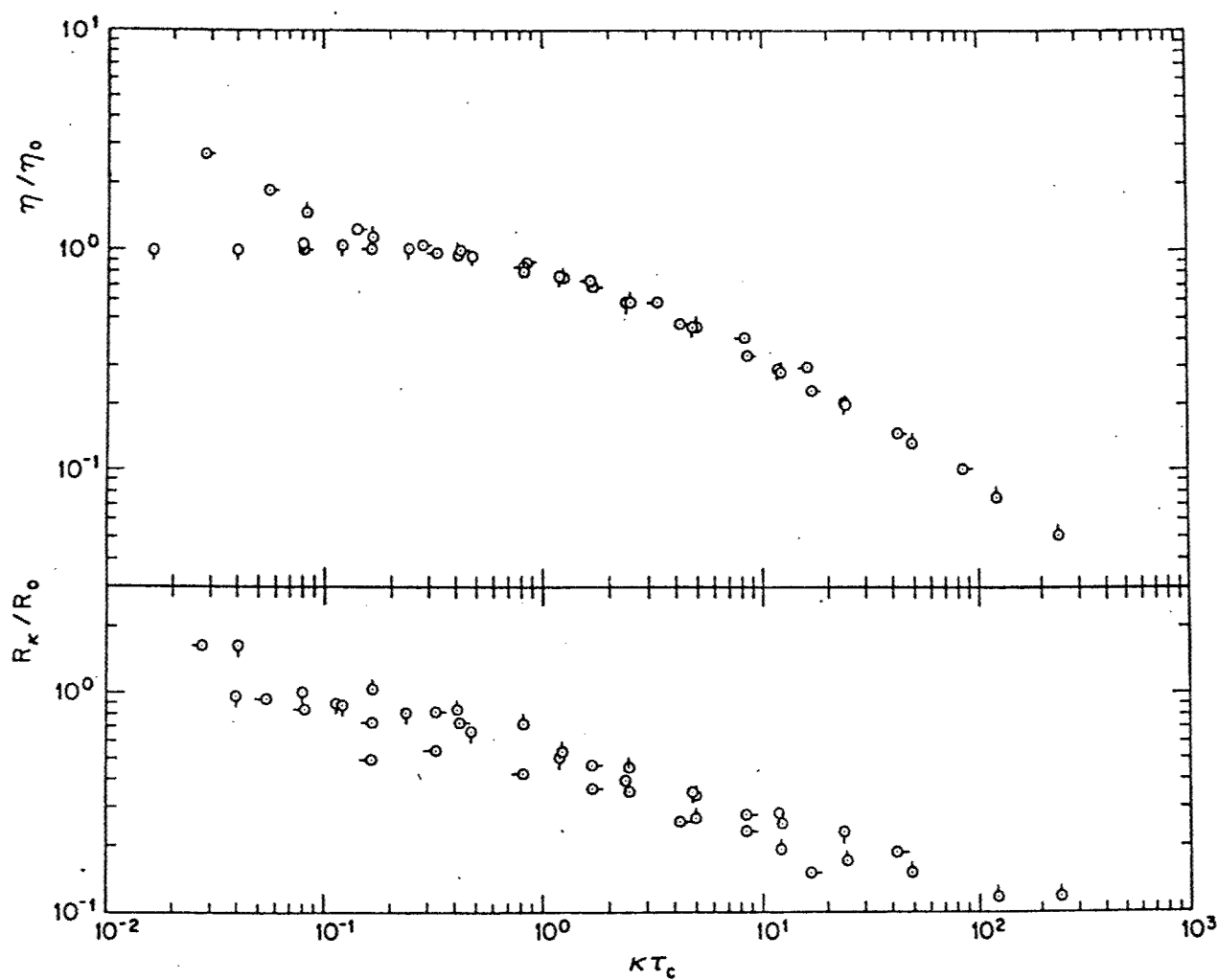


Figure 35

Plot of η_x/η_0 and R_x/R_0 for a solution that undergoes a transition in the range $10^\circ < T < 60^\circ\text{C}$ (3.23 wt %).

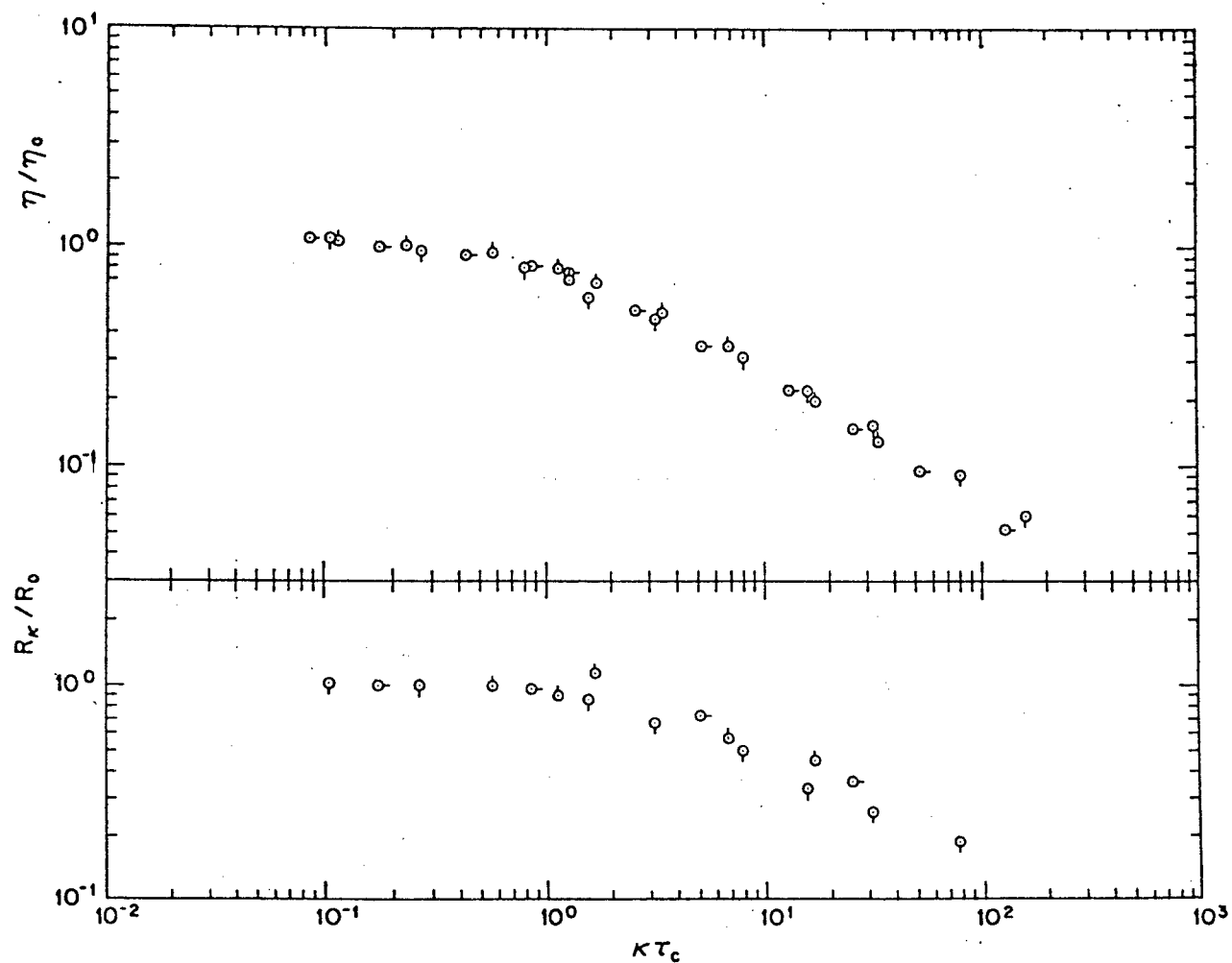


Figure 36 Plot of η_κ/η_0 and R_κ/R_0 for a nematic solution (4.27%).

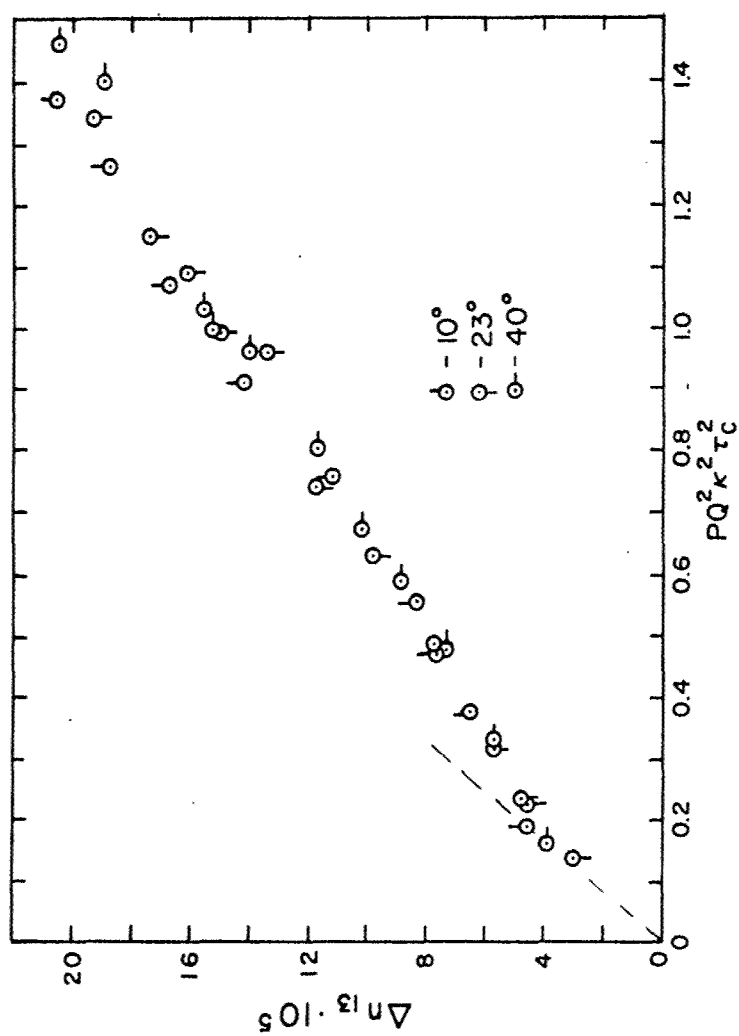


Figure 37 The birefringence versus a reduced square shear rate (see text) for solution of PBT in MSA at the indicated temperature (2.55 wt %).

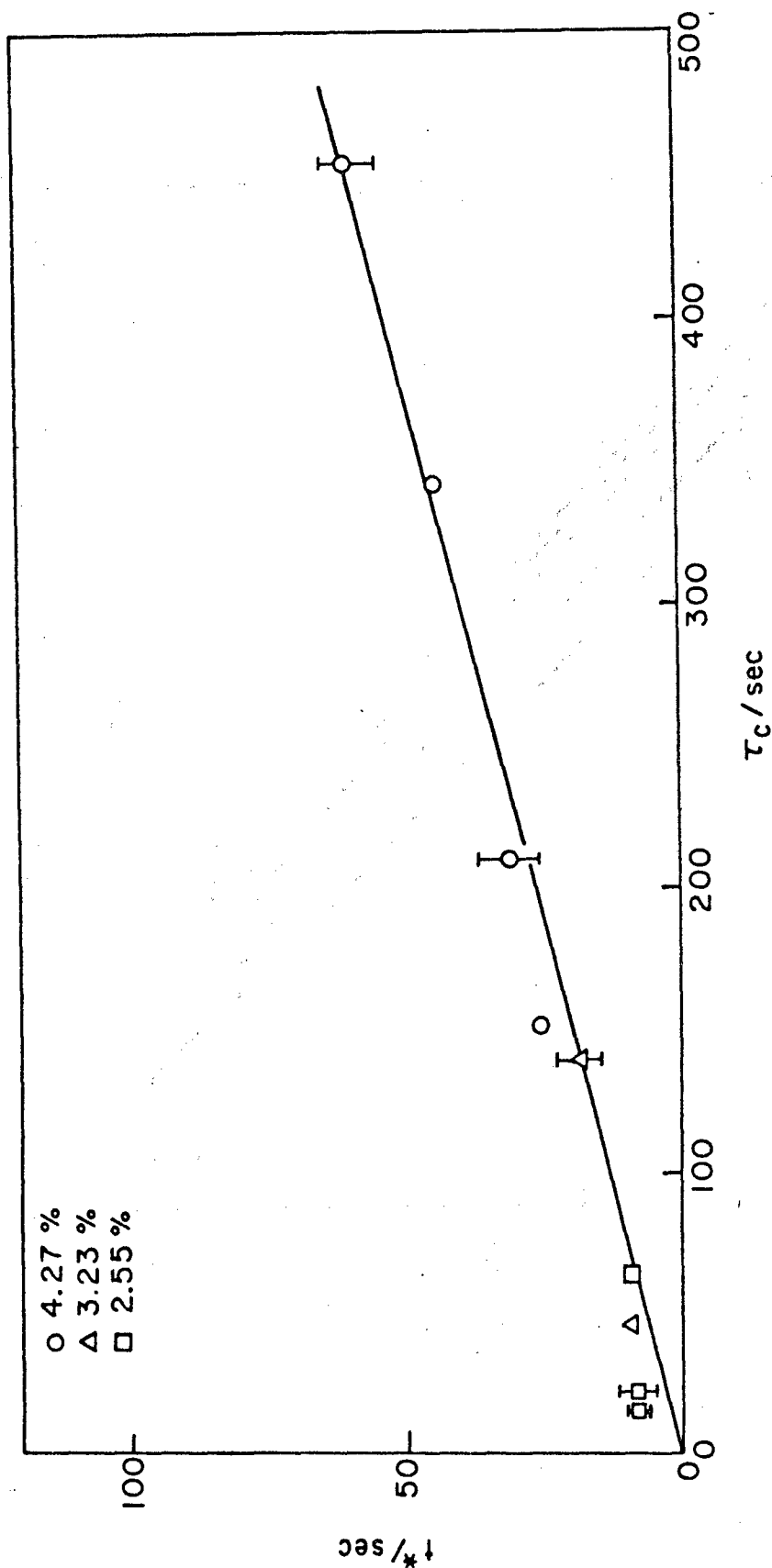


Figure 38 Rheological time constant τ_N (Eqn. 93) versus the characteristic time (Eqn. 94) for solution of PBT in methane sulfonic acid.

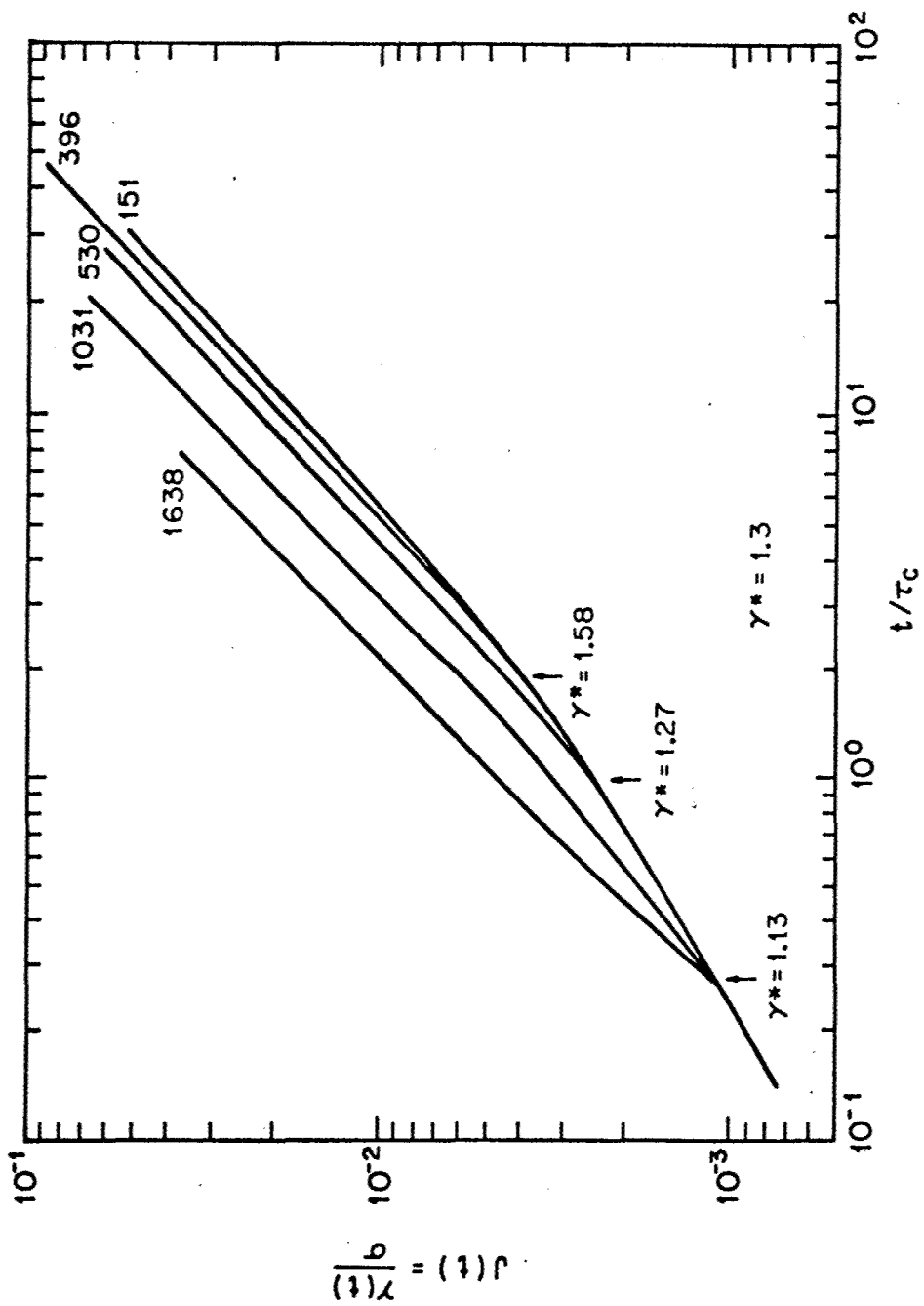


Figure 39 Creep compliance plotted against t/τ_c for various stress levels for an isotropic solution (2.55% at 300C).

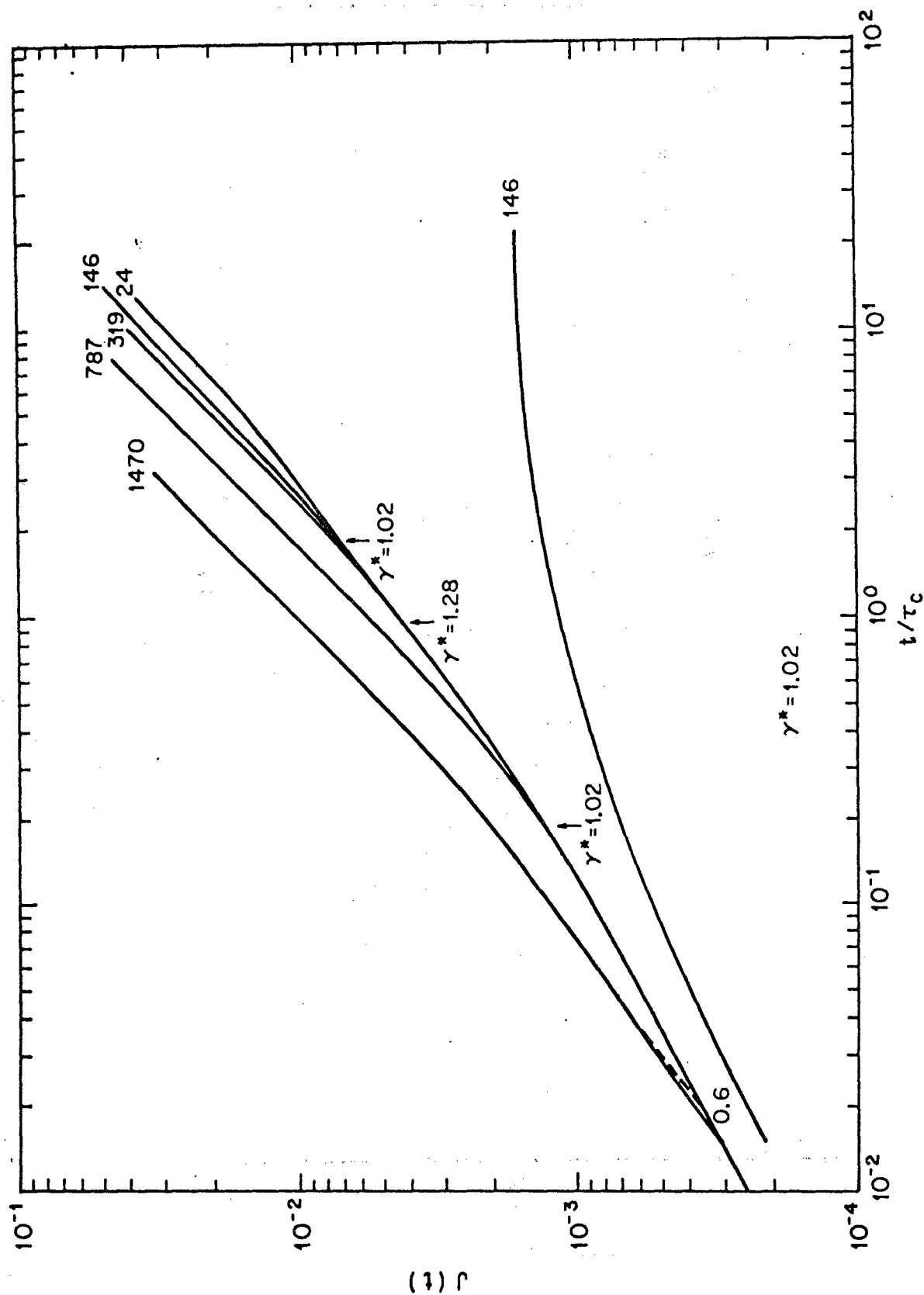


Figure 40 Creep compliance curves plotted against t/τ_c for various stress levels, for the 3.23% solution at 198°C (nematic). Also shown is the transient recovery curve for a particular stress level.

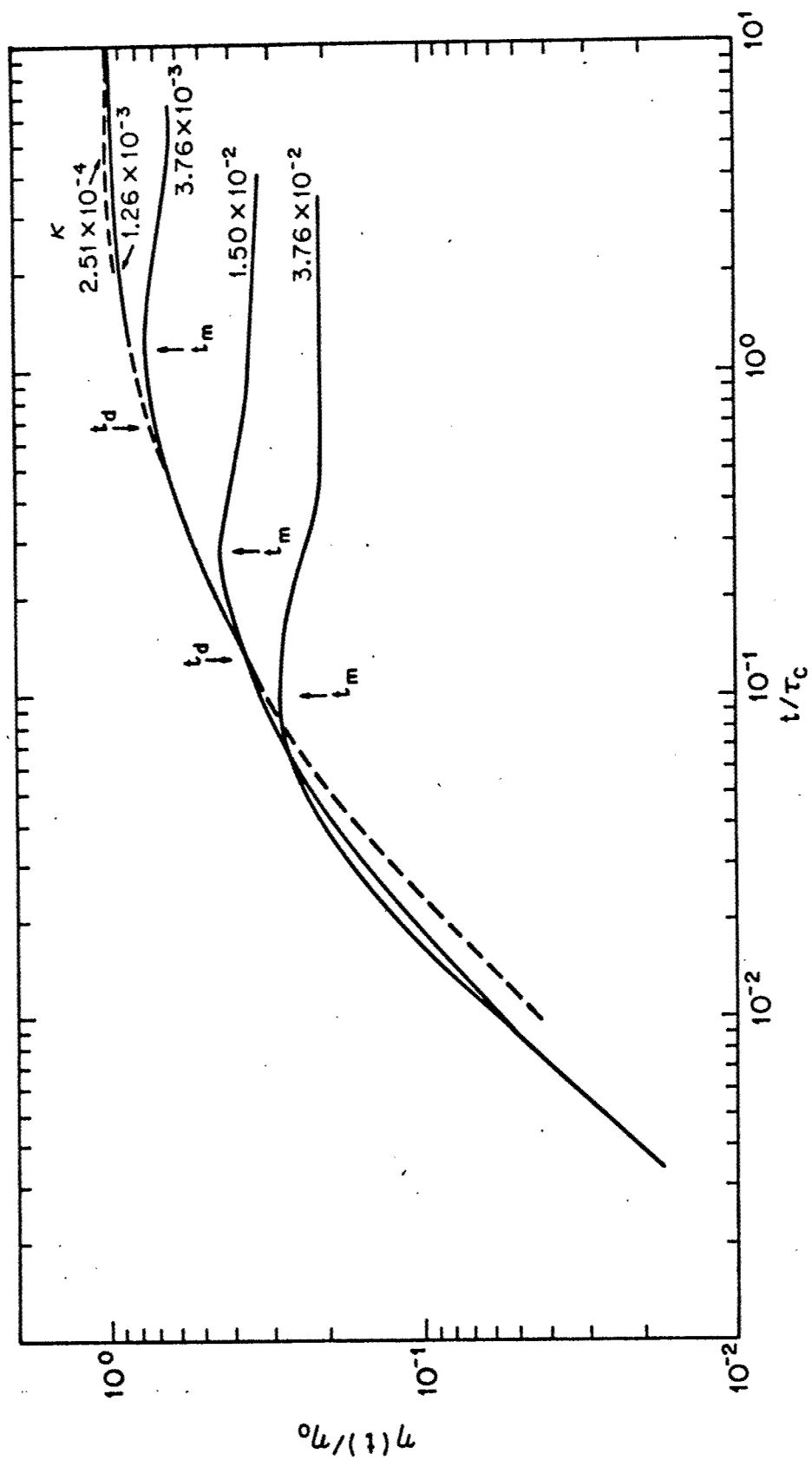


Figure 41 Stress growth curves plotted against t/τ_c for the 4.27% solution of PBT-53 in MSA at 10.5°C (nematic). 136

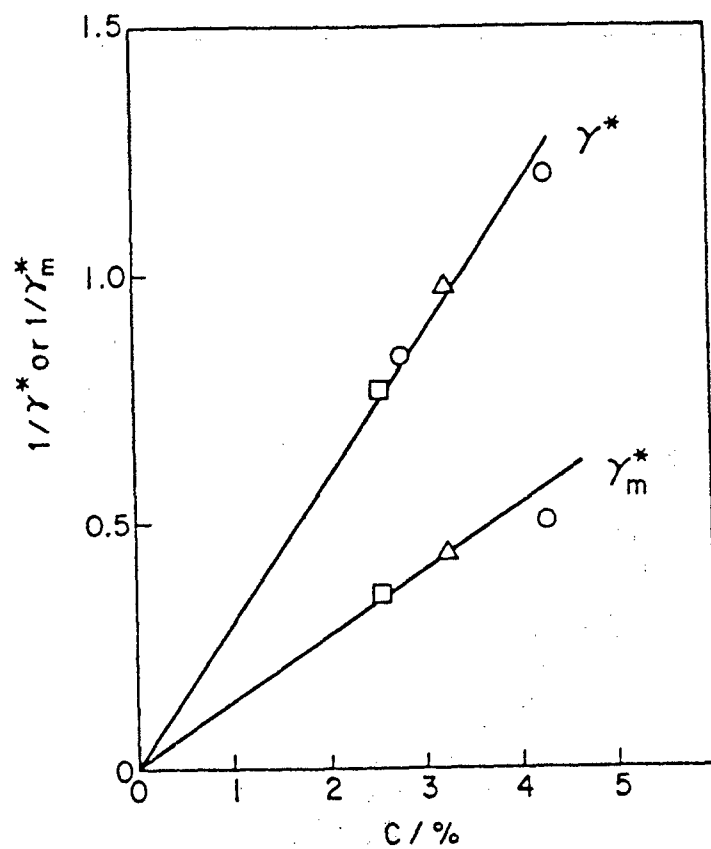


Figure 42

Inverse of the critical strains γ_m and γ^* as a function of concentration for solutions of PBT-53 in MSA.

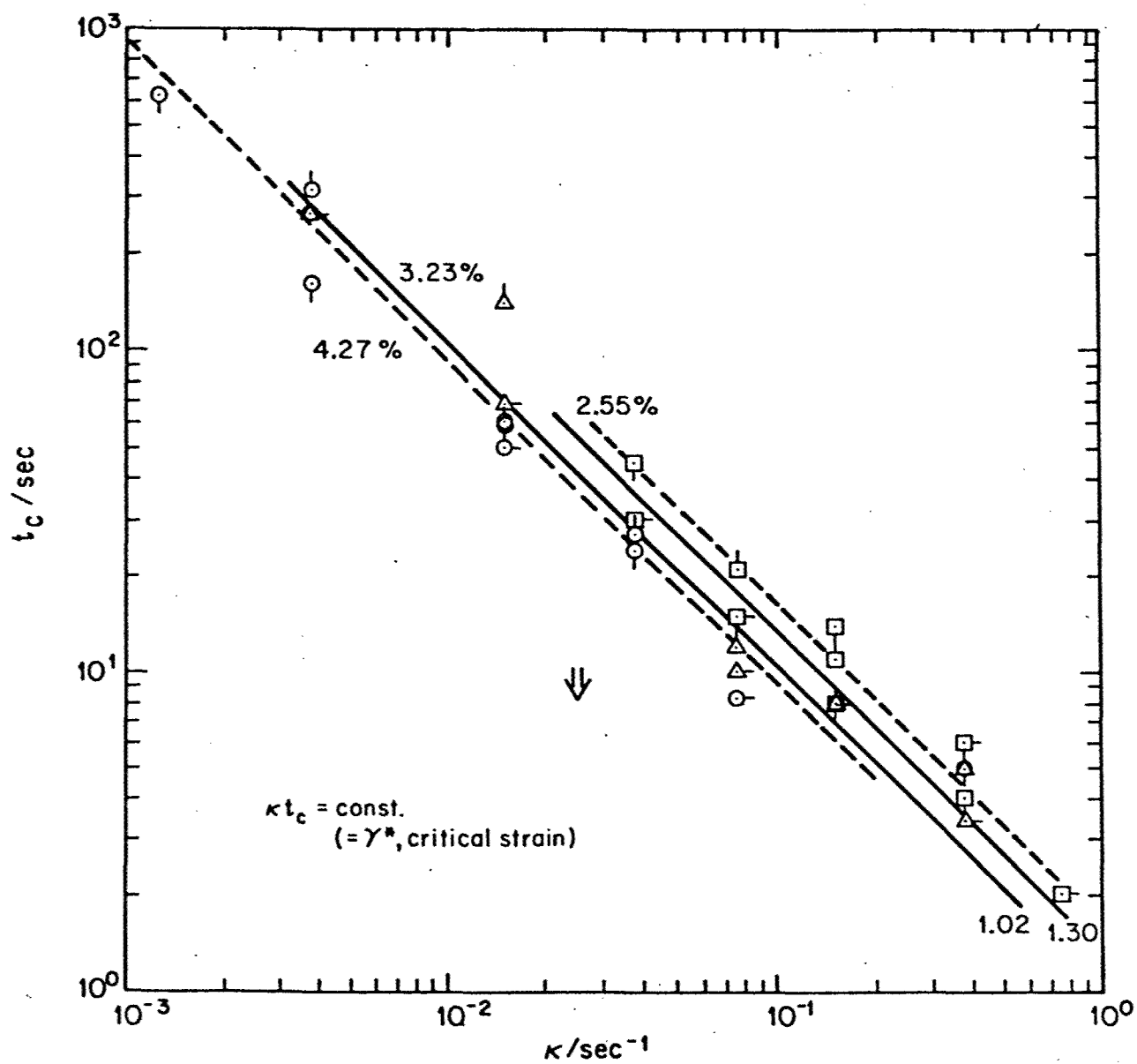


Figure 43

Plot of the parameter κt_c from stress-growth measurements against κ for the three different concentrations.

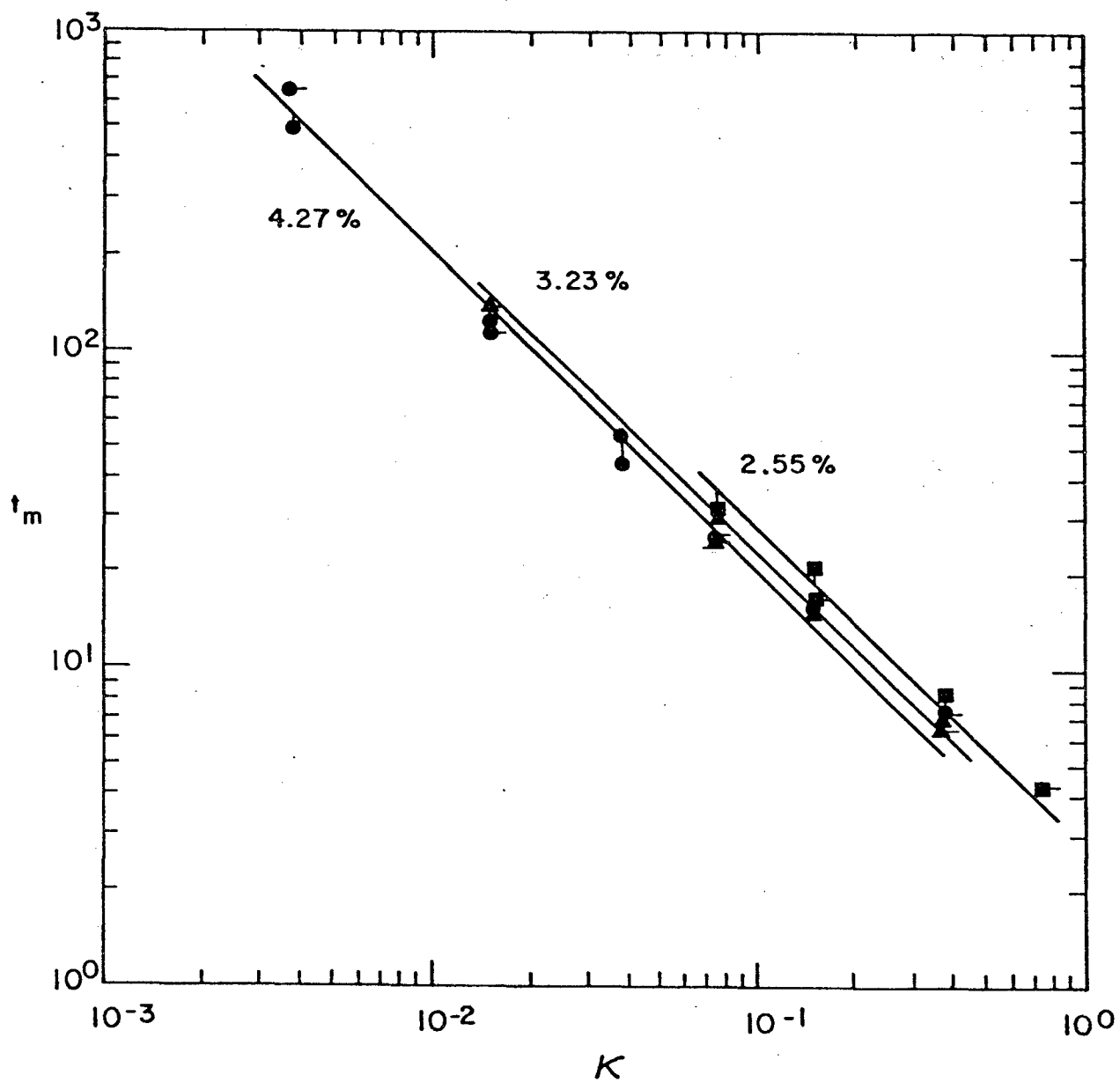


Figure 44

The time t_m to reach a maximum stress in stress growth as as function of shear rate for solutions of PBT-53 in MSA.

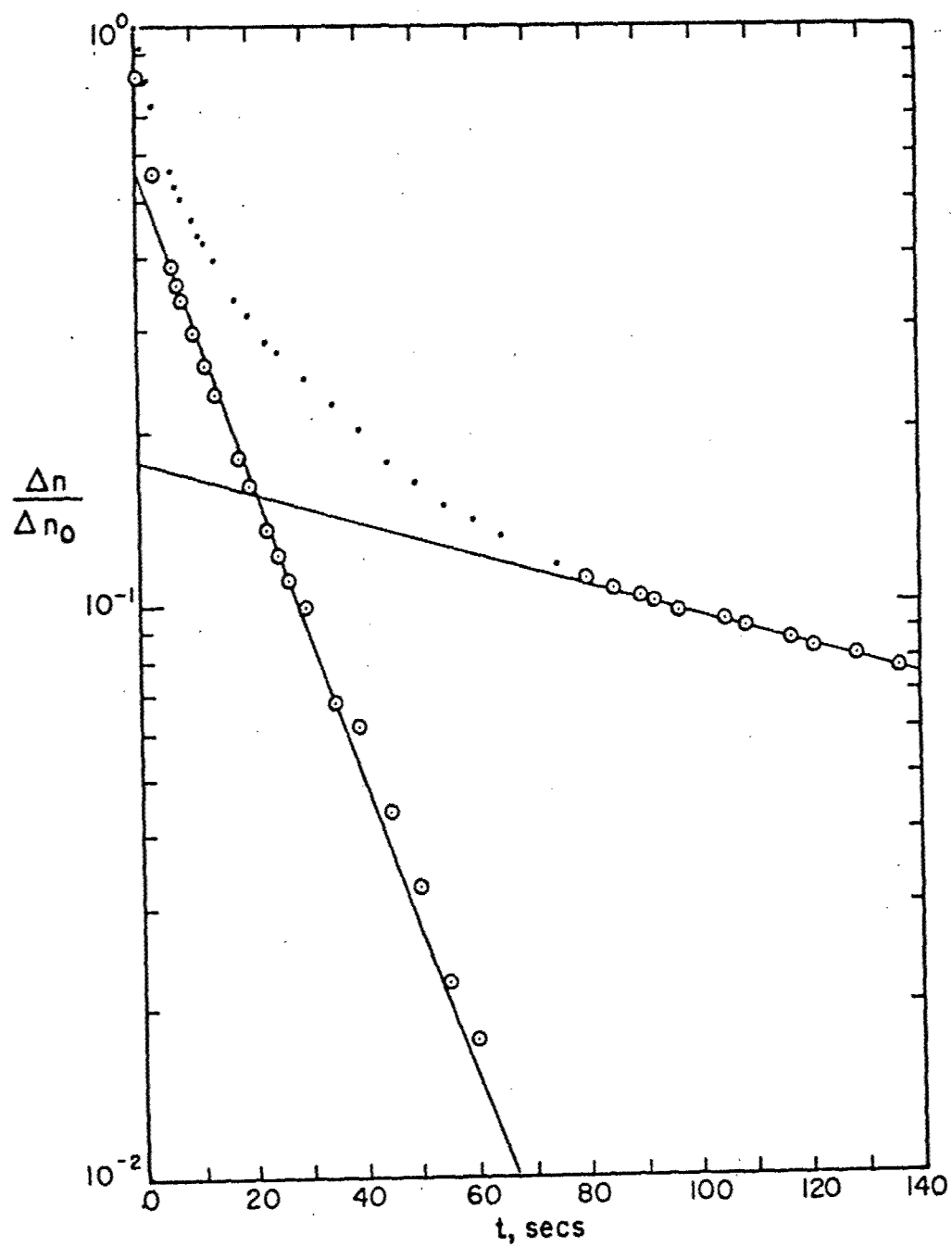


Figure 45 A typical birefringence relaxation curve, showing the resolution into two exponentials.

III. SOLUTION PROCESSING OF RODLIKE POLYMERS INTO RIBBONS

A.-F. Charlet and G.C. Berry

1. INTRODUCTION

Ribbons of rodlike polymers, such as poly(p-phenylenebenzobisthiozole), PBT, and the ladder polymer poly [(7-oxo-7, 10 H-benz-[de] imidazo [4¹, 5¹: 5,6] - benzimidazo -(2,1 - a) isoquinoline - 3,4 : 10,11 - tetrayl) - 10 - carbonyl 1], BBL, have been prepared from solutions in polyphosphoric acid, PPA, and methane sulfonic acid, MSA, respectively. Because of the high viscosity of the solutions in PPA, flow induced orientation could be maintained even without coagulation. The orientation of such ribbons could later be increased during tensile creep. X-Ray diffraction patterns obtained for ribbons prepared under different formation and post-formation processing conditions will be discussed below.

2. FABRICATION OF RIBBONS OF ROD-LIKE POLYMERS

2.1 Apparatus

The Wong Ribbon Fabrication Apparatus⁴⁰ has been improved by adding a heat exchanger to permit operation over a wider range in temperature; in our studies, water was used as heating fluid, and the temperature was kept at 80°C. A schematic drawing is shown in Figure 46. The solution of PBT is warmed to 160°C in container C and then pushed by nitrogen pressure through the stainless steel tube T, into the 4.75 mil gap between the moving Mylar tape and the stationary shear plate.

BBL solutions were not very viscous, and a 2 ml syringe was used to lead them into the gap, at room temperature. The shear rate κ is adjusted by controlling the velocity v of the tape with a motor M:

$$\kappa = \frac{v}{\ell} \quad (129)$$

where ℓ is the distance between the tape and the stationary shear plate; v was in the range of 0.01 to 1 cm/s.

The total strain γ is constant and given by

$$\gamma = \frac{L}{\ell} \quad (130)$$

where L is the length of ribbon subjected to shear stress; here, $L = 6$ cm, $\ell = 0.012$ cm so that $\gamma = 500$.

A coagulation bath B was used in some cases.

2.2 Solutions

2.2.1 PBT In PPA

Five solutions described below were provided by Celanese Research Co.

Number of Reference	Reaction Mixture Number	Concentration in wt %
28555-28-1	2895-32	2.95%
28555-29-1	3271-17	3.9 %
28555-29-2	3271-17	7.8 %
28555-28-2	2895-32	9.2 %
SRI - PBT	3271-15	10 %

All solutions have been degassed for a few days under vacuum at 120°C for 2.95% and 3.9% solutions, 160°C for 7.8% and 180°C for 9.2% and 10%. These temperatures were chosen to facilitate the degassing process. As a result of the high viscosity at lower temperatures, gases escaped very slowly and had a tendency to expand, increasing the solution volume rather than to diffuse through it.

The solutions with concentration 3.9% and 7.8%, coming from the same reaction mixture 3271-17 formed a kind of gel after heat treatment and did not flow. Moreover, a white precipitate appeared--these materials were not processed.

Ribbons either uncoagulated or coagulated, obtained from the three other solutions are listed in Table 18 and Table 19. For easy reference, each sample has been attributed a number; the digits before the dash

give the approximate concentration in weight %; the digits after the dash come from graduations of the regulator used to control v , and vary almost linearly with v . Designations and U C refer to samples prior to coagulation and after coagulation, respectively.

TABLE 18

UNCOAGULATED RIBBONS

Number	v (cm/s)	K (s ⁻¹)
--------	---------------	---------------------------

Concentration = 2.95%

3-60 U	0.016	1.33
3-80 U	0.040	3.33
3-100 U	0.060	4.97

Concentration = 9.2%

9-540 U	0.63	52.22
9-733 U	0.85	70.45
9-1000 U	1	82.88

Concentration = 10%

10-100 U	0.064	5.30
10-130 U	0.078	6.46
10-150 U	0.1	8.29
10-200 U	0.114	9.45
10-230 U	0.155	12.84
10-280 U	0.217	17.98

TABLE 19

RIBBONS COAGULATED IN WATER

Number	v (cm/s)	K (s ⁻¹)
--------	---------------	---------------------------

Concentration = 2.95%

3-100 C	0.060	4.97
---------	-------	------

Concentration = 9.2%

9-540 C	0.63	52.22
---------	------	-------

Concentration = 10%

10-100 C	0.064	5.30
10-130 C	0.078	6.46
10-150 C	0.1	8.29
10-200 C	0.114	9.45
10-230 C	0.155	12.84
10-280 C	0.217	17.98

When starting an experiment, the velocity v was set at an arbitrary value and eventually varied; its limits were imposed by experimental conditions: as v was decreased, the tension on the Mylar tape increased until the point where it broke; as v was increased, the width of the ribbon formed decreased until no material came out at all.

In general, solutions were greenish. Uncoagulated ribbons are yellow if dry, but became orange on adsorption of moisture from the air. Once dry, coagulated ribbons, also orange, show blue reflections, possibly due to orientation.

After processing, ribbons were kept in a dessicator with a drying agent.

With the 2.95% solution, interchain forces were too low to maintain ribbons, which mostly split into fibers. Only a few specimens were obtained, but disorientation occurred on storage; the ribbons collapsed and spread into large spots.

2.2.2 BBL In MSA

In Table 20 are listed ribbons obtained from solutions of BBL in MSA prepared at Carnegie-Mellon University. BBL was provided by F.E. Arnold, (Polymer Laboratory, Wright-Patterson Air Base, Ohio). Before use, it was dried under vacuum at room temperature for three days and then mixed with distilled methane sulfonic acid and stirred until homogeneous.

TABLE 20
CONDITIONS FOR RIBBON FORMATION

Sample Number	Concentration in wt %	v cm/s	κ^{-1} s	Coagulant
1	3.58 %	0.5	41.44	H ₂ O
2	3.58 %	0.5	41.44	H ₂ SO ₄ 5% (by wt)
3	5.84 %	0.5	41.44	H ₂ O
4	5.84 %	0.2	16.58	H ₂ O

For sample 1, coagulation was too fast and the ribbon adhered to the Mylar tape; the latter had to be dissolved, an appropriate solvent being phenol; the ribbon was then thoroughly washed with acetone and water.

Sample 2 was to be coagulated with 20% H₂SO₄ solution, but since coagulation was not complete at that acid level, the concentration had to be reduced to 5% to obtain coagulation as seen from the change in color of the ribbon.

All solutions were dark red; dry coagulated ribbons appear to be golden brown and shiny.

Observation of the ribbon through crossed polarizer and analyzer did not reveal any birefringence. No orientation was seen from X-Ray diffraction analysis in the conditions of exposure, i.e., with the X-Ray beam perpendicular to the plane of the ribbon; it would be interesting to take X-Ray diffraction films with the beam parallel to the plane of the ribbon, to see if any, interplanar orientation might exist in the plane of the ribbon.

BBL ribbons are very brittle and no creep experiment was performed since all samples broke in a direction perpendicular to the long axis of the ribbon.

3. TENSILE CREEP AND RECOVERY

3.1 Apparatus

A detailed description of the tensile creep and recovery apparatus has been given previously.⁴⁸ A schematic drawing of the apparatus is given in Fig. 47.

The sample, usually 4cm long, is held between two clamps, the lower clamp being fixed and the upper clamp attached to the bottom of a thin walled Invar tube. This tube terminates in the core of a linear variable differential transformer (LVDT), which is attached to a fine wire. The force is supplied by applying a weight on the other end of the lever arm; 50 and 100 g were used; additional weight was added to eliminate bows in the sample, especially for coagulated ribbons. Change in length of the order of 10^{-5} cm is detected by the LVDT. The entire apparatus is enclosed in glass and the environment can be controlled; all experiments reported here were done in nitrogen with a partial vacuum of 30 cm Hg, at room temperature. Another LVDT mounted in series with the first one but outside the glass is used to determine the calibration constant k found to be 0.0101 cm/mv.

3.1.1 Results

Tensile creep and recovery will be described below for uncoagulated and coagulated ribbons of PBT formed from solutions with 9-10% polymer. The X-Ray diffraction results to be discussed in the next section, show that the ribbons processed from the 2.95% solution are nearly unoriented. However, the X-Ray pattern was taken after the uncoagulated sample was stored for one week, and during this time, disorientation

could have occurred. This can be true for the coagulated sample too. Since coagulation was done after some days of storage. The tendency for failure under very small tension or torsion (after two weeks of storage) discouraged attempts to perform creep experiments with coagulated and uncoagulated ribbons. Breakage occurred, as for BBL, in the direction perpendicular to the long axis of the ribbon both uncoagulated and coagulated ribbons. None of these samples exhibited birefringent behavior when examined about two weeks after formation.

3.1.2 Young's Modulus

The Young's modulus E (in g/den) is given by

$$E = \frac{\sigma}{\epsilon} \quad (131)$$

where σ is the stress (in g/den) and ϵ the strain:

$$\sigma = \frac{W}{W_L} \quad (132)$$

$$\epsilon = \frac{\Delta l}{l_0} \quad (133)$$

Here W is the weight loaded on the specimen, which has weight W_L per 9,000 m, l_0 is the length of ribbon between the clamps (in cm), and Δl is the change in length read from the recorded curve calculated from the change Δv in the recorder responses:

$$\Delta l = k \Delta v \quad (134)$$

where $k = 0.0101/s$ (cm/mv) with S a scale factor ($S = 0.5, 1, 2, 4$ or 8).

A series of weights ranging from 10 to 100 g was applied to the sample

and for each weight, E was calculated; the average value is reported in Table 21. The sample was allowed to creep for one day with a 100 g weight applied, and recover overnight. Then, another series of weights was applied to determine E again. E was found larger in most cases after creep and recovery, except for 10-150U and 10-280U samples that exhibit a decrease in E. This is unexpected behavior and should be checked as it could arise from experimental error.

For four samples, 9-540 U, 9-733 U, 10-280 C and 9-540 C, E increased by 40 to 50%; however, these results give too large a value for E after creep because of an error in calculation of the denier of the sample. The entire sample was weighed after creep. It was later found that solvent was lost by contact with polyethylene sheets on which ribbons were stored and on the clamps, thus leading to an error in the estimate for denier. As a consequence, the factor of about 10 between the concentrations of polymer in uncoagulated and coagulated ribbons processed at the same v is not maintained for E. To eliminate this error, only the central part of the sample was weighed after being left under the vacuum for one day to eliminate residual humidity.

It can also be noted that the increase in E is more important with uncoagulated ribbons than with coagulated ones. This is reasonable since solvent promotes chain mobility, permitting orientation in the elongational stress field.

Results for E do not appear to be related coherently either to the velocity of the tape, particularly for uncoagulated ribbons, or to the deniers. Although great care was taken in choosing the samples in the central part of the ribbons, there are large differences in E from one sample to another. These could arise from a variation in the structure of the ribbon due to an irregular flow of the solution. Thickness would be the most affected.

TABLE 21

PROPERTIES OF PBT RIBBONS

Sample Number	Deniers	E ^(a) (g/den)	X Ray ^(c) pattern	E ^(b) (g/den)	X Ray ^(c) pattern	Relative Change in E
10-100U	1102.5	47.3	-	Sample broke	-	----
10-150U	1025.6	35.6	0	34.0	Sample lost	-2.8%
10-200U	967.5	65.7 ^(d)	0	87.5 ^(d)	0	+33.2%
10-280U	994.2	81.2 ^(d)		75.5 ^(d)		-7%
9-540U	789.5	34.6	-	49.2	-	+42.2%
9-733U	472.5	63.6 ^(d)	0	88.0 ^(d)	0	+38.4%
9-1000U	680	42.0	-	53.3	-	+26.8%
10-100C	360	241.0		298		+20.0%
10-130C	321.4	186.6		230		+23.5%
10-200C	340.5	204.3		249.5		+22.1%
10-280C	260.5	223.4		307.0		+37.4%
9-540C	402.6	171.4		255.7		+49.2%
(e) 10-130*	165.7	506	0	597	0	+18%
(e) 9-540*		460	0	----	0	

(a) Average value of E calculated with the first series
of weights added before creep and recovery.

(b) Average value of E calculated with the second series
of weights added after creep and recovery.

(c) See section IV.

(d) These values have to be regarded with caution; see text.

(e) See section II 2 and 3, OTHER EXPERIMENTS.

3.1.3 Tensile Creep Compliance

Plots of the tensile creep compliance D and the recoverable compliance D_R , versus time are given in Figs. 48-51. D and D_R are of the order of 10^{-2} den/g for uncoagulated ribbons and 10^{-3} for coagulated ones; both increase slightly over the period of time extended to four decades. Although the $E(t)$ curves would suggest a solid-like behavior, there is not complete recovery. As would be suspected, PBT recovery is faster and more complete for coagulated than for the uncoagulated precursor.

Linear viscoelastic behavior would exhibit the same initial jump in strain for creep and recovery, and thus the same value for the initial tensile creep and recoverable compliances. This is not observed for the samples studied here. The jump obtained for the recovery is close to the one obtained subsequently in creep when the second series of weight was added, as shown in Table 22 (10-150 U is an exception). These results indicate that some of the orientation gained during creep persists after recovery, resulting in a higher modulus for the ribbon in subsequent deformation.

3.1.4 Other Experiments

As E was increased after creep, another type of experiment was devised. Some samples were allowed to creep for one day and were then coagulated in water with the 100 g weight still applied. Contact with water resulted in shrinkage almost immediately and splitting into fibers or two ribbons due to the constraint to shrinkage in the neighborhood of the clamps. These samples will be labelled with a star (*). After drying the sample, creep and recovery was performed and E calculated.

TABLE 22

CREEP AND RECOVERY DATA

Sample	(a) $D \times 10^2$ den/g	(b) $D_R \times 10^2$ den/g	(c) $D \times 10^2$ den/g	Relative difference between (b) D_R and (c) D
10-100U	2.10	1.17	---	-----
10-150U	3.32	1.72	2.94	+70.9%
10-200U	1.39	0.98	1.14	+14%
10-280U	1.21	0.86	1.32	+32%
9-540U	2.35	1.92	2.03	+5.7%
9-733U	1.55	1.10	1.14	+3.6%
9-1000U	2.20	1.73	1.87	+8.1%
10-100C	0.403	0.328	0.335	+2.1%
10-130C	0.497	0.420	0.435	+3.4%
10-200C	0.497	0.390	0.401	+2.8%
10-280C	0.456	0.325	0.326	+0.3%
9-540C	0.571	0.389	0.391	+0.5%
10-130*	0.186	0.165	0.167	+1.2%
9-540*	0.206	0.185	----	-----

(a) Initial tensile creep compliance

(b) Initial Recoverable compliance

(c) Tensile creep compliance calculated as $\frac{1}{E}$ after creep and recovery when the second series of weights is added.

Two samples, 10-200* and 10-100* split into fibers and broke when clamped in a direction perpendicular to the long axis of the ribbon.

PBT 9-540* gave a very encouraging result, since E calculated was 460 g/denier, i.e, 2.7 times greater than the Young's modulus found for the same sample coagulated, 9-540C, without the intervening creep. (This sample recovers up to 90%, Table 22).

Creep was performed on half of a fourth sample, 10-130* after it had split into two parts along the long axis of the chains. To avoid breakage, only a 50 g weight was added for the creep experiment. The average value for E before creep is 500 g/den, and E after creep is 597 g/den i.e, respectively 2.7 and 2.6 times greater than the values obtained for 10-130C sample.

4. X-RAY DIFFRACTION

Oriented polymers exhibit typical X-ray diffraction patterns, already discussed by Berry.⁴⁸

Films show characteristic sets of arcs with Bragg's spacings found to be 3.45\AA° and 5.17\AA° ; comparing with results reported by Berry on BBB, 3.45\AA° would arise from interplanar distances and 5.17\AA° from interchain spaces in a same plane; 15\AA° was not seen in the conditions of exposure. The 5.17\AA° is smaller than 8\AA° found for BBB; this is not surprising since PBT repeat unit is not as wide as BBB.

4.1 Experimental Conditions

A flat camera was placed at 6cm from the specimen with the X-ray beam coming perpendicularly to the plane of the sample. Exposure time was set to 20 hours except in some cases where it was increased to 40 or 60 hours. The X-Ray beam was produced with a copper target. The tube power was set to 700 w (35 kV, 20 mA).

4.2 Results

A 20 hours exposure gave nothing with 2.95% ribbons but with two ribbons stuck together, and a 60 hour exposure time, a very faint ring appeared at 3.45\AA° ; this suggests that the chains are little oriented in the plane of the ribbon, at the time of experiment, i.e, after one week storage, but that no further orientation occurred. Chains do not appear to be regularly arranged in a same plane, and 5.17\AA° ring was not seen (see Fig. 52).

A film was taken for each PBT sample listed In Table 21, and for the * labelled samples before and after creep experiment; usually, 2 sets of arcs were characteristic on these films, with a varying intensity and shape according to the orientation.

Two kinds of patterns were obtained; the first kind, indicated with a line in Table 21, shows fine, thin, sharp arcs, and by comparison with E values, it is seen that they correspond to samples with Young's modulus; in the low end of the observed range. This is illustrated in Fig. 53a, (10-100U). In the other patterns, arcs have become shorter in the longitudinal direction, and more spotty. Such patterns are indicated by a circle in Table 21; and occur when E is high. An example is shown in Figure 54 (10-200U after creep) and figure 10 (9-540*); 10-130* also gave this kind of pattern.

Most of the time, especially noticeable with uncoagulated ribbons, films are much more intense and sharp after creep; see Figure 53 a and b (10-100U). If present at all, such effects are less pronounced with coagulated ribbons. Surprisingly, these latter give a faint pattern built up with very large spots instead of fine arcs. This change could be attributed to solvent which can act as side chain and so increase the number of diffractant centers giving same Bragg's spacings as PBT. Another reason is that coagulation can result into distruction of of centers of diffraction, due to rupture of some chains and decrease intensity of X-Ray films.

5. CONCLUSIONS

The special processing used here to fabricate oriented ribbons is promising for PBT; further studies should involve fabrication of ribbons at higher and lower shear rates, with improvement in the regularity and reproducibility of the samples. A measurement of the intensity of X-ray patterns would be necessary to relate the results with E values. It would be worth it to go on research with the * labelled samples for their Young's modulus seem to be greatly increased.

A. Teflon Roller
 B. Coagulation Bath
 C. Stainless Steel Container
 G. Guiding Rod
 H. Heat Exchanger

I. Backing Plate
 J. Shearing Plate
 N. Capitan Attached to Motor M.
 O. Nitrogen Inlet
 P. Polymer Solution

R. Rubber Roller
 S. Adjustable Screw and Dovetail
 T. Stainless Steel Tube
 W. Weight

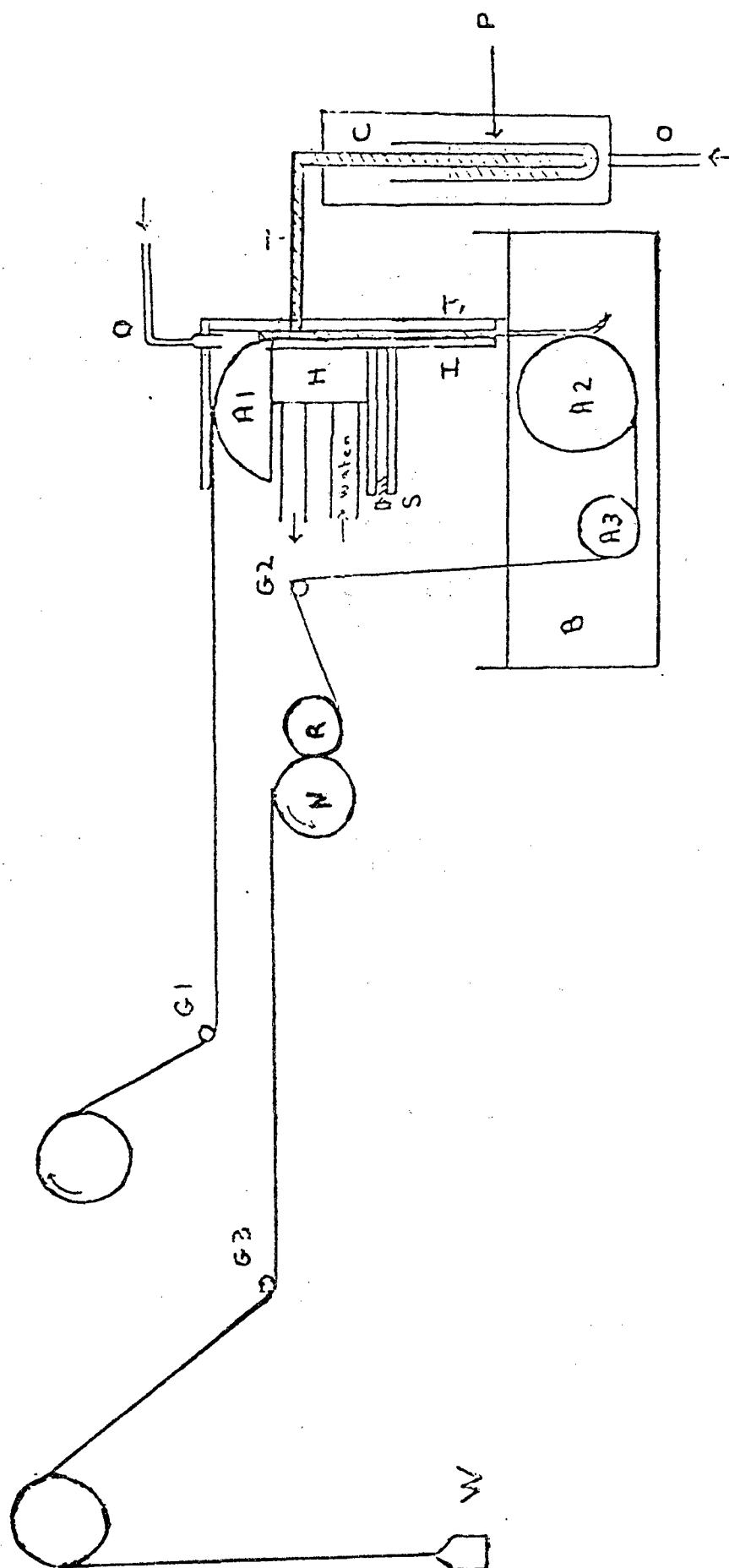


Figure 46 Ribbon fabrication apparatus

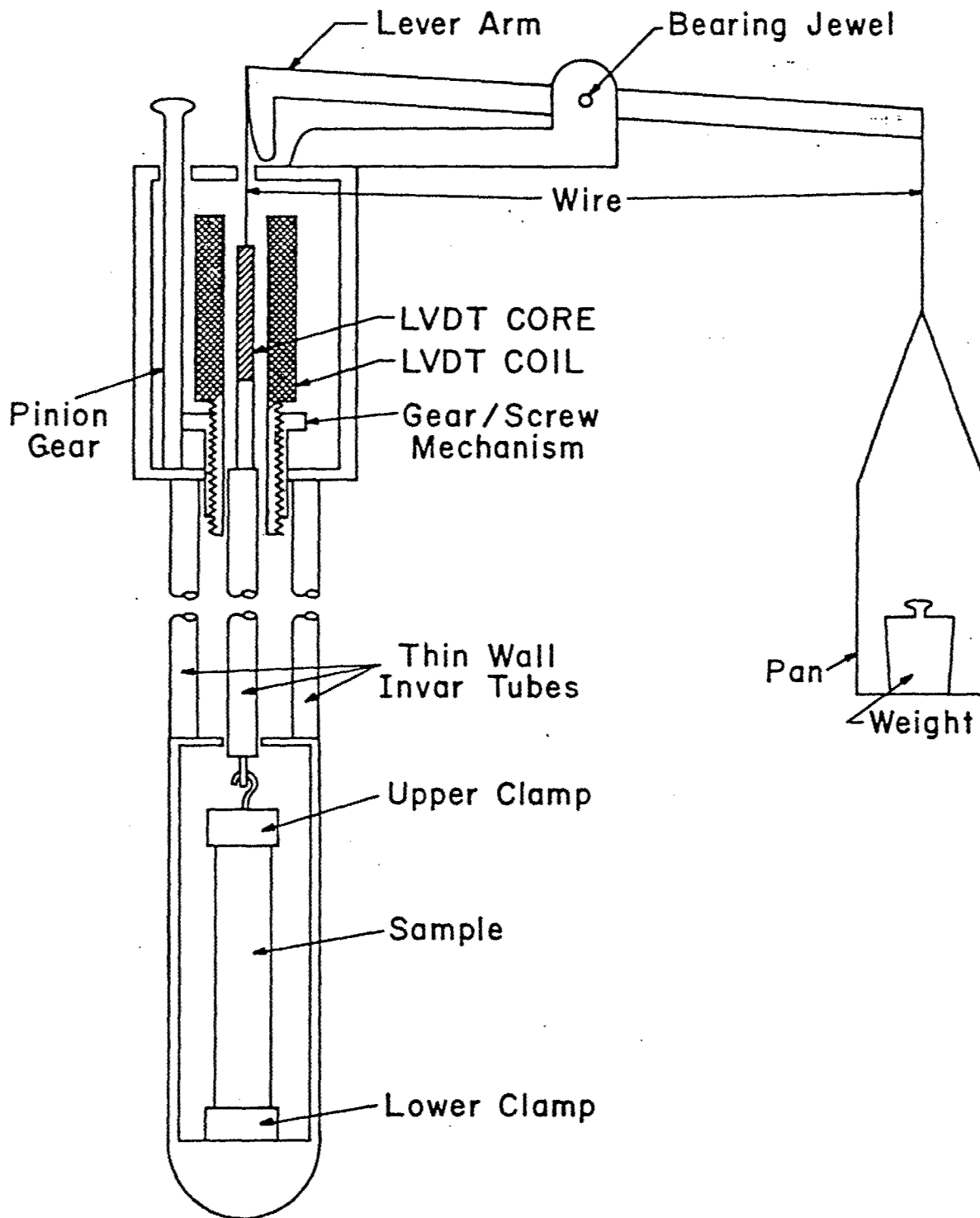


Figure 47 Schematic drawing of tensile creep apparatus.

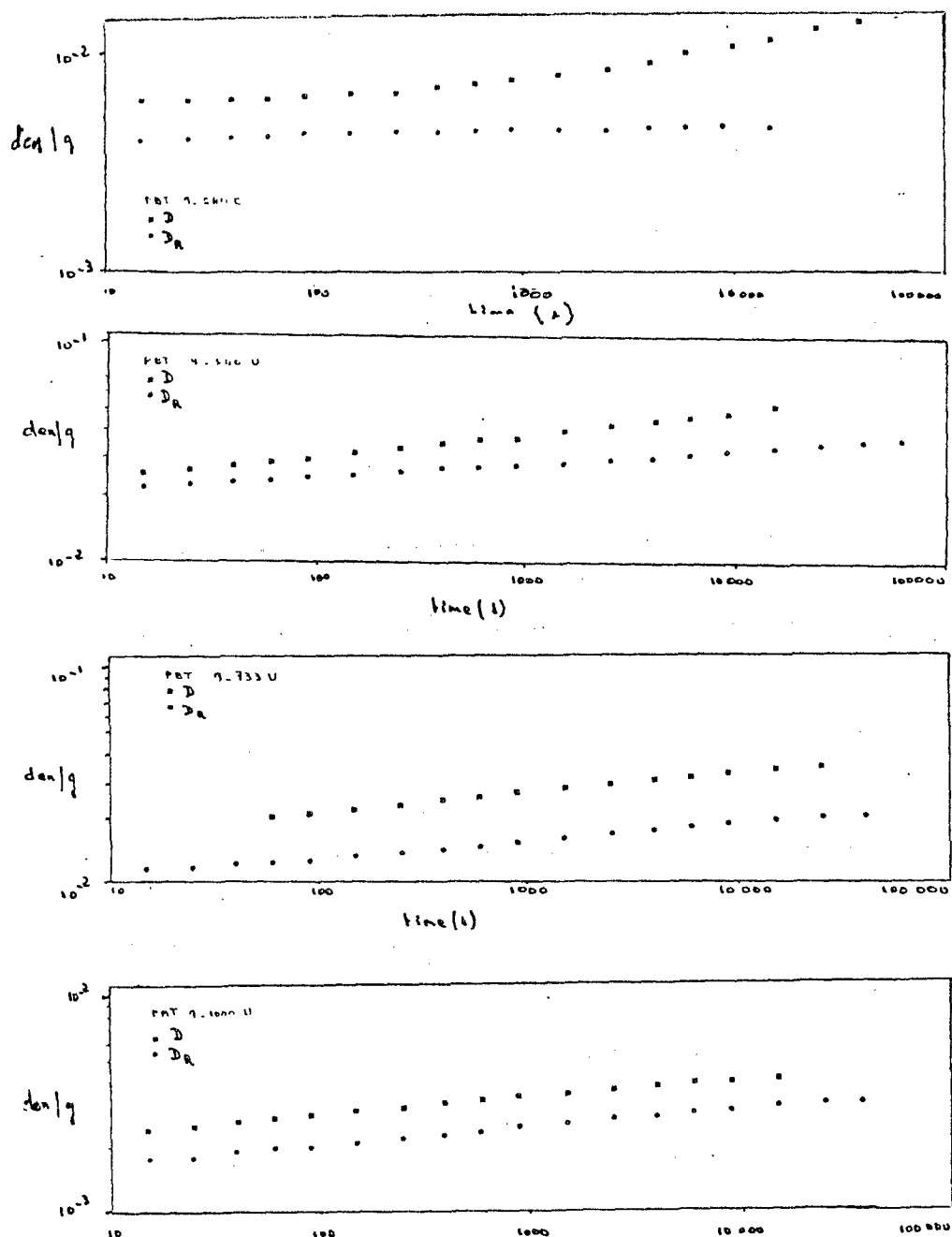


Figure 48 Creep and Recovery for several ribbons prepared with 9.2 weight percent PBT solution:

- a) 9-540 C
- b) 9-540 U
- c) 9-733 U
- d) 9-1000 U

Series U are prior to removal of PPA solvent, and series C are after removal of PPA.

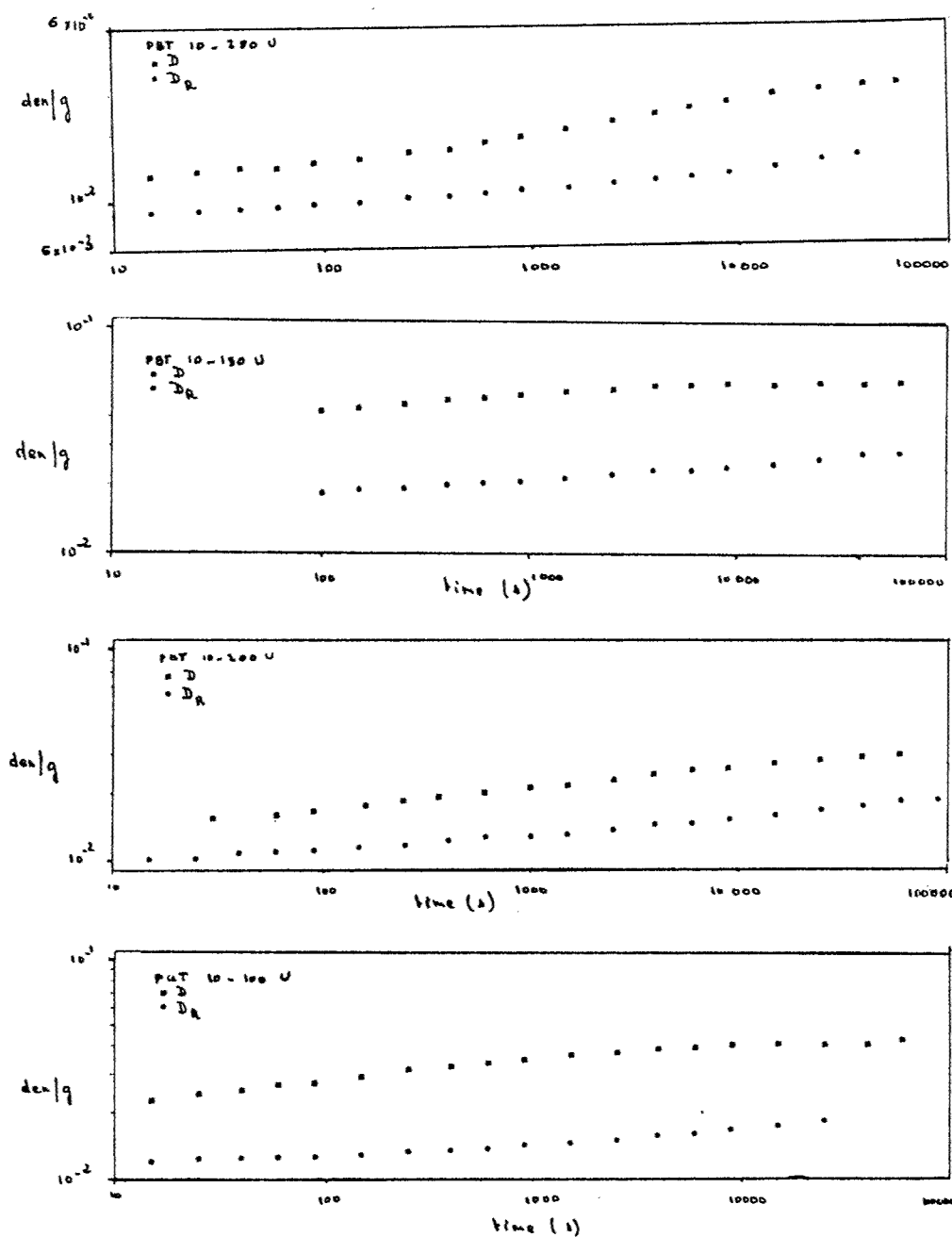


Figure 49 Creep and recovery for several ribbons prepared with 10 weight percent PBT; all prior to removal of PPA solvent:

- a) 10-280 U
- b) 10-150 U
- c) 10-200 U
- d) 10-100 U

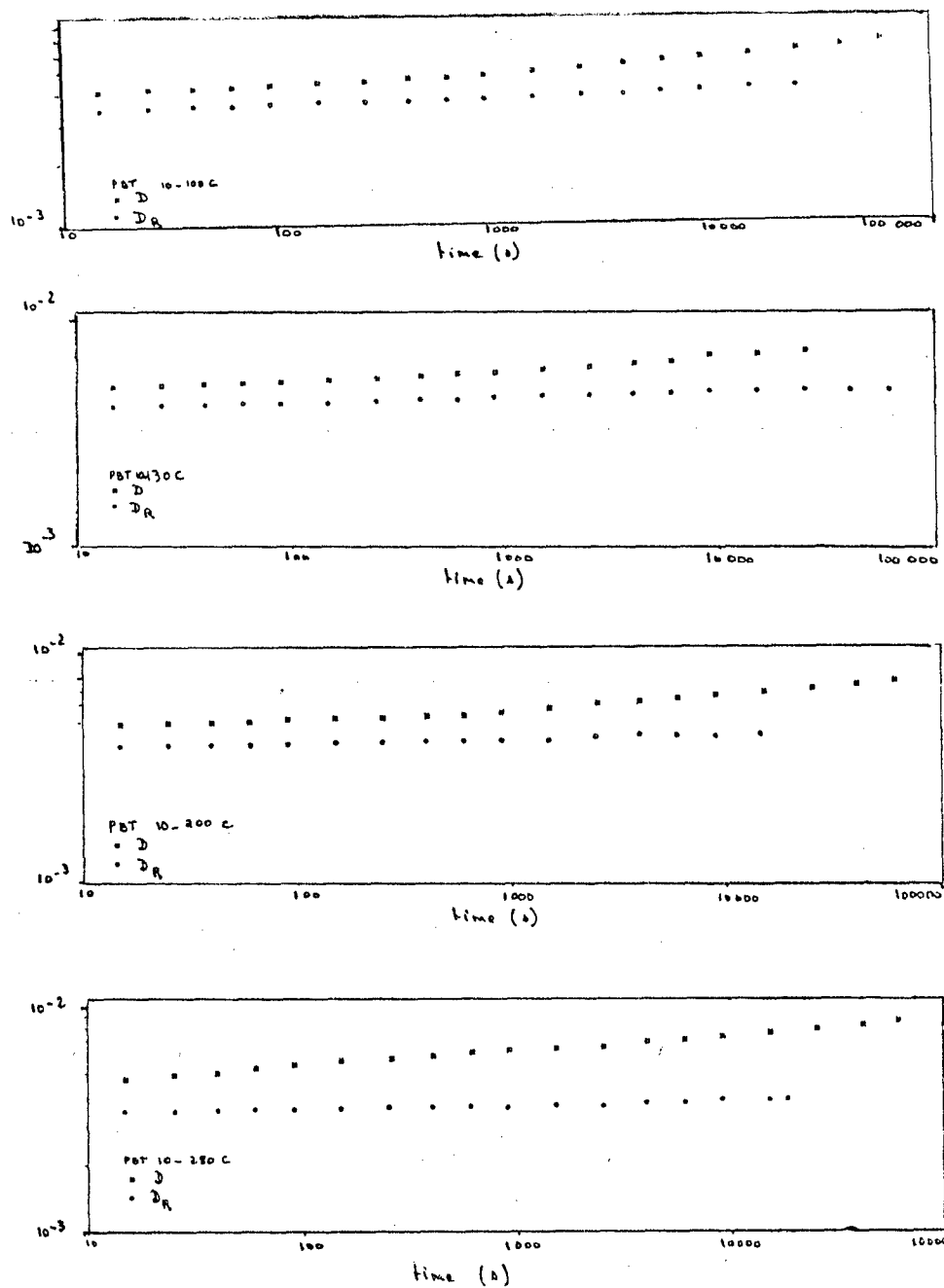


Figure 50 Creep and recovery for several ribbons prepared with 10 weight percent PBT; all after removal of PPA solvent:

- a) 10-100 C
- b) 10-130 C
- c) 10-200 C
- d) 10-200 C

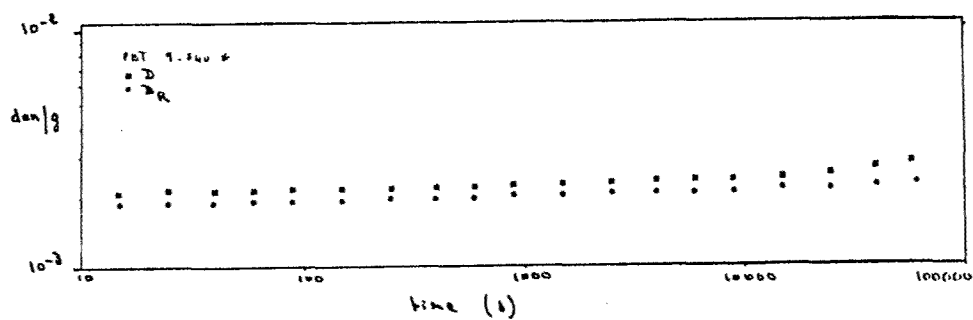
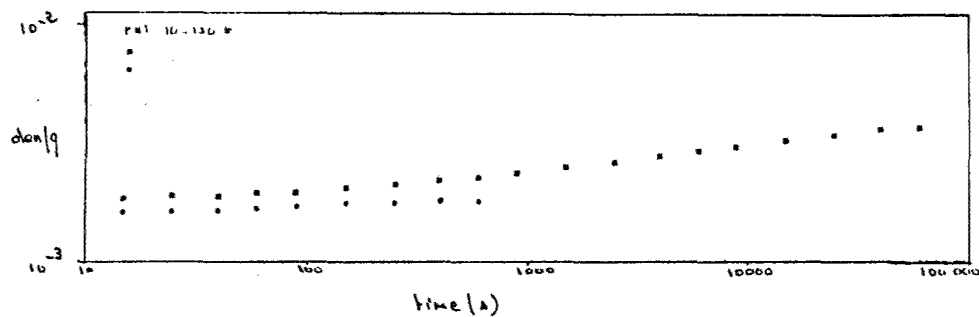


Figure 51 Creep and Recovery for PBT ribbons given post formation creep treatment prior to removal of PPA solvent. Data are for ribbons after removal of PPA:

- a) 10-130*
- b) 9-540*

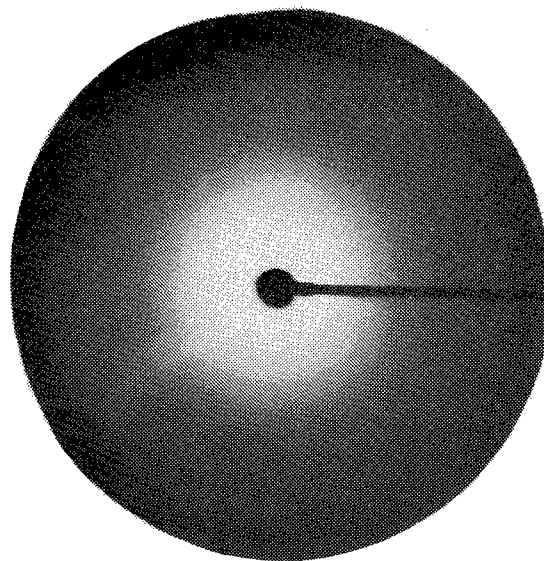
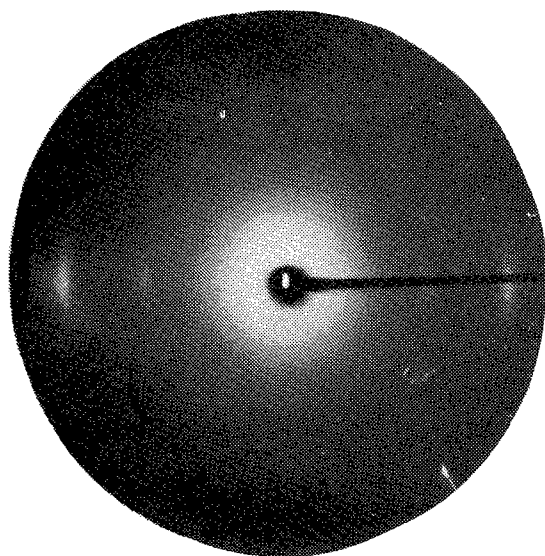
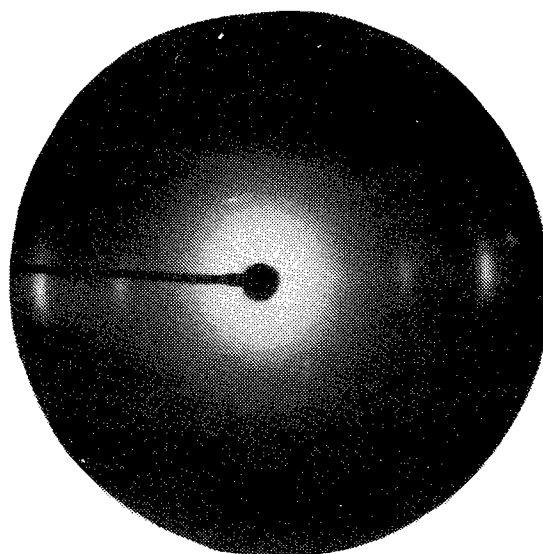


Figure 52 X-ray diffraction from ribbon PBT 3-100 U. Specimen 6 cm from film.



(a)



(b)

Figure 53 X-ray diffraction from ribbon PBT 10-100 U; a) before creep; b) after creep and recovery. Specimen 6 cm from film with ribbon axis vertical and x-ray became perpendicular to the plane of the ribbon. Major equatorial reflections are at 3.45 and 5.17 Å.

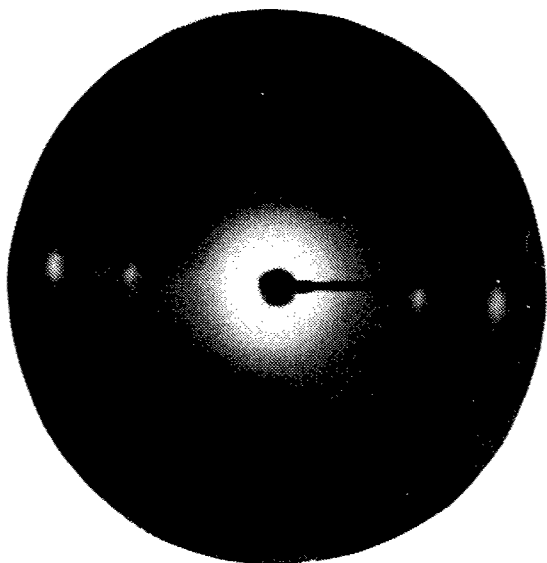


Figure 54 X-ray diffraction from ribbon PBT 10-200 U after creep and recovery. Conditions are as specified in Fig. 8 caption.

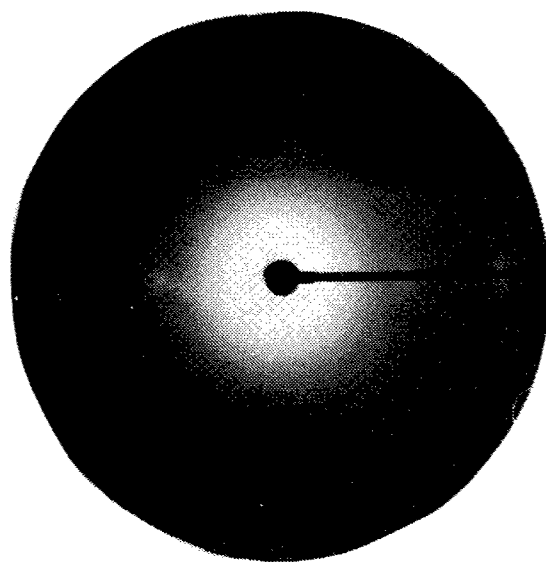


Figure 55 X-ray diffraction from ribbon PBT 9-540* after creep and recovery. Conditions are as specified in Figure 8 caption.

REFERENCES

1. C.-P. Wong, H. Ohnuma and G. C. Berry, J. Poly. Sci., Poly. Symp. 65, 173 (1978).
2. G. C. Berry, J. Poly. Sci., Poly. Symp. 65, 143 (1978).
3. G. C. Berry, Discuss Farad. Soc. 49, 121 (1970).
4. C.-P. Wong and G. C. Berry in Structure-Solubility Relationships in Polymers, ed. F. W. Harris and R. B. Seymour, Academic Press, New York, 1977, p. 71.
5. R. J. Gillespie and E. A. Robinson, in Non-Aqueous Solvents, T. C. Waddington, ed., Academic Press, New York, 1965, Chapter 4.
6. G. S. Manning, J. Chem. Phys. 51, 924 (1969).
7. G. C. Berry and P. R. Eisman, J. Poly. Sci., Poly. Phys. Ed. 12, 2253 (1974).
8. E. R. Pike and E. Jakeman, Adv. Quantum Electronics 2, 1 (1974).
9. B. J. Berne and R. Pecora, Dynamic Light Scattering, Wiley-Interscience, New York, 1976, Chapter 8.
10. D. B. Cotts and G. C. Berry, Macromolecules, in press.
11. T. E. Helminiak, F. E. Arnold and C. L. Benner, Polymer Preprints, Am. Chem. Soc. 16 (1), 683 (1975).
12. J. F. Wolfe, B. H. Loo and F. E. Arnold, Polymer Preprints, Am. Chem. Soc. 20 (1), 82 (1979).
13. P. Metzger Cotts and G. C. Berry, to be published, P. Metzger, Ph.D. Thesis, Carnegie-Mellon University, Pittsburgh, PA, 1979.
14. A. Fratini, private communication.
15. P. Picker, E. Tremblay and C. Jolicœur, J. Solution Chem. 3, 377 (1974).
16. M. Bertolotti, in Photon Correlation and Light Beating Spectroscopy, E. Z. Cummins and E. R. Pike, ed., Plenum Press, New York, 1973, Chapter 3.
17. N. Ben-Yosef, S. Zweigenbaum and A. Weitz, Appl. Phys. Lett. 21, 436 (1972).
18. F. Perrin. Compt. Rend. P. 178, 1978 (1924).

References (continued)

19. D. J. R. Laurence, in Physical Methods in Macromolecular Chemistry, B. Carrol, ed., Marcel Dekker, 1969 , Chapter 5 .
20. T. Kojima, J. Poly. Sco., Poly. Phys. Ed. 18, 1685 (1980).
21. P. J. Flory, Proc. Roy. Soc. (London) A234, 60 (1956).
22. H. Yamakawa and W. H. Stockmayer, J. Chem. Phys. 57, 2843 (1972).
23. G. C. Berry, P. Metzger Cotts and S.-G. Chu Brit. Poly. J., in press.
24. H. Yamakawa and M. Fujii, Macromolecules 6, 407 (1973); 7, 128 (1974).
25. S. I. Abdel-Khalik and R. B. Bird, Biopolymers 14, 1915 (1975).
26. J. R. Parks and J. Van Wazer, J. Am. Chem. Soc. 79, 4890 (1957).
27. J. C. Holste, private communication.
28. See, for e.g., J.D. Ferry, "Viscoelastic Properties of Polymers", Wiley, New York, 1970 (2nd Ed.).
29. H. Markovitz, J. Phys. Chem., 69, p. 671 (1965).
B.D. Coleman and H. Markovitz, J. Appl. Phys., 35, p. 1 (1968).
30. (a) C.-P. Wong and G.C. Berry, Polymer, 20, p. 229 (1979).
(b) G.C. Berry, B.L. Hager and C.-P. Wong, Macromolecules, 10, 361 (1978).
(c) C.-P. Wong, H. Ohnuma and G.C. Berry, J. Polym. Sci., Polym. Symp., 65, p. 173 (1978).
31. W.W. Graessley, Adv. in Polymer Science, 16 Sec. 3, (1974).
32. H. Janeschitz-Kriegl, Adv. in Polymer Sci., 6, pp. 170-318 (1964).
33. B.D. Coleman, E.H. Dill and R.A. Toupin, Archives for Rational Mech. and Analysis, 39, p. 358 (1970).
34. C.-P. Wong and G.C. Berry, Journal of Polymer Science, Polymer Physics Ed., 13, p. 1761 (1975).
35. B.D. Coleman, H. Markovitz and W. Noll, "Viscometric Flows of Non-Newtonian Fluids", Springer-Verlag, New York, 1966
(a) p. 52
(b) p. 54.
36. H. Benoit, Thesis, University of Strasbourg, 1950.
37. B.H. Zimm, Rev. Scientific Instruments, 29, p. 360 (1958).

References (concluded)

38. W. Philippoff, Trans. Soc. Rheol., 5, p. 163 (1961).
39. (a) F.D. Dexter, J.C. Miller and W. Philippoff, Trans. Soc. Rheol., 5, p. 193 (1961).
(b) W.T. Foreman, J. Chem. Phys., 32, p. 277 (1960).
(c) J. Wahl and F. Fischer, Mol. Cryst., Liq. Cryst., 22, p. 359 (1973).
(d) J. Wahl and F. Fischer, Opt. Comm., 5, p. 344 (1972).
(e) K. Skarp and T. Carlson, Mol. Cryst., Liq. Cryst., 49, p. 75 (1978).
40. G.C. Berry, et al., Technical Report AFML-TR-79-4115, August 1979.
41. C. Cohen, private communication.
42. (a) M. Doi and S.F. Edwards, J. Chem. Soc., Faraday Trans. II, 74, p. 560 (1978).
(b) M. Doi and S.F. Edwards, J. Chem. Soc., Faraday Trans. II, 74, p. 918 (1978).
43. (a) J.L.S. Wales and W. Philippoff, Rheol. Acta., 12, p. 25 (1973).
(b) K. Osaki, N. Bessho, T. Kojimoto and M. Kweata, J. Rheol., 23, p. 457 (1979).
(c) F.H. Gortemaker, M.G. Hansen, B. deCindio and H. Janeschitz-Kriegl, Rheol. Acta, 15, p. 242 (1976).
44. See, for e.g., V.N. Tsvetkov, et al., "Structure of Macromolecules in Solution", Vo. 3, Chap. 7, Eng. Transl., National Lending Library for Science and Technology, Boston Spa, England, 1971.
45. P. Metzger, Ph.D. Thesis, Carnegie-Mellon University, Pittsburgh, PA 1979.
46. K. Nakamura and G.C. Berry, to be published.
47. V.N. Tsvetkov, et al., European Polymer J., 12, p. 517 (1976).
48. G. C. Berry, J. Polymer Sci., Phys. Ed., 14, p. 451 (1976).